

IMPEDANCE MATCHING FEED NETWORK TO  
IMPROVE MICROSTRIP ANTENNA MANUFACTURABILITY

RONALD S. LEWIS







**Impedance Matching Feed Network to Improve  
Microstrip Antenna Manufacturability**

by

©Ronald S. Lewis

B.Sc.(Honours), Acadia University (1998)  
M.Sc., Memorial University of Newfoundland (2003)

A thesis submitted to the  
School of Graduate Studies  
in partial fulfillment of the  
requirements for the degree of  
Master of Engineering

Faculty of Engineering and Applied Science  
Memorial University of Newfoundland

May 2007



Library and  
Archives Canada

Bibliothèque et  
Archives Canada

Published Heritage  
Branch

Direction du  
Patrimoine de l'édition

395 Wellington Street  
Ottawa ON K1A 0N4  
Canada

395, rue Wellington  
Ottawa ON K1A 0N4  
Canada

*Your file* *Votre référence*  
*ISBN: 978-0-494-31267-4*  
*Our file* *Notre référence*  
*ISBN: 978-0-494-31267-4*

**NOTICE:**

The author has granted a non-exclusive license allowing Library and Archives Canada to reproduce, publish, archive, preserve, conserve, communicate to the public by telecommunication or on the Internet, loan, distribute and sell theses worldwide, for commercial or non-commercial purposes, in microform, paper, electronic and/or any other formats.

The author retains copyright ownership and moral rights in this thesis. Neither the thesis nor substantial extracts from it may be printed or otherwise reproduced without the author's permission.

**AVIS:**

L'auteur a accordé une licence non exclusive permettant à la Bibliothèque et Archives Canada de reproduire, publier, archiver, sauvegarder, conserver, transmettre au public par télécommunication ou par l'Internet, prêter, distribuer et vendre des thèses partout dans le monde, à des fins commerciales ou autres, sur support microforme, papier, électronique et/ou autres formats.

L'auteur conserve la propriété du droit d'auteur et des droits moraux qui protègent cette thèse. Ni la thèse ni des extraits substantiels de celle-ci ne doivent être imprimés ou autrement reproduits sans son autorisation.

---

In compliance with the Canadian Privacy Act some supporting forms may have been removed from this thesis.

Conformément à la loi canadienne sur la protection de la vie privée, quelques formulaires secondaires ont été enlevés de cette thèse.

While these forms may be included in the document page count, their removal does not represent any loss of content from the thesis.

Bien que ces formulaires aient inclus dans la pagination, il n'y aura aucun contenu manquant.

  
**Canada**

# Impedance Matching Feed Network to Improve Microstrip Antenna Manufacturability

by

Ronald S. Lewis

## Abstract

Experimental investigation of frequency bandwidth dependence on geometrical characteristics of microstrip patch antennas (MPAs) has shown that variations in impedance are a dominant bandwidth limiting factor. Other functional techniques to increase MPA bandwidth exist such as increasing the thickness of the substrate or decreasing the substrate permittivity, but there are obvious tradeoffs to these methods including cost, increased mass and spatial footprint. In this work, there is a supposition regarding the restriction of basic design elements including choice of substrate materials, thereby limiting the discussion to the first method in order to attack the MPA narrow bandwidth problem in the context of manufacturability.

These MPAs suffer from variations in material electrical properties as well as inaccuracies and variations of machining during fabrication which result in a shifting of the resonant frequency of the patch antenna. The narrowband nature of MPAs may result in a completely non-radiating build of hardware due to this real variability during the manufacturing process. Low cost printed circuit board (PCB) fallout for digital interconnect is not significant; however, variations in material have very sig-

nificant impacts on MPA performance. Thus with the advent of wireless commercial electronics, methods to add robustness to RF designs are of increasing importance.

A rigorous process of computer simulation is applied to examine geometric manipulation of MPAs and how the introduction of two coplanar design element, capacitively gap coupled parasitic elements and an impedance matching network feed line, can improve and increase MPA bandwidth sufficiently to overcome small errors encountered in the MPA fabrication process.

## Acknowledgements

I would like to take this opportunity to thank my Supervisor Dr. Siu D. O'Young for providing both moral and financial support and for his energy, drive and enthusiasm to create an enriching learning environment and experience.

I would like to thank the Faculty of Engineering and Applied Science and the School of Graduate Studies for providing me with financial support in the form of a fellowship and various teaching assistantships.

I would like to thank the Atlantic Canada Opportunities Agency for their support of the Remote Aerial Vehicles for Environmental Monitoring Project. It was through this exciting Unmanned Aerial Vehicle project that I was given an opportunity to conduct research for a truly interesting local and contemporary real world application. At this point, I also would like to recognize Provincial Aerospace Limited for their industry support of the RAVEN project. This project would not have the promising life that it does without PAL's industry presence and maritime aerospace expertise.

Furthermore, I wish to recognize Mr. Ian Timmins for his invaluable guidance and assistance with this research topic. Thanks also to Mr. Roy Crocker and Mr. Chris Batten at Technical Services for assistance in the fabrication process.

Last, but not least, thank you to my wife and family for their continued love, support and patience.

# Contents

<b>Abstract</b>	<b>ii</b>
<b>Acknowledgements</b>	<b>iii</b>
<b>Contents</b>	<b>iv</b>
<b>List of Figures</b>	<b>x</b>
<b>List of Tables</b>	<b>xiv</b>
<b>List of Symbols</b>	<b>xvi</b>
<b>List of Acronyms</b>	<b>xix</b>
<b>1 General Introduction</b>	<b>1</b>
1.1 Beginnings . . . . .	1
1.2 Scope . . . . .	4
<b>2 Antennas and General Parameters</b>	<b>8</b>

2.1	Antennas and their types . . . . .	8
2.2	Parameters . . . . .	10
2.2.1	Radiation pattern . . . . .	11
2.2.2	Polarization . . . . .	14
2.2.3	Radiation intensity . . . . .	15
2.2.4	Directivity . . . . .	17
2.2.5	Gain . . . . .	18
2.2.6	Input impedance . . . . .	19
2.2.7	Reflection coefficient and associated parameters . . . . .	20
2.2.8	Bandwidth and Q-factor . . . . .	22
<b>3</b>	<b>Literature Review</b>	<b>25</b>
3.1	General . . . . .	25
3.2	Patch element . . . . .	29
3.3	Feeding techniques . . . . .	32
3.3.1	Direct probe coupling . . . . .	33
3.3.2	Coplanar microstrip coupling . . . . .	34
3.3.3	Electromagnetic proximity coupling . . . . .	36
3.3.4	Aperture coupling . . . . .	38
3.3.5	Coplanar waveguide . . . . .	41
<b>4</b>	<b>Problem Statement and Modelling Methods</b>	<b>46</b>

4.1	Narrow frequency bandwidth . . . . .	46
4.1.1	General methods to improve bandwidth . . . . .	47
4.1.2	Characterizing the problem . . . . .	49
4.2	Modelling . . . . .	53
4.2.1	Transmission line model . . . . .	53
4.2.2	Cavity model . . . . .	54
4.2.3	Multi-port network model . . . . .	55
4.2.4	Full-wave models . . . . .	55
<b>5</b>	<b>Basic Rectangular MPA with Coplanar Microstrip Feed Line</b>	<b>56</b>
5.1	Design . . . . .	57
5.1.1	Rectangular patch . . . . .	57
5.1.2	Microstrip feed line . . . . .	60
5.2	Simulation . . . . .	61
<b>6</b>	<b>Coplanar Gap-coupled Parasitic Elements</b>	<b>70</b>
6.1	Design . . . . .	71
6.2	Simulation . . . . .	73
<b>7</b>	<b>Impedance Matching Feed Line Network</b>	<b>79</b>
7.1	Design . . . . .	80
7.2	Simulation . . . . .	84
<b>8</b>	<b>Measurements and Discussion</b>	<b>90</b>

8.1	Radiation pattern measurements . . . . .	91
8.1.1	General setup . . . . .	91
8.1.2	Azimuthal plane results . . . . .	95
8.1.3	Elevation plane results . . . . .	100
8.2	Return loss and VSWR measurements . . . . .	108
8.2.1	Control RMPA results . . . . .	108
8.2.2	Tuned RMPA results . . . . .	111
8.2.3	Modified RMPA results . . . . .	115
8.2.4	Summary statistics . . . . .	119
<b>9</b>	<b>Conclusion</b>	<b>121</b>
9.1	Summary . . . . .	122
9.2	Original contributions . . . . .	124
9.3	Recommendations . . . . .	124
9.4	Future work . . . . .	125
	<b>Bibliography</b>	<b>127</b>
<b>A</b>	<b>Simulation Results</b>	<b>146</b>
A.1	Data . . . . .	146
A.1.1	Control RMPA return loss . . . . .	146
A.1.2	Tuned RMPA with coupling strips return loss . . . . .	150

A.1.3	Modified RMPA with coupling strips and impedance matching network return loss data . . . . .	154
A.2	Plots . . . . .	158
A.2.1	Smith charts . . . . .	158
A.2.2	Characteristic impedance . . . . .	159
A.2.3	Real and imaginary impedance . . . . .	161
A.2.4	Far field radiation . . . . .	162
A.2.5	Accepted gain . . . . .	164
A.2.6	Current distribution . . . . .	165
<b>B</b>	<b>Measurement Results</b>	<b>167</b>
B.1	Return loss data . . . . .	167
B.1.1	Control RMPA . . . . .	167
B.1.2	Tuned RMPA . . . . .	171
B.1.3	Modified RMPA . . . . .	175
B.2	Radiation pattern data . . . . .	179
B.2.1	Control RMPA azimuthal data . . . . .	179
B.2.2	Tuned RMPA azimuth data . . . . .	180
B.2.3	Modified RMPA azimuth data . . . . .	181
B.2.4	Control RMPA elevation data . . . . .	182
B.2.5	Tuned RMPA elevation data . . . . .	183
B.2.6	Modified RMPA elevation data . . . . .	184

<b>C MATLAB Code</b>	<b>185</b>
C.1 RMPA dimensions . . . . .	185
C.2 Feed line dimensions . . . . .	188
C.3 Impedance matching network . . . . .	191
C.3.1 M-script . . . . .	191
C.3.2 Running M-script . . . . .	195

# List of Figures

2-1	Basic antenna operation . . . . .	9
2-2	Reference axis . . . . .	11
2-3	Hertzian dipole power patterns . . . . .	13
2-4	Directional antenna radiation pattern . . . . .	14
2-5	Polarization: circular and polar . . . . .	15
2-6	Steradian . . . . .	16
2-7	Antenna in transmit mode . . . . .	19
2-8	Basic antenna circuit model . . . . .	20
3-1	Rectangular MPA construction . . . . .	26
3-2	RMPA circular polarization techniques . . . . .	31
3-3	Yagi-Uda MPA array . . . . .	32
3-4	Probe coupling . . . . .	34
3-5	L-probe coupling . . . . .	34
3-6	Coplanar microstrip coupling . . . . .	35

3-7	Modified coplanar microstrip coupling . . . . .	36
3-8	Proximity coupling . . . . .	37
3-9	Unconventional proximity coupling . . . . .	38
3-10	Aperture coupling . . . . .	38
3-11	Orthogonal aperture coupling . . . . .	39
3-12	Coplanar waveguide proximity coupling . . . . .	42
3-13	CPW feed examples . . . . .	43
3-14	Capacitive and inductive CPW feeds . . . . .	44
3-15	Single sided CPW feeds . . . . .	45
4-1	Effect of dielectric substrate electrical variability on return loss . . . . .	50
4-2	Effect of over/under etching on return loss . . . . .	52
5-1	MPA physical and electrical length . . . . .	59
5-2	RMPA layout . . . . .	62
5-3	Control RMPA simulation model . . . . .	62
5-4	Control RMPA - simulated return loss . . . . .	63
5-5	Control RMPA - simulated VSWR . . . . .	67
5-6	Control RMPA - simulated accepted gain (dB). . . . .	68
5-7	Control RMPA - simulated accepted gain in polar coordinates . . . . .	69
6-1	Tuned RMPA simulation model with gap coupled parasitic strips . . . . .	72
6-2	Tuned RMPA - simulated return loss . . . . .	74

6-3	Tuned RMPA - simulated VSWR . . . . .	74
6-4	Tuned RMPA - simulated accepted gain (dB). . . . .	76
6-5	Tuned RMPA - simulated accepted gain in polar coordinates . . . . .	77
7-1	Impedance matching network . . . . .	81
7-2	$g_i$ parameter chart . . . . .	83
7-3	Modified RMPA simulation model with impedance matching network	85
7-4	Modified RMPA - simulated return loss . . . . .	85
7-5	Modified RMPA - simulated VSWR . . . . .	87
7-6	Modified RMPA - simulated accepted gain (dB). . . . .	88
7-7	Modified RMPA - simulated accepted gain in polar coordinates . . . . .	89
8-1	RF anechoic chamber . . . . .	92
8-2	Antenna and hardware configuration for anechoic measurements . . . . .	92
8-3	Yagi-Uda antenna in azimuthal measurement configuration . . . . .	93
8-4	Control RMPA antenna in azimuthal measurement configuration . . . . .	94
8-5	RMPA azimuthal plane measurement configuration . . . . .	95
8-6	Control RMPA - Azimuthal radiation pattern . . . . .	96
8-7	Tuned RMPA - Azimuthal radiation pattern . . . . .	96
8-8	Modified RMPA - Azimuthal radiation pattern . . . . .	97
8-9	RMPA azimuthal radiation patterns . . . . .	98
8-10	Control RMPA - Azimuthal radiation pattern in polar coordinates . . . . .	99
8-11	Tuned RMPA - Azimuthal radiation pattern in polar coordinates . . . . .	99

8-12	Modified RMPA - Azimuthal radiation pattern in polar coordinates . . .	100
8-13	Yagi-Uda antenna in elevation measurement configuration . . . . .	101
8-14	Control RMPA antenna in elevation measurement configuration . . .	101
8-15	RMPA elevation plane measurement configuration . . . . .	102
8-16	Control RMPA - Elevation radiation pattern . . . . .	103
8-17	Tuned RMPA - Elevation radiation pattern . . . . .	103
8-18	Modified RMPA - Elevation radiation pattern . . . . .	104
8-19	RMPA elevation radiation patterns . . . . .	105
8-20	Control RMPA - Elevation radiation pattern in polar coordinates . .	106
8-21	Tuned RMPA - Elevation radiation pattern in polar coordinates . . .	107
8-22	Modified RMPA - Elevation radiation pattern in polar coordinates . .	107
8-23	Control RMPA - Measured return loss . . . . .	109
8-24	Control RMPA - Measured VSWR . . . . .	110
8-25	Tuned RMPA - Measured return loss . . . . .	112
8-26	Tuned RMPA - Measured VSWR . . . . .	114
8-27	Modified RMPA - Measured return loss . . . . .	115
8-28	Modified RMPA - Measured VSWR . . . . .	119

# List of Tables

3.1	MPA characteristics . . . . .	28
3.2	General MPA applications . . . . .	28
4.1	Electric variation affect on return loss . . . . .	51
5.1	Simulated return loss for control RMPA . . . . .	64
6.1	Simulated return loss for tuned RMPA with coupling strips . . . . .	75
7.1	Parameters for impedance matching netowrk . . . . .	84
7.2	Simulated return loss for modified RMPA . . . . .	86
8.1	Received amplitude drop-off from peak . . . . .	105
8.2	Real return loss for control RMPA . . . . .	109
8.3	Real return loss for control RMPA quality factor . . . . .	110
8.4	Real return loss for tuned RMPA . . . . .	112
8.5	Real return loss for tuned RMPA quality factor . . . . .	113
8.6	Real return loss for modifed RMPA - upper pole . . . . .	116

8.7	Real return loss for modified RMPA - lower pole . . . . .	117
8.8	Parameters of interest: simulation versus actual . . . . .	120
8.9	Frequency shifts and pole reductions . . . . .	120

# List of Symbols

$x, y, z$	cartesian coordinates
$\theta, \phi, r$	spherical coordinates
$D$	largest antenna dimension
$R$	farfield distance from antenna
$\lambda$	signal wavelength in free space
$l$	Hertzian dipole length
$\vec{E}, \vec{H}$	electric and magnetic field vectors
$d\Omega$	solid angle differential element
$U(\theta, \phi)$	radiation intensity
$ \cdot $	magnitude operator
$\vec{P}_a$	Poynting vector
$\vec{H}^*$	magnetic field vector complex conjugate
$U_0$	radiation intensity for an isotropic source
$P_r$	average radiated power
$d\vec{S}$	spherical surface differential element

$D(\theta, \phi)$	directivity
$\epsilon_r$	radiation efficiency
$P_{IN}$	power delivered to antenna
$G(\theta, \phi)$	gain
$G(dB)$	gain expressed in dB
$V_t$	transmission device voltage
$Z_{in}$	input impedance
$R_{in}$	antenna resistance at terminals
$X_{in}$	antenna reactance at terminals
$R_r$	radiation resistance
$R_L$	loss due to conduction or dielectric effects
$I$	current
$Z_0$	characteristic impedance
$\Gamma$	reflection coefficient
$RL(dB)$	return loss expressed in dB
$VSWR$	voltage standing wave ratio
$B$	bandwidth
$f_r$	resonant frequency
$\Delta f$	range of frequencies
$f_2, f_1$	upper and lower frequency
$Q_t$	total quality factor

$Q_{rad}$	quality factor due to radiation losses
$Q_c$	quality factor due to conduction losses
$Q_d$	quality factor due to dielectric losses
$Q_{sw}$	quality factor due to surface waves
$\epsilon_r$	relative dielectric constant
$\tan \delta$	loss tangent
$L$	patch length
$\lambda_d$	wavelength in substrate
$c$	free space speed of light
$h$	thickness of dielectric material
$W$	patch width
$\epsilon_{re}$	relative effective dielectric constant
$L + \Delta L$	patch electric length
$w$	feed line width
$\ell$	feed line length
$\beta$	signal propagation constant
$k_0$	signal wave number
$m_L, b_L$	regression line variables
$Y$	admittance
$f_c$	centre frequency

# List of Acronyms

**CPW** Coplanar Waveguide

**CCPW** Channelised Coplanar Waveguide

**e/m** Electromagnetic

**FCPW** Finite Ground Coplanar Waveguide

**FR-4** Flame Resistant 4

**GCPW** Grounded Coplanar Waveguide

**IEEE** Institute of Electrical and Electronic Engineers

**MPA** Microstrip Patch Antenna

**PCB** Printed Circuit Board

**RF** Radio Frequency

**RMPA** Rectangular Microstrip Patch Antenna

**RL** Return Loss

**VSWR** Voltage Standing Wave Ratio

**UAV** Unmanned Aerial Vehicle

# Chapter 1

## General Introduction

### 1.1 Beginnings

The seminal work on the microstrip patch antenna (MPA) concept is attributed to G. Deschamps and W. Sichak, “Microstrip Microwave Antennas” and first appeared at the Third Symposium on the United States Air Force Antenna Research and Development Program in 1953 [1]. However, it was only declassified a decade later and was not available for public consumption until 1965. Two years after the original presentation of the Deschamps-Sichak work, a patent was filed by H. Gutton and G. Baissinot. French Patent number 703113 is concerned with developing a flat aerial for ultra high frequencies [2]. Ultra high frequencies (UHF) are in the range of 300 Megahertz (MHz) to 3 Gigahertz (GHz) and have wavelengths roughly measuring anywhere from 10 cm to 1 m in free space.

It was not until the early 1970's that the first actual MPA fabrications appear in recognized literature. In 1972, Howell [3] first reported a design and fabrication of several L-band (1-2 GHz) and C-band (4-8 GHz) linearly polarized MPAs. Howell observed that narrow bandwidth results from the large impedance transformation to match the antenna. As well, techniques to alter the polarization to purify its circularity are offered and details concerning the introduction of a second resonant frequency are given. A follow up work of Howell delves into the topic of circular polarization in greater detail and a general MPA design protocol is established [4]. During this time, Munson describes an MPA like system integrated into a cylindrical rocket fuselage [5]. The use of microstrip technology is driven in this instance by the physical design specifications of the application. The author identifies the need for a 'paper thin' antenna which can conform to a rocket without disturbing air flow or intruding into the rocket and causing mechanical interference. He highlights not only the beneficial physical aspects of microstrip technology for this particular application, but also its relative cost effectiveness. In his conclusion, Munson goes so far as to suggest that, "It may be entirely possible to cover the entire outer surface of a missile or aircraft with [a microstrip] antenna without large cost or weight penalties." Authors elsewhere in the literature agree with this opinion citing the need for conformal missile and spacecraft antennas as the impetus of a grander scale of MPA research work in the 70's as opposed to the wider selection of available microstrip substrates [6], [7].

Since the aforementioned original works, MPA technology has blossomed into a

vibrant area of research over the course of the last several decades. In 1979, at New Mexico State University the first workshop on MPAs was held. The Workshop on Printed Circuit Antenna Technology resulted in a dedicated special issue of IEEE Transactions on Antennas and Propagation in January, 1981 [8]. That publication contained almost 30 articles directly involving MPA technology and stimulated research for a generation. Since then, there have been hundreds of research articles appearing in reputable publications and several texts written specifically on the subject. This is partly due to advances in printed circuit substrates. The nature of microstrip line technology versus stripline technology is that there is significant energy loss due to radiation because of the former's open structure. A stripline is a microstrip line embedded in a substrate instead of etched on the surface of the substrate. When MPAs were first proposed, dielectric substrates generally had low-permittivity which further contributed to energy losses. Technology has since improved and evolved to make available substrates that have higher permittivity and low-loss thereby reducing energy losses and increasing the effectiveness and utility of MPAs [9].

In addition to the beneficial physical traits of MPAs, low fabrication costs, and simultaneously fabricated feed lines and matching networks result in antennas which are amenable to mass production. Features such as differing polarizations (particularly circular achieved with a single feed line), introducing dual-frequencies and integration with microwave integrated circuits are all relatively easy to fabricate with MPA technology. This manifestation of antenna technology lends itself to certain applications.

The previously mentioned qualities are attractive to aerospace and satellite engineering applications as well as mobile communications for modern personal computer systems.

A particular problem of interest is that of communications on an Unmanned Aerial Vehicle (UAV). Typically, these vehicles depend on lightweight communication and sensor systems. As well, there are bandwidth conservation issues in the sense a UAV be outfitted with multiple devices which transmit and receive RF signals. Hence MPA physical qualities and multi channel operation ability make this technology attractive for UAV applications. Although not explicitly stated, the successful integration of MPA technology on UAV is also a motivation for this work. The academic problem of the thesis is framed in the context of increasing frequency bandwidth sufficiently at a given frequency to overcome material variability as part of a large scale MPA fabrication process with high volume.

## **1.2 Scope**

In this work, the design and testing of a technique to overcome the classical narrow bandwidth problem for an MPA with an operating resonant frequency of 900 MHz is described. The experiment will focus on modifying the frequency bandwidth in such a way as to successfully account for slight variations in the resonant frequency resulting from significant, but industry reasonable inaccuracies involved in MPA fabrication processing such as at Memorial University of Newfoundland's Technical Services.

These inaccuracies are common to all printed circuit board (PCB) manufacturing processes.

Many different approaches exist to tackle this problem; however, the goal of the author was to do so in a cost-effective manner using solely the common low cost materials and standard fabrication processes available. Modifying the MPA physically by adding active hardware devices or by using different dielectric substrates is not considered as an option in the discussion contained herein.

The second chapter is a general introduction to the language and terminology of antennas. It includes an overview of antenna function and types. Much of the discussion in this chapter is centred around general antenna parameters and their usage in evaluating antenna performance. Many of the essential antenna parameters are defined and explained.

The third chapter is the literature review for the thesis. It provides a general background to MPA antennas for a non-specialist. The MPA structure is divided into two substructures: the radiating patch and the microstrip feed line. Both substructures are examined in some detail. Relevant results from the literature will be considered as they relate in this context and be discussed thusly. These sections survey the journal publications related to the experiment and are a commentary on the state of research.

Chapter four is concerned with the narrow bandwidth problem and characterizes the problem studied in this thesis. Several MPA modelling methods are explained.

The fifth, sixth and seventh chapters focus on the design of an optimal 900 MHz

antenna element that can overcome reasonable fabrication variations in order to function according to specification. In the fifth chapter, the control for the experiment, a rectangular MPA model with simple coplanar microstrip feed line is designed using current analytic methods available in the literature. A high accuracy finite element (method of moments) computer simulation is used for model analysis and evaluation of certain antenna parameters for comparison to experimental measurements. The sixth chapter describes the insertion of the first of two additional coplanar design elements into the existing control MPA model. A set of gap coupled strips are added to the design along the non-radiating edges of the control MPA for tuning purposes. The design approach is detailed and then treated by a course of computer simulation. The last of the design chapters, chapter seven, describes the analytic derivation of an impedance matching feed network as prescribed by Pues and Van de Capelle [10]. Computer simulation to adjust the model is employed in order to optimize the antenna performance parameters of interest.

The role of simulation in the sixth and seventh chapters differs significantly from chapter five. In chapter five, computer simulation is employed purely as an assessment tool for the purposes of evaluating certain antenna parameters of interest for the control model. In the subsequent two chapters, simulation is a design as well as an assessment tool. The simulation reconfigures the models of chapters six and seven to optimize specific antenna parameters according to specification.

Chapter eight describes the experimental test measurement results and compares

the actual measurements with the computer simulation. The parameters compared for this work are the radiation pattern and reflection coefficient in the form of return loss and voltage standing wave ratio (VSWR). A measure of the radiation patterns of the fabricated patch antennas signifies a base level of functionality for the MPAs. It is possible to ascertain if the fabricated MPAs exhibit the general radiation characteristics of MPAs and more importantly if the fabricated MPAs perform adequately in the range of the desired resonant frequency of 900 MHz. MPAs normally have bandwidth on the order of a percent or less. Improvement in this bandwidth to at least a level of several percent is a desired outcome of this work. The return loss measurements are the true measure of the MPAs ability to function according to specification and a gauge of the success of this work.

The conclusion is contained in the ninth and final chapter of this work. It includes a summary of the experimental measurement results and a series of recommendations that pertain to extensions of this work. The novel concepts found in the thesis are stated and future research problems stemming from this topic are offered.

There are several appendices in the thesis. They include simulation data, actual measurement data and the code for several MATLAB programs used in the course of this work.

# Chapter 2

## Antennas and General Parameters

This chapter includes definitions and explanations of the terminology used in this thesis. The non-specialist can appreciate this casual introduction to antennas. A more rigorous exposition of the subject is available in C. Balanis' fundamental text [11] or W. Stutzman and G. Thiele's book [12].

### 2.1 Antennas and their types

An antenna is a conductive mechanism that converts electromagnetic waves on a transmission line to electromagnetic waves propagating in free space. The IEEE Standard Definitions of Terms for Antenna [13] formally defines an antenna as, "that part of a transmitting or receiving system which is designed to radiate or to receive electromagnetic waves." Figure 2-1 depicts the basic structure of an electrical system utilizing antennas to transmit electromagnetic waves (a signal). This radiation

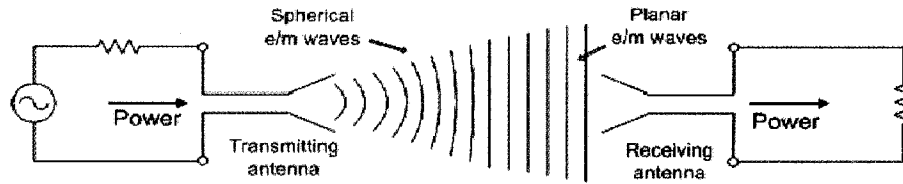


Figure 2-1: Basic antenna operation between a transmitting and receiving device.

of electromagnetic waves originates from charge acceleration on the transmitting antenna resulting from an oscillating current, a constant current moving along a curved medium, or a current encountering a truncation, a load or some type of discontinuity. The resulting radiated energy will excite surface currents on a receiving antenna which can then be converted into a useable signal by a specified electronic device. In addition to the aforementioned capacity of energy transmission, antennas are often required to focus radiated energy in a particular direction. They can be designed to accentuate radiation toward certain spatial areas of interest and suppress it in other areas (see Sections 2.2.4 and 2.2.5). This feature can be attractive to certain applications such as satellite communications and satellite television receivers.

There are multiple antenna configurations currently in use. Pozar [14] groups them into several categories:

- Wire antennas include dipoles, monopoles, loops, sleeve dipoles, Yagi-Uda arrays and related structures. Such antennas generally have low gains and are often used at lower frequencies HF to UHF (3 MHz to 3 GHz). The advantages of this type of antenna are that they are typically light-weight, low cost and of

simple design.

- Aperture antennas include open-ended waveguides, rectangular or circular horns, reflectors and lenses. Common applications for aperture type antennas utilize microwave and millimetre wave frequencies. These antennas usually have high gains.
- Printed antennas include printed slots, printed dipoles, printed monopoles and microstrip patch antennas. These antennas can be made with photolithographic methods, with both radiating elements and associated feed circuitry fabricated on dielectric substrates. Printed antennas are often used at microwave and millimetre wave frequencies, and can be arrayed for high gain.
- Array antennas consist of regular arrangements of antenna elements with a feed network. Pattern characteristics such as beam steering angle and side lobe levels can be controlled by adjusting amplitude and phase distributions of the individual array elements.

## 2.2 Parameters

Antenna parameters are used quite often to describe an antenna and quantify its performance. It is essential to have a regimental method for describing antenna parameters so that practitioners can be assured they are speaking the same language when it comes to antenna theory and design. Some important parameters will be

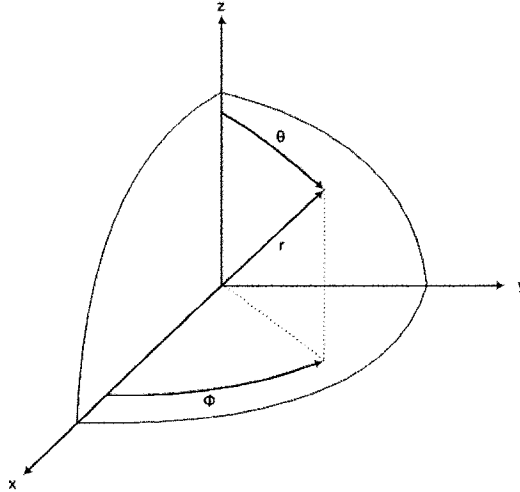


Figure 2-2: The standard reference axis used to describe antenna parameters. A point is described in terms of rectangular  $(x, y, z)$  or spherical  $(\theta, \phi, r)$  coordinates.

discussed. Before engaging this topic further, recall the antenna coordinate system as seen in Figure 2-2. Both rectangular and spherical coordinates are commonly used to describe an antenna's parameters.

### 2.2.1 Radiation pattern

A radiation pattern or antenna pattern is the spatial distribution of a quantity which characterizes the electromagnetic field generated by an antenna [13]. It is expressed as a function of the elevation angle,  $\theta$ , the azimuth angle,  $\phi$ , and the radial distance,  $r$ , from the centre of the antenna. Radiation patterns are typically measured in the Fraunhofer or far-field region. It is in this region that the distance from the antenna can be overlooked and the field pattern is reduced to a function of  $\theta$  and  $\phi$ , that is,

the region of the field of an antenna where the angular field distribution is essentially independent of the distance from a specified point in the antenna region [13]. Let  $D$  represent the largest dimension of the antenna. To be valid,  $D$  must also be large compared to the signal wavelength ( $D > \lambda$ ). For example, on a circular parabolic dish it would be the diameter and on a rectangular microstrip patch it would be the length. Then the far-field region,  $R$ , is defined mathematically to be

$$R > \frac{2D^2}{\lambda}, \quad (2.1)$$

when  $D$  is large compared to  $\lambda$  [11].

It is necessary to be clear when discussing specific radiation patterns of an antenna. Sometimes it is the power pattern which is the radiated parameter of interest, but it can also be the electric or magnetic fields which are the patterns of significance (referred to as amplitude field patterns). The electric field is an indicator for directivity for example. Radiation properties have come to include several concepts such as: power flux density, radiation intensity, field strength, directivity, phase and polarization.

For a simple illustration of some antenna radiation patterns, consider basic patterns for a Hertzian or infinitesimal dipole in Figure 2-3. Note that a Hertzian dipole is a dipole antenna which is sufficiently small compared to its transmission wavelength ( $l \ll \lambda$ ) such that it can be treated as a point for analysis purposes. In three dimensions, the power pattern for the Hertzian dipole is realized as a torus with no hole, but

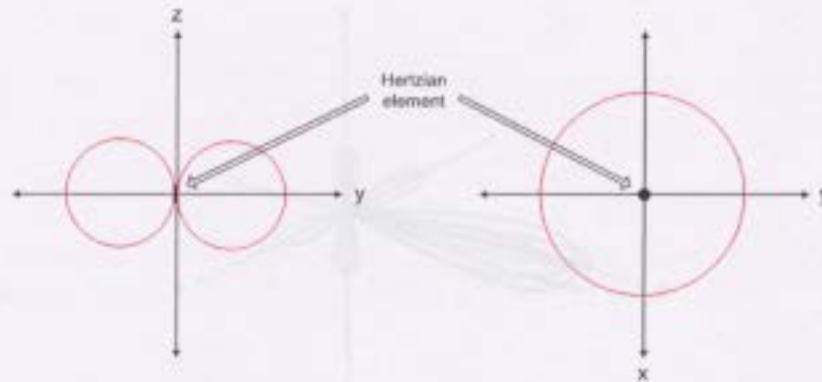


Figure 2-3: Radiated power patterns for a Hertzian dipole in the elevation plane ( $\theta$ -plane) and in the azimuthal plane ( $\phi$  - plane).

rather a point for its centre. Antennas with the quality of having a constant pattern in the azimuthal direction, like the Hertzian dipole, are called omnidirectional.

The radiation pattern for an antenna or array of antennas is not always geometrically symmetric or uniform. In fact, directionality is often a design requirement for most antennas. It will be shown that MPAs are directional because of their structure. Consider the given general illustration of a radiation pattern in Figure 2-4. Along the  $y$ -axis is the main lobe and along the  $x$  and  $z$  axes are minor or side lobes. Most of the antenna's energy is focused through a main lobe. Sometimes back lobes exist which are oriented in the opposite direction to that of the main lobe (although none are pictured in Figure 2-4). A lobe is a portion of the radiation pattern bounded by regions of relatively weak radiation intensity [11]. The main or major lobe is then the radiation lobe containing the direction of maximum radiation [13].

by an antenna taken over its radiation sphere. See Figure 2-3 for example.

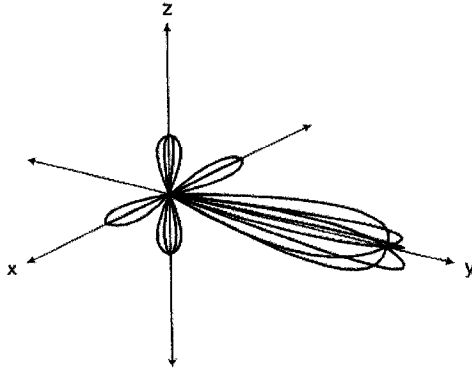


Figure 2-4: Power pattern for directional antenna with main lobe along the  $y$ -axis and four minor side lobes.

### 2.2.2 Polarization

Polarization is a fundamental parameter design consideration and an antenna term which requires further clarification. This term can be used as a descriptor for the antenna itself as well as for the type of radiation pattern emitted by the antenna. Technically, polarization of a wave refers to the polarization of the plane wave used to represent the radiated wave at a point lying in the far-field of the antenna and in a specified direction from the antenna. In short, it describes the tip of the E-field vector for a radiating antenna. Generally, this polarization pattern is elliptical but there are special cases where it is linear or circular. It is also possible to designate elliptical polarization as either right handed or left handed based on the curl in the E-field vector in the direction perpendicular to the direction of propagation. The polarization pattern of an antenna is the spatial distribution of the field vector excited by an antenna taken over its radiation sphere. See Figure 2-5 for example.

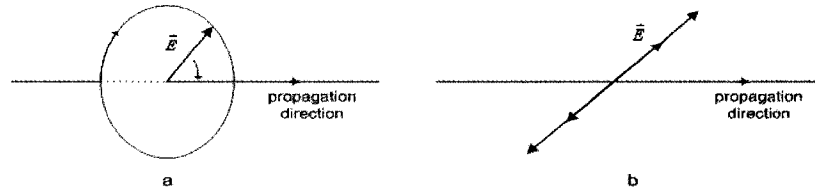


Figure 2-5: Examples of (a) Left-handed circular and (b) linear polarization patterns where the electric field vector is denoted by  $\vec{E}$ .

Polarization may be used to isolate different forms of communication . Some devices such as television typically utilize horizontally polarized signals, whereas satellite communication signals are circular due to the unknown orientations of the transmitter and receiver. When referring to a specific antenna, it is not uncommon to make reference to the antenna's polarization.

### 2.2.3 Radiation intensity

It is necessary to consider the higher dimensional analogue to the radian. A steradian is the solid angle with vertex at the centre of a sphere radius  $r$  subtended by a surface area equal to  $r^2$ . The element of the solid angle is denoted by  $d\Omega$ . A geometric interpretation of a steradian can be found in Figure 2-6.

Now, radiation intensity in a given direction is the power radiated from an antenna per unit solid angle [11], denoted by

$$U \equiv U(\theta, \phi) = r^2 |\vec{P}_a| \text{ W/sr}$$



Figure 2-5: Examples of (a) Left-handed circular and (b) linear polarization patterns where the electric field vector is denoted by  $\vec{E}$ .

Polarization may be used to isolate different forms of communication. Some devices such as television typically utilize horizontally polarized signals, whereas satellite communication signals are circular due to the unknown orientations of the transmitter and receiver. When referring to a specific antenna, it is not uncommon to make reference to the antenna's polarization.

### 2.2.3 Radiation intensity

It is necessary to consider the higher dimensional analogue to the radian. A steradian is the solid angle with vertex at the centre of a sphere radius  $r$  subtended by a surface area equal to  $r^2$ . The element of the solid angle is denoted by  $d\Omega$ . A geometric interpretation of a steradian can be found in Figure 2-6.

Now, radiation intensity in a given direction is the power radiated from an antenna per unit solid angle [11], denoted by

$$U \equiv U(\theta, \phi) = r^2 |\vec{P}_a| \text{ W/sr}$$

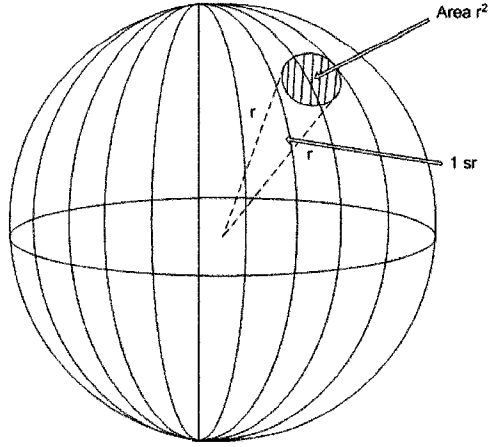


Figure 2-6: Geometric representation for steradian (sr).

where

$$\vec{\mathcal{P}}_a = \frac{1}{2} \text{Re}\{\vec{E} \times \vec{H}^*\}$$

is the time averaged Poynting vector. The Poynting vector given by  $\vec{\mathcal{P}} = \vec{E} \times \vec{H}$ , is the instantaneous power density measured in  $\text{W}/\text{m}^2$ . For an isotropic source, that is a lossless antenna which radiates power equally in all directions, the radiation intensity is constant and given by

$$U_0 = \frac{P_r}{4\pi}$$

where

$$P_r = \int \vec{\mathcal{P}}_a \cdot d\vec{S}$$

is the average radiated power of the antenna and  $d\vec{S}$  is the spherical surface element of a spherical surface surrounding the antenna.

## 2.2.4 Directivity

Directivity is the ratio of the radiation intensity in a given direction from the antenna to the radiation intensity averaged over all directions and given by

$$D(\theta, \phi) = \frac{U}{U_0}.$$

Note that directivity is a dimensionless quantity and in some cases is considered in the direction of its maximum value [11]. It is possible to consider directivity as a standardized measure of how much more intensely an antenna radiates in a direction compared to an isotropic radiator transmitting with the same total amount of power. In practice, the antenna should be of significantly larger size compared to its wavelength in order to achieve directivity appreciably more than unity. For instance, phased arrays or full-wave antennas have been used to get such results. However, in the case of some single element antennas such as dipoles problems can arise because as the length of the dipole increases beyond one wavelength, the number of lobes increases [11]. Although this may result in greater directivity in the direction of maximum radiation, it introduces nulls in the radiation pattern and can detrimentally impact main lobe beamwidth.

### 2.2.5 Gain

Gain is closely related to directivity. It is possible to define an antenna's radiation efficiency,  $\varepsilon_r$ , by the ratio of the total power radiated by an antenna to the net power accepted by the antenna from the connected transmitter [13]. That is

$$\varepsilon_r = \frac{P_r}{P_{IN}}$$

where  $P_{IN}$  is the power delivered to the antenna itself (ignoring any transmission line ohmic losses). A mathematical definition of gain can be expressed in terms of directivity

$$G(\theta, \phi) = 4\pi \left( \frac{U}{P_{IN}} \right) = \varepsilon_r D.$$

Intuitively, the higher the antenna gain then the higher the energy output of an antenna in a given direction. If an antenna has high gain in a particular direction, then it focuses much of its energy in that direction. Technically, gain is the ratio of the radiation intensity, in a given direction, to the radiation intensity that would be obtained if the power accepted by the antenna were radiated isotropically [13]. Gain is commonly expressed in dB by

$$G(dB) = 10 \log(G).$$

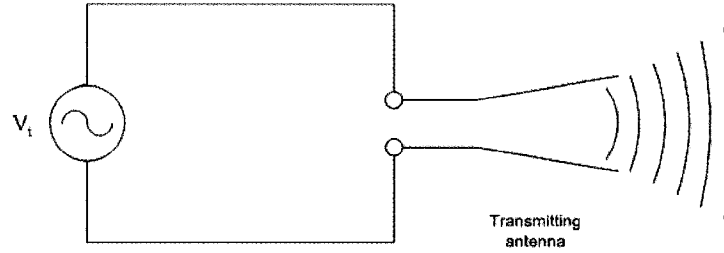


Figure 2-7: Antenna in transmit mode connected to a source.

### 2.2.6 Input impedance

The impedance presented by an antenna at its terminals is known as the input impedance [13]. The input impedance,  $Z_{in}$ , relates to the ability of an antenna to accept power from a source as in Figure 2-7.

Impedance is a complex quantity and defined by

$$Z_{in} = R_{in} + jX_{in}$$

where  $R_{in}$  is the antenna resistance at the terminals (ohms) and  $X_{in}$  is the antenna reactance at the terminals (ohms). The real resistive part of  $Z_{in}$  can be further subdivided into two components

$$R_{in} = R_r + R_L$$

where  $R_r$  is the radiation resistance given by  $2P_r/|I|^2$  for a feed current of  $I$ , and  $R_L$  is loss due to conduction or dielectric effects (i.e. heat dissipation). Input impedance is

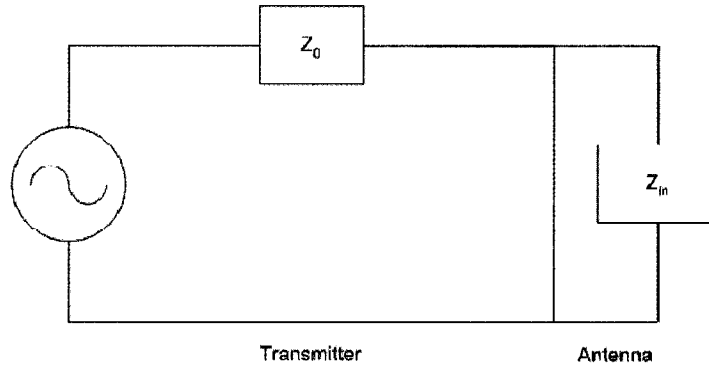


Figure 2-8: Basic circuit model for an antenna.

almost always treated as a function of frequency [11]. There are only a limited number of cases where analytical methods have been used to determine an antenna's input impedance; most require experimental analysis to determine the input impedance.

### 2.2.7 Reflection coefficient and associated parameters

It is possible to consider an antenna using a simple circuit representation depicted in Figure 2-8.

The characteristic impedance,  $Z_0 = R_0 + jX_0$ , is the impedance attributed to the transmission source and feed line. Ideally, for maximum power transmission there needs to be a matching of the characteristic and input impedances. Indeed, conjugate matching is required for this to occur, i.e.  $Z_0 = Z_{in}^*$ . In most cases when there is not an ideal match, power is reflected back toward the transmitter. A measure of this reflected energy is known as the reflective coefficient and calculated as a ratio of the difference to the sum of the input impedance of the antenna and the characteristic

impedance of the feed line

$$\Gamma = \frac{Z_{in} - Z_0}{Z_{in} + Z_0}.$$

The return loss of the antenna, in decibels (dB), is a parameter which gives a good indication of the power that is actually transmitted (or lost) by the antenna and is not reflected back to the transmitter. Loss in this case is a good thing. The return loss of an antenna is defined as

$$RL(dB) = 20 \log |\Gamma|.$$

A small  $\Gamma$  indicates a small return loss, i.e. not too much reflection.

Another parameter which is a good indicator of the impedance matching or mismatching is the Voltage Standing Wave Ratio (VSWR). If not all power is throughput and there are reflections then standing waves are created. The VSWR can be expressed as a function of the reflection coefficient

$$VSWR = \frac{1 + |\Gamma|}{1 - |\Gamma|}.$$

It can also be expressed as a ratio of the maximum voltage amplitude to the minimum voltage amplitude. In practice,  $1 \leq VSWR \leq \infty$  with a perfectly matched antenna having a  $VSWR = 1$ ; however, a  $VSWR$  of 2 is sufficient for most applications and this corresponds to a return loss of approximately  $-9.54$  dB. This represents approximately an 89% power throughput for the antenna. This value constitutes an

acceptable operational specification which will be used in the thesis. Return loss performance above the  $-9.54$  dB level will be judged to be unsatisfactory for operation.

### 2.2.8 Bandwidth and Q-factor

Bandwidth refers to the range of frequencies within which the performance of the antenna, with respect to some characteristics will conform to a specified standard [13]. Quantifying the frequency bandwidth for an antenna depends on the nature of that antenna. If an antenna is broadband, then its bandwidth is referred to as a ratio of its higher acceptable operating frequency to its acceptable lower operating frequency. In the case of a narrowband antenna, the bandwidth is expressed as a percentage. It is calculated by the difference in higher and lower operating frequencies divided by the antenna's resonant frequency within that band,

$$B = \frac{\Delta f}{f_r}. \quad (2.2)$$

The resonant frequency,  $f_r$ , of an antenna is defined as a frequency at which the input impedance of an antenna is nonreactive [13] and  $\Delta f = f_2 - f_1$  is the range in frequencies for which a certain return loss level is achieved. Usually, the value of bandwidth is specified at a given value of return loss or VSWR. For example, a certain antenna may have a 1% bandwidth at  $-10$  dB.

The quality factor or  $Q$ -factor, is another parameter of interest used to describe antennas performance. It is representative of an antenna's losses [11]. A larger  $Q$ -

factor is indicative of narrower bandwidth and lower efficiency. In its general form it is defined by

$$\frac{1}{Q_t} = \frac{1}{Q_{rad}} + \frac{1}{Q_c} + \frac{1}{Q_d} + \frac{1}{Q_{sw}}$$

where

$Q_t$  is the total quality factor,

$Q_{rad}$  is the quality factor due to radiation (space wave) losses,

$Q_c$  is the quality factor due to conduction (ohmic) losses,

$Q_d$  is the quality factor due to dielectric losses,

$Q_{sw}$  is the quality factor due to surface waves.

In practice, the quality factor is determined from actual experimental measurements. The analytical derivation of this value can be tedious [15]. However, there are simpler definitions in order to compute  $Q_t$  as mentioned in [6] and [11]. Formulae used to calculate  $Q_t$  are

$$Q_t = \frac{f_r}{f_\beta - f_\alpha} \quad (2.3)$$

and a slightly refined

$$\frac{f_r}{f_\beta - f_\alpha} = \frac{VSWR - 1}{Q_t \sqrt{VSWR}}$$

which takes into account impedance matching at the input terminals of the antenna. Similar to equation (2.2), the parameter  $Q_t$  is defined in terms of some frequency

band  $\Delta f = f_\beta - f_\alpha$ . In this situation,  $\Delta f$  is taken as the band over which the power reflected is not more than one-fifth ( $\sim -7$  dB) of that absorbed at resonance when matched to the feed line [6]. The definition of  $Q_t$  given by equation (2.3) will be employed in this work.

# Chapter 3

## Literature Review

### 3.1 General

A basic MPA, in a physical sense, is simply a printed circuit board (PCB). What makes a printed circuit into an actual MPA is its ability to radiate energy in a manner suitable to an antenna engineer and the end user. All printed circuits emit energy, but when this energy is being utilized for electronic signal transmission the PCB can be qualified as an MPA. The Institute of Electrical and Electronics Engineers (IEEE) defines an MPA as an antenna which consists of a thin metallic conductor bonded to a thin grounded dielectric substrate [13]. The radiation behaviour of an MPA is unstable and it is highly sensitive to changes in the dielectric substrate, the patch element and the feed line. Depicted in Figure 3-1 is an illustration of an MPA in its basic form.

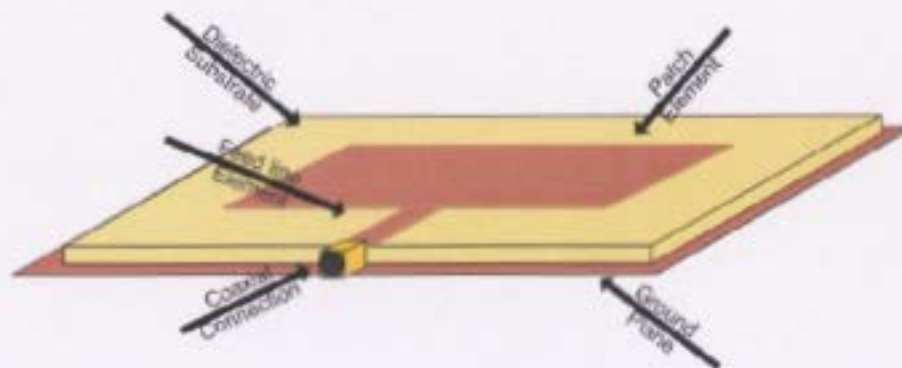


Figure 3-1: General construction of a rectangular MPA with coplanar microstrip feedline.

Progress in research has resulted in contemporary MPAs having notable variation in structure. The basic design components do not change except for the layering complexity and element placement changes. Zurcher and Gardiol [9] describe a semi-inverted orientation in which the patch is separated from the feed by a dielectric layer and the patch itself is on the underside of the top most dielectric layer known as the Strip-Slot-Foam-Inverted Patch antenna or SSFIP design. Employing multiple layers is a common technique which allows for multiple frequency operations. Many researchers have examined this stacking technique in detail [16], [17].

For the purposes of this work, a single layer design and a static dielectric substrate will be considered. However, despite the fact that the material itself is a known quantity, some slight variability in its physical properties is expected once the fabrication process is engaged. So in this context, the MPA can be separated into two fundamental elements: the radiating or patch element and the feed line element. Although both will be treated separately in the following discussion, it is important to appre-

ciate the interplay between these two elements in a finished design and their coupled contribution to an MPA's overall behaviour. IEEE formally states the feed line is a transmission line interconnecting an antenna and a transmitter or receiver or both [13]. However, references to the feed line element contained herein consider only the printed component of the transmission line, i.e., that portion of the antenna that is fabricated at the same time as the patch. A 50 ohm coaxial cable will connect the fabricated MPA to the transmitter and technically it is the coaxial cable and the printed feed line element which composes the true feed line as per IEEE standards.

A list of the generally accepted strengths and weaknesses of MPA technology is found in Table 3.1. The list is not exhaustive, but captures the noteworthy characteristics of MPAs. This Table originates in [16]. The authors of that work also list conventional applications associated with MPA use in Table 3.2. MPA technology has been extensively developed since the writing of [16] in 1989. In particular, the problems of small bandwidth and polarization purity are very active areas of research as will be discussed shortly. Techniques to address the polarization purity by patch geometrical and topological manipulation and feed placement have been refined. As well, bandwidth has been increased using different feed methods and modifying patch configurations.

<b>Advantages</b>	<b>Disadvantages</b>
Thin profile	Low efficiency
Light weight	Small bandwidth
Simple to manufacture	Extraneous radiation from feeds, junctions and surface waves
Can be made conformal	Tolerance problems
Can be integrated with circuits	High-performance arrays require complex feed systems
Simple arrays readily created	Polarization purity difficult to achieve

Table 3.1: MPA characteristics

<b>Applications</b>	
Aircraft antennas	Communication and navigation Altimeters Blind-landing systems
Missiles and telemetry	Stick-on sensors Proximity fuses Millimetre devices
Missile guidance	Seeker monopulse arrays Integral radome arrays
Adaptive arrays	Multi-target acquisition Semiconductor integrated array
Battlefield communications and surveillance	Flush mounted on vehicles
SATCOMS	Domestic direct broadcast satellite receiver Vehicle-based array Switched-beam array
Mobile radio	Hand telephones and pagers Manpack systems
Reflector feeds	Beam switching
Remote sensing	Large lightweight apertures
Biomedical	Applications in microwave cancer therapy
Covert antennas	Intruder alarms Personal communication

Table 3.2: General MPA applications

## 3.2 Patch element

The antenna element, radiating element or patch resonator (these terms are used interchangeably) is typically a simple geometric pattern etched onto the surface of the dielectric substrate over a ground plane. In general, these patterns are simple shapes: rectangular, square, dipole, elliptical, circular or triangular. However, it is not uncommon to find instances of more complex geometries developed in order to deal with narrow bandwidth or to modify other MPA parameters.

The rectangular and circular shaped patch resonators tend to be the most widely used in literature, the former probably being the most popular. The very early works of Munson [18] and Howell [3] utilize a rectangular patch. Munson applies both a tapered microstrip line feed network and a quarter-wave transformer parallel feed network, whereas, Howell's method differs significantly by using a relatively simple matched feed line.

The likely attraction of the rectangular shape is that its basic geometry lent itself to early attempts at modelling and serious theoretical investigation. In 1975, Derneryd [19] described the basic rectangular patch with a simple microstrip feed line configuration similar to Figure 3-1. He proposed an equivalent circuit network topology for bandwidth calculations and reported on limited experimental findings. Several years later in a subsequent work, he undertook a more extensive examination of the rectangular patch antenna element [20]. Derneryd's study included the radiation patterns, input impedance, mutual conductance and directivity from an

analytical perspective. Shortly thereafter, Lo *et al* [21] proposed a theory based on cavity modelling and positively tested the theory against experimental results. This work with the cavity model has been acknowledged as the first theoretical solution to include the electromagnetics of the MPA [22]. It also included many canonical forms beyond rectangular including circular, elliptical, annular, triangular and wedge shaped.

One of the running themes of MPA research is polarization purity. The novelty of MPAs is their ability to transmit or receive circularly polarized waves with only a simple single feed point and no need of an external polariser. Figure 3-2 includes some of the techniques that have been applied to rectangular patches in order to optimize circular polarization [22]. It has been shown that slight geometric manipulations and physical modifications result in improved circular polarization, alter resonant frequency and offer some control over other antenna parameters.

Cutting corners as a method to improve circular polarization was first studied by Kerr [23] in 1978 and has since been explored by others including [24]-[26]. The works [24], [25], also study the effect of varying probe placement. Several other authors treat this subject in detail [27], [28].

It has been reported in [22] that the introduction of shorting posts to affect antenna parameters was inspired by the work of Kerr. Several papers appeared at the end of the 1970's and early 1980's dealing with this subject [29]-[31] and the topic has been covered very recently in [32].

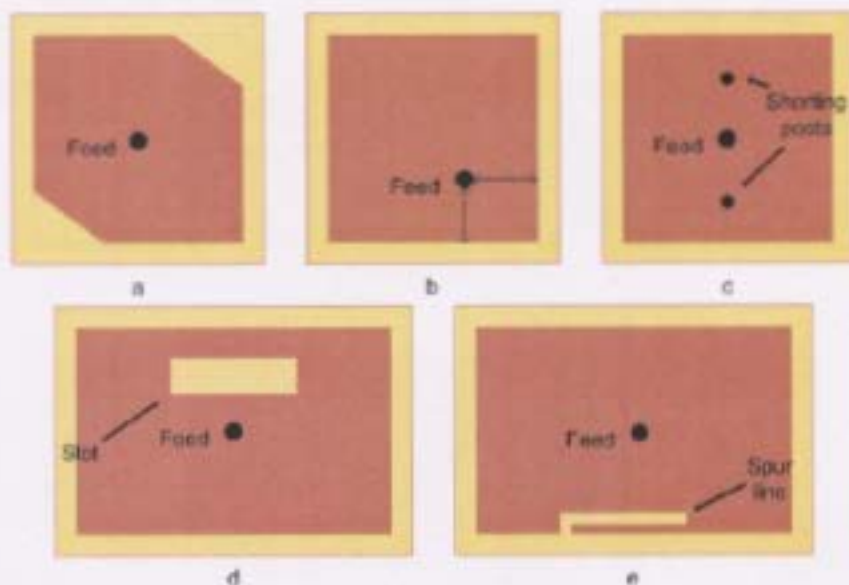


Figure 3-2: Five simple known methods to affect circular polarization of probe fed rectangular resonators: (a) cutting corners, (b) probe placement, (c) shorting posts, (d) slots, and (e) spur lines.

Introduction of slots in the MPA, another original Kerr technique according to [22], appeared in 1977 in [23], [33]. This particular method has been quite popular in the literature since its inception. Patch resonator slotting has become a popular design tactic to manipulate MPA properties. It is a continuing theme in MPA research which has been studied in various contexts. Slotted rectangular MPAs are examined in [34], [35] and an U-shaped slot is applied in [36]-[38]. The effect of slotting has also been explored in relation to circular [39], triangular [40] and octagonal [41], [42] patch elements. One could consider the square shaped ring of [26] and the annular rings of [43]-[45] as slotted. The slotting concept has been extended recently. In 2004, a rectangular MPA was designed with reconfigurable slots [46] and a year later ground plane slotting and its effect on polarization was explored for several regular



Figure 3-3: Compact Yagi-Uda MPA array. Notice the half-ground plane and etched reflector segment on the underside of the dielectric substrate.

geometries in 2005 [47]. Spur lines, that is, slotting connected to the perimeter of the patch element, has been inspected in rectangular patches [35] and in triangular patches [48].

Thus far, several basic patch shapes have been discussed. Several other interesting patterns have been analyzed in the literature including an H-shaped resonator [49], an U-shaped antenna [50], an asymmetrical double-T configuration [51], and a MPA with a resonator the shape of a bowtie [52]. However, the actual number of possible patch geometries is limitless. This is shown by the design work in [53] using genetic algorithms and mentioned briefly in the survey work [54]. Figure 3-3 is a non-standard MPA configuration which illustrates the versatility of printed antenna development and the ability to realize complex three dimensional antennas in planar form.

### 3.3 Feeding techniques

Generally, most of the works mentioned in the previous section are probe fed. That is, a coaxial cable is employed to connect the patch to the transmission device. There are only a few distinct of ways to feed the patch with energy. Several will be discussed

here in some detail. Differing techniques have distinct advantages which range in ease of design fabrication and ease of modelling to significant reduction in coupling with the radiating element.

### **3.3.1 Direct probe coupling**

The traditional feed method involves coaxial feed or probe coupling [7]. A recent and simple illustration of the coaxially fed MPA is described in [56] and can be seen in Figure 3-4. This method employs the centre conductor of a coaxial line to transfer the power directly to the patch while the outer conductor is connected to the ground plane. As has already been discussed, placement of the coaxial connection influences the impedance match and mode excitation. The ability to control impedance levels by manipulating feed placement is an attractive feature of this feed technique. However, one shortcoming of this type of feed is that the connection requires a solder joint. Hence an array with a large number of elements fed in this way will be rather tedious to fabricate and a high number of joints of this nature may compromise the integrity and reliability of the array. Also, probe coupling results in narrow bandwidth and can be difficult to model, specifically for thicker substrates [11].

Some authors have experimented with probe coupling by generalizing to a higher number of probes. In [57], an array of sequentially rotated feed positions is described to control the polarization purity. Dual banding using stacked multi probe fed elements is examined in recent works [58], [59]. An L-shaped direct probe has been used

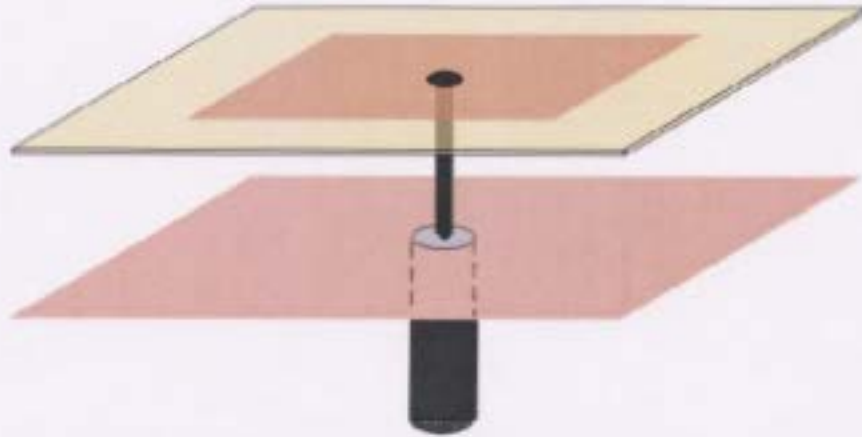


Figure 3-4: Layered view of a probe or coaxial coupled MPA. (Note that the centre conductor is lengthened in the illustration to show its connectivity to the patch element.)



Figure 3-5: Cross-section of a basic L-probe fed MPA. Note that different dielectric substrates may make up the two parallel layers.

in [50]. A cross-section of an L-probed MPA is depicted in Figure 3-5.

### 3.3.2 Coplanar microstrip coupling

The coplanar microstrip feed line is etched upon the same side of the dielectric substrate along with the radiating element (see Figure 3-6). It can be thought of as an extension of the radiating element and was the other early MPA feed method used in mid 70's [19]. The distinct advantage presented by this feed technique is its



Figure 3-6: Typical coplanar microstrip feedline.

ease of manufacturability, but drawbacks include bandwidth/feed radiation trade-offs and excitation of higher order modes which leads to cross-polarization [7]. It can be printed on a substrate at the same time as the antenna element and therefore has a higher reliability over a direct probe, especially in large arrays. However, a disadvantage of this type of feed is the amount of coupling between the feed line and the patch. Moreover, this type of feed lends itself to narrower bandwidth antennas which may or may not be desirable in all cases.

Generally, the microstrip feed line is the basic building block of MPA feeds, likely due to the ease of its fabrication. Manipulation of its basic coplanar form has been investigated using several approaches. Insetting the feed by notching the patch has been discussed in [7], [46] and modifying the feed orientation examined in [60]-[62]. Several of the latter authors have also explored altering the geometry of the feed line by introducing open circuited stubs and modifying segment widths as a means to affect impedance. Matching techniques have been analyzed extensively in many works including [10], [17], [52], [61]-[64].

The previous transformations to the coplanar feed line were purely geometrical. In recent works, several researchers have introduced topological changes to the feed

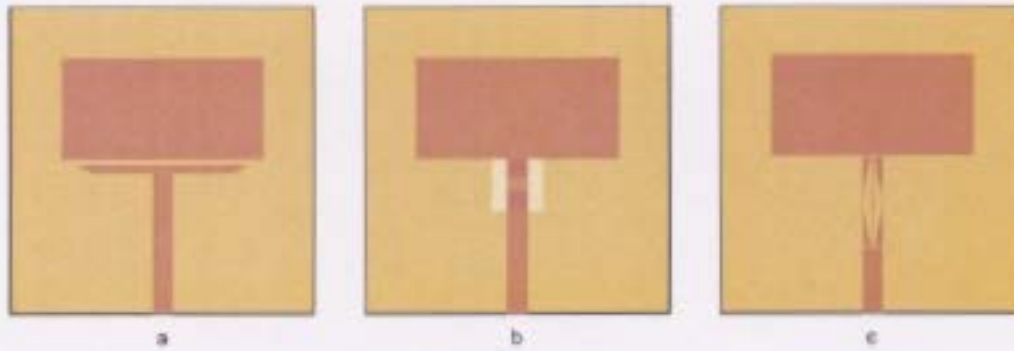


Figure 3-7: Current modifications to microstrip feedlines (a) gap coupled T feed, (b) defected ground structure (H-slotted ground plane), and (c) compact microstrip resonant cell structure.

line, that is, the feed line is punctured or discontinuities are introduced. In [65] the authors present a dual feed capacitive or gap coupled coplanar feed line. While in the contemporary works [66], [67], special cases of photonic bandgap structures are studied. Examples of different arrangements are shown in Figure 3-7.

### 3.3.3 Electromagnetic proximity coupling

The feed technique of electromagnetic coupling employs a feed line stub etched into a substrate over ground, but situated below a substrate to which a patch element is etched. An illustration of the basic design is in Figure 3-8. Its original manifestation was developed in the context of printed dipoles in [68], [69]. Benefits of proximity coupling are that the upper substrate can be relatively thick thereby improving bandwidth while the feed line can be on a thinner substrate which reduces spurious radiation and coupling [7]. Although there are no solder joints to be assembled, there

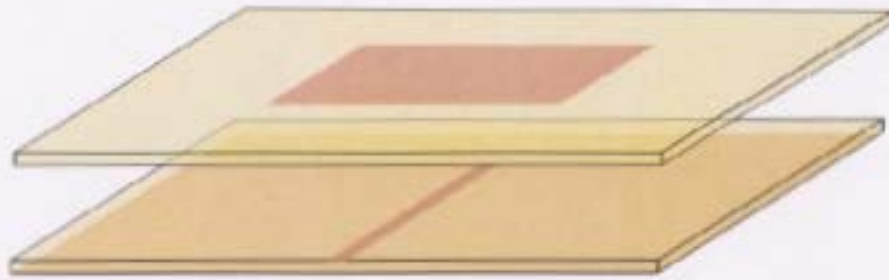


Figure 3-8: Layered view of a proximity coupled MPA. The feedline is printed on a grounded substrate layer, there is no ground plane on the upper dielectric substrate layer.

can be difficulties achieving the proper alignment of the patch over the feed line stub. Hence fabrication can be slightly more challenging compared to the simple coplanar microstrip feed.

Straightforward illustrations of the proximity coupling methods using a straight segment feed line stub are found in [7], [70]-[72]. A split, segmented semi-circular type line called a symmetric dual-stub is designed in [73]. Examples of slightly differing configurations employing proximity coupling have been developed. A double-II feed line is used to couple with a U-slotted antenna. The patch in this instance is printed on the underside of the upper substrate and the feed line is separated by an air gap with variation in this distance being shown to affect the impedance bandwidth of the device. The author in [26] uses proximity feed to couple orthogonal sides of a square ring slot antenna. These variations on the proximity coupled construction are depicted in Figure 3-9.

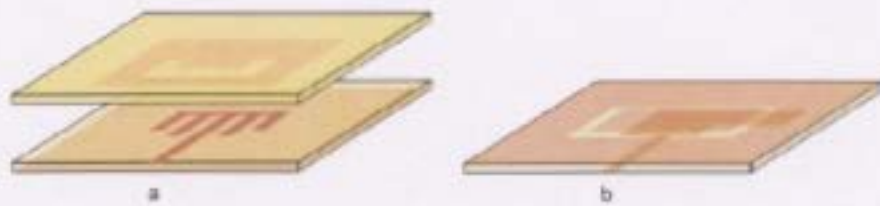


Figure 3-9: Unconventional proximity coupling configurations: (a) double- $\Pi$  stub proximity feed U-slot patch and (b) single layer proximity feed square ring slot antenna. (Note that design (a) is as it appears and not separated into layers for illustrative purposes.)



Figure 3-10: Layered view of apercutre coupled feed MPA.

### 3.3.4 Aperture coupling

Aperture or slot coupling closely resembles proximity coupling. The difference between the aperture-coupled and the electromagnetically coupled (proximity) microstrip feeds is that the bottom plane is inverted and an aperture or slot is cut in the ground plane to facilitate the energy transfer between the feed line and the radiating element.

Figure 3-10 illustrates an aperture coupled RMPA with a rectangular slot.

The substrate arrangement of the slot coupled design closely mirrors that of a proximity coupled MPA design. Typically a thin, high-dielectric-constant substrate

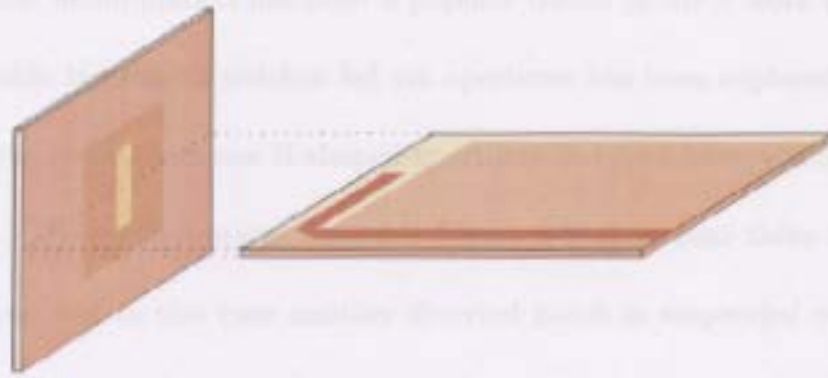


Figure 3-11: Aperture coupled MPA proposed by Pozar in 1992.

is used for the feed line and a thicker, lower dielectric substrate is employed beneath the patch element. A generally smaller aperture when compared to the resonant patch dimensions inhibits feed line spurious radiation interference with the antenna's radiation pattern and polarization purity. The aperture coupling technique was first studied in the mid 1980's in [74]-[76]. In [77], Pozar employs a circular slot as well as an unconventional configuration that has the feed line substrate perpendicular to the patch-aperture substrate as shown in Figure 3-11.

The aperture coupling design has since been modified using cross slotting and feed lines which are not oriented orthogonal to the slot in several works including [78]-[81]. Innovations in aperture coupled MPAs have been realized in multiple works. Improvements range from modifying the aperture shape to a dog bone [82] to introducing relatively simple dual feed techniques using parallel feed line segments as in [83]. Slight modifications of the feed lines have been explored using impedance matching and Wilkinson power dividers in [84]. Dual feeds of more intricate design and aper-

ture geometric manipulation has been a popular theme in MPA work since 2000. A dual-fed double layering of patches fed via apertures has been explored in [85], [86]. In these works the authors use H-shaped apertures and feed lines which terminate in a  $90^\circ$  bend. The configurations resemble Figure 3-9(a) in that there is the typical aperture layer, but in this case another inverted patch is suspended over the lower aperture fed radiator. This technique is loosely known as the strip-slot-foam-inverted patch or SSFIP principle and is covered in detail in [9]. The authors of [87] extend the SSFIP technique using a single feed aperture, but place another layer below the feed line segment with a ground reflector. A more simple design using orthogonally oriented dual feed line segments and modified H-shaped coupling slots is presented in [88]. However, in their design the authors do not employ an upper dielectric substrate layer, but rather suspend a circular patch over the apertures creating an air gap or superstrate. An appreciably more complicated two port feed line is designed in [89]. This architecture has four H-shaped fed apertures and the resonating patch element is a modified square ring slotted antenna with an air gap between the ground (aperture) layer and the patch dielectric substrate.

Also worth mentioning in this section are a series of hybrid fed MPAs. Such works bear mentioning because each involves an aperture coupling to feed the MPA. In a 2002 work, a suspended circular radiating patch is fed directly with a feed line-conducting post combination and via an H-shaped aperture [90]. Various configurations using a Wilkinson power divider (single port), two ports and an array

are compared. A coplanar microstrip and dual H-aperture fed patch appear in [86]. The design has additional layers. The patch-ground-feed layers are inserted between a foam-shielding layer and foam-inverted patch layer. Lastly, Lau and Luk [91] combine an L-probe with an aperture couple in order to drive an air gapped square resonator. The design is singly fed, but uses a Wilkinson power divider beneath a circular ground plane with a simple slot segment. Each of these three works employ hybrid feeding methods to broadband the MPA and optimize its dual polarization.

### **3.3.5 Coplanar waveguide**

The final type of MPA feed to be discussed is the coplanar waveguide (CPW) feed line in Figure 3-12. The CPW feed method is similar to an aperture-coupled feed line except the feed line (the coplanar waveguide) is etched into the ground-aperture layer, that is, the CPW and aperture are coplanar. This feed line technique is preferred in certain applications such as microwave monolithic integrated circuits [15]. The waveguide feed also reduces the amount of spurious radiation compared to other methods; however, proper alignment of the waveguide and patch is a challenge and there are no significant gains in bandwidth compared to the simple coplanar feed line. In the basic design, there is only one dielectric substrate and the CPW and aperture are etched into the ground plane opposite the patch element. This single substrate construction is attractive in terms of its stability and design simplicity, although it is not uncommon to find examples in which the aperture is printed on a separate layer

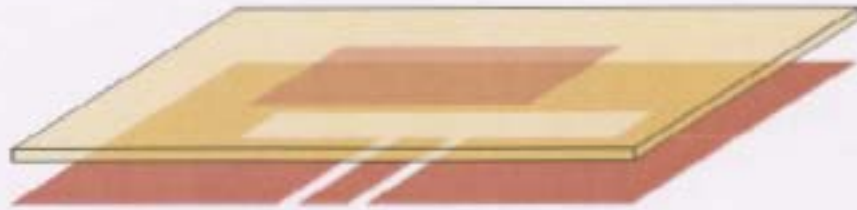


Figure 3-12: Layered view of coplanar waveguide feed MPA.

as the CPW feed line.

The CPW type feed in any manifestation does not have the history of its counterpart feed line methods. The 1992 work [92] contends that there is only one paper in the literature which treats the subject. This contention would place the birth of the CPW in Greisler [93] in 1976. Moreover, these authors attempt to address why there has been a deficit of research into the theory and design of CPW fed MPAs. In [92], the authors actually fabricate a CPW fed MPA using stationary store foam board  $\epsilon_r = 1.06$  as a substrate (which is comparable to air), some copper tape and a sharp knife. Notable progress in CPW research has since taken place. Theoretical analysis of CPW feed lines roughly agrees with the timeline suggested by the aforementioned paper in 1991 [94] and in 1995 this work was extended [95].

Another article appeared in 1992 which describes different types of CPW feed lines in multi substrate layered designs [96]. A grounded CPW, a finite ground CPW and a channelized CPW are fabricated and evaluated. The CPW feeds a rectangular patch via a simple slot aperture in this two-substrate design. These differing design types are in Figure 3-13.



Figure 3-13: Different types of CPW feeds: (a) GCPW, (b) FCPW and (c) CCPW. Note the black segments in (c) represent metallic strips mounted on the edge of the substrate and extending to the ground plane (on reverse).

There can also be slight differences in the termination of a CPW feed. The single dielectric substrate configuration of a CPW can couple with the patch capacitively or inductively. The differences between these two different forms have been studied in [97], [98] and are pictured in Figure 3-14.

Naturally, advancements applied to other feed techniques in the late 1970s and 1980s were applied to CPW fed MPAs. For example, stacking a parasitic element on top of a single layer, inductive CPW with a dog bone slot is studied in [99] and the stacked parasitic element with a capacitive CPW feed is examined in [100]. In [101] the authors study a capacitive CPW feed with stubs that are not perpendicular to the parallel slot lines of the CPW feed line. In an earlier work, Lee and Simons [102] introduce a series gap and tuning stubs in the midsection of the CPW centre conductor. A regular rectangular aperture couple is used in this two-layer substrate design and in addition, they explore widening the distance between the CPW slot lines before and after the series gap. In each of these aforementioned works the

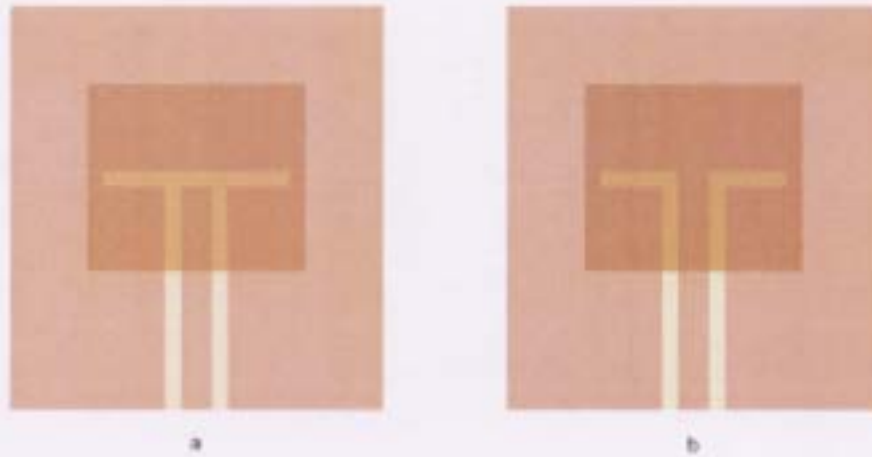


Figure 3-14: CPW fed MPAs with differing geometries: (a) capacitive coupling and (b) inductive coupling.

CPW is a grounded CPW. Another article [103] involves a single substrate layered capacitively coupled GCPW, but the patch side of the substrate has an extended ground surrounding the rectangular patch.

Innovations employing CPW feed techniques are common in the literature. There are examples of single-sided designs with no ground backing. A finite width CPW or FCPW is formed by widening the terminating end of the CPW centre strip conductor [104]. In a similar fashion, an asymmetric double-T is printed on the same side as an inductive CPW in [51]. These two single sided MPA designs are shown in Figure 3-15.

Other interesting arrangements include a CPW loop feed rectangular patch [105] in which the authors employ an extended substrate in both a single and double layer configuration, but the latter is inverted such that there is no aperture-ground plane

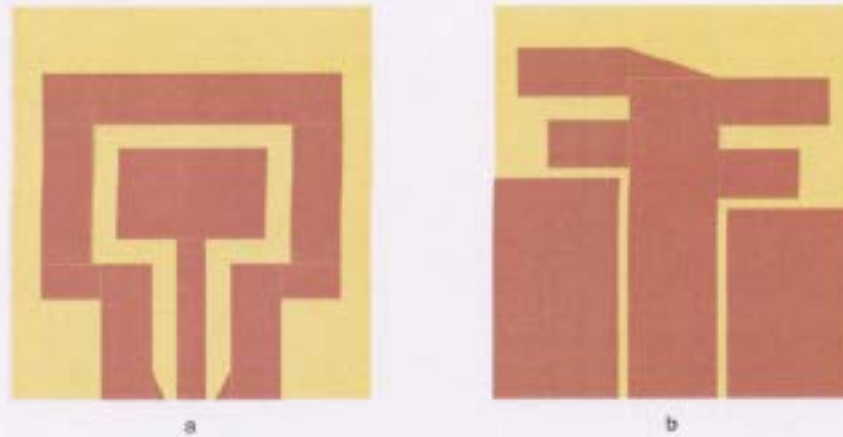


Figure 3-15: Two single substrate - same side CPW fed patch elements with no ground plane: (a) FCPW and (b) asymmetric double-T microstrip dipole.

separating the patch substrate from the extended GCPW. Iwasaki [106] uses a single GCPW sandwiched between two substrates to feed back-to-back patch elements. A non-leaky CPW fed MPA is designed in [107], by using the conventional double substrate layer aperture coupled inductive CPW fed with an additional ungrounded substrate layer inserted between the ground-aperture and the CPW feed layers.

An excellent resource describing a plethora of modern MPA designs with various patch and feed line element configurations is Wong's 2002 book [108]. The text focuses on overcoming the inherent narrow band of MPAs by implementing a host of design techniques (many of which have been highlighted here) and maintaining a compact form for the MPA device. The designs tend to involve only simple layering (at most two dielectric substrates), but focus on geometric and topological complexity to accomplish satisfactory results.

# Chapter 4

## Problem Statement and Modelling

## Methods

### 4.1 Narrow frequency bandwidth

The characteristic of generally narrow frequency bandwidth, which will be referred to bandwidth henceforth, has been a source of much investigation within the MPA community. Despite the fact that MPAs tend to resonate well at a specific frequency, they compare poorly to conventional antennas which tend to be of wider bandwidth around their resonant frequency. This characteristic can be a beneficial feature of the patch antenna. Consider a system which utilizes multiple frequencies that are close to each other such as a device with different transmit and receiving channels or a system which utilizes global positioning systems and satellite communications.

For example, the operating frequency for GPS is 1.515 GHz and for Iridium Satellite Personal Communication System is 1.610 GHz. A series of MPAs, when tuned appropriately, eliminates the need for filtering, thereby conserving resources that would normally be devoted to cleaning up communication signals and portioning and partitioning the frequency band. However, many researchers have recognized the utility of the physical and cost aspects of MPAs and have studied ways to make improvements in bandwidth.

#### **4.1.1 General methods to improve bandwidth**

Sanchez-Hernandez and Robertson [109] list several methods or techniques to improve bandwidth:

- multilayer structures
- parasitic elements coupled to the main patch
- tuning stubs and loads
- diode use
- shorting pins
- adjustable air gap between substrate and ground plane
- aperture-coupled parallel resonators and slotted patches
- specifically shaped patches

The authors conclude their survey by stating that many of the examples listed can be problematic when it comes to design and fabrication stages. Often, there are trade-offs in bandwidth improvement and/or degradation in other antenna characteristics. Also, they point out that discrepancies between simulated and measured results frequently occur because of inconsistencies and inaccuracies in the fabrication process. It is noted that the authors do not mention manipulating the feed line in order to affect the frequency bandwidth of the MPA. There are some other more complex methods suggested such as using a wedge shaped dielectric substrate or by using antennas that utilize dichroic surfaces.

Balanis [11] quantifies the narrow bandwidth at a fraction of a percent to a few percent which agrees with [77]. Other less conservative authors [110] put the bandwidth at one to five percent and [6] put it at one to four percent. However, it is important to note that in realizing gains in MPA bandwidth there are necessary concessions in performance or design complexity. In [77] the author goes so far as to mention a specific case of a 25% bandwidth improvement of a simple design which subsequently has been found to resonate in different modes at different frequencies thereby resulting in polarization changes at different operating frequencies. Some of the conventional antennas such as dipoles or Yagi-Uda arrays can achieve bandwidths on the order of approximately 10%.

In the earlier discussion, several challenges of MPA designs were highlighted including polarization purity and achieving satisfactory radiation patterns. A more

general review of the positive characteristics and challenges of MPA design can be found in [9].

### 4.1.2 Characterizing the problem

The motivation for this work is due to the narrow bandwidth of an MPA. Variability in material properties and the fabrication process can result in poor performance at a desired frequency. In the context of a larger scale MPA fabrication process, electrical property variation and/or over/etching will contribute toward an unsatisfactory number of manufactured MPA that must be rejected because of unsuitable operating frequency capability. Some preliminary computer simulated return loss results will frame the problem at hand and provide justification for the bandwidth widening approaches applied in this work. The material used to fabricate antennas is a glass-epoxy known as Flame Resistant 4 or FR-4. It is low cost, readily available and the most common substrate used for general electronics systems. The electrical properties of interest for this material are its dielectric constant,  $\epsilon_r$ , and dissipation factor or loss tangent,  $\tan \delta$ . The design process undertaken in this thesis fixes the electrical properties of FR-4 at  $\epsilon_r = 4.4$  and  $\tan \delta = 0.02$ ; however, in practice an acceptable range for  $\epsilon_r$  is 3.9 to 4.7 and for  $\tan \delta$  is 0.01 to 0.035. The result of this electrical variability as seen in Figure 4-1 are resonant pole shifts and changes in return loss levels. Figure 4-1 displays the return loss for the extremes values of the accepted range in dielectric constant and dissipation factor. Generally, a lower dielectric constant results in

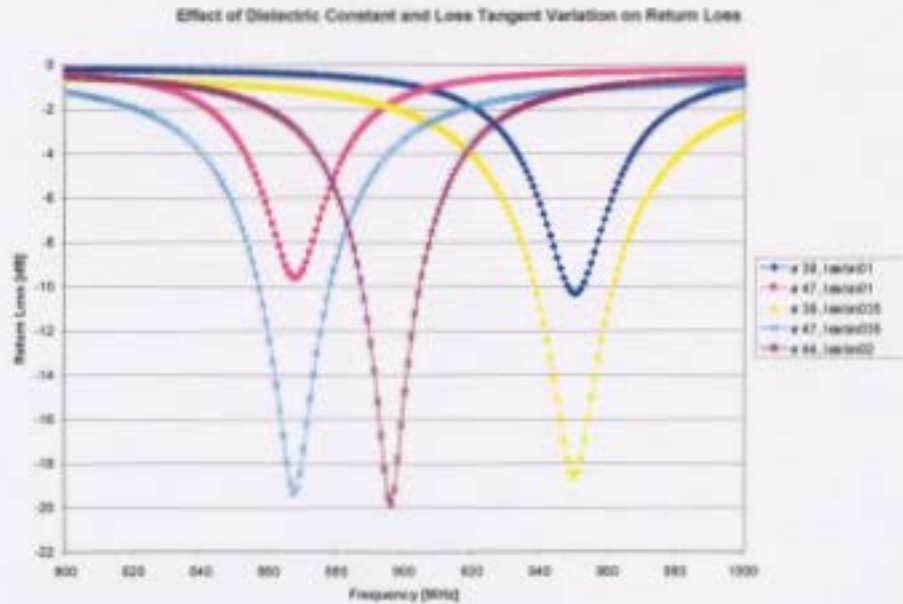


Figure 4-1: Return loss effect of dielectric constant and loss tangent variability on a 896 MHz RMPA.

a right shift or increase of the resonant frequency. A smaller loss tangent tends to cause a weakening of the resonance, that is, a higher return loss level is observed at the various resonant frequencies.

Particular points of interest from this simulation can be found in Table 4.1. According to this computer simulation result, an MPA designed to operate at 900 MHz with the ideal electrical property values ( $\epsilon_r = 4.4$  and  $\tan \delta = 0.02$ ) does not perform satisfactorily if there is significant variation in these values.

Simulation results can also be used to show the effect of over and under etching on a MPA's return loss. Over and under etching occurs when traces or patterns are made to large or small respectively by the PCB milling machine or excessive

Dielectric, Loss tan.	$f_r$ [MHz]	RL @ 900 MHz
$\epsilon_r$ 3.9, $\tan \delta$ 0.01	950	-0.90 dB
$\epsilon_r$ 4.7, $\tan \delta$ 0.01	868	-1.49 dB
$\epsilon_r$ 3.9, $\tan \delta$ 0.035	950	-2.12 dB
$\epsilon_r$ 4.7, $\tan \delta$ 0.035	867	-3.38 dB
$\epsilon_r$ 4.4, $\tan \delta$ 0.02	896	-14.81 dB

Table 4.1: Electric variation affect on return loss

exposure to acid in the fabrication process thereby removing too much copper. At lower frequencies, over/under etching effects are not as adverse on MPA return loss. This is because the wavelengths are relatively large when compared to the etching error. However, with higher frequencies (gigahertz range) where the wavelengths are on the order of millimetres and smaller, the etching errors can be quite detrimental. Figure 4-2 shows the simulated effect of under and over etching by 2 mm on the patch dimensions of an MPA (the feed line dimensions were not altered for this simulation). There is some noticeable frequency shifting resulting from the dimension variations but it is not as severe as with the electrical variability.

The method applied in the thesis concerns the implementation of two coplanar design elements into a RMPA model to increase the frequency bandwidth of the fabricated RMPA. A basic RF design methodology is utilized

- Analytical formulae employed to establish a basic working model,
- EM simulation applied for high accuracy solutions to Maxwell's Equations,
- Optimization according to specification using gradient-based search methods,
- Measurements for specification verification.

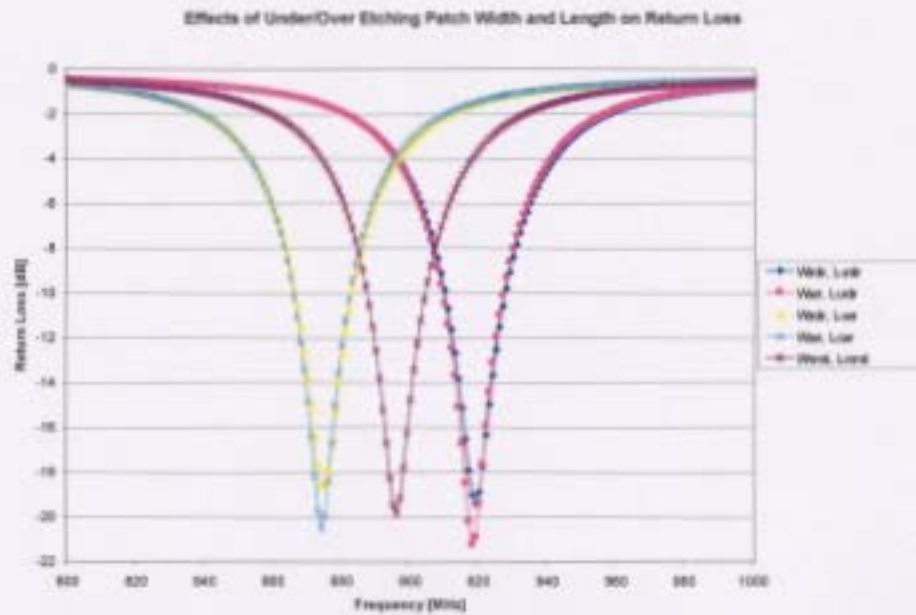


Figure 4-2: Return Loss effect of over/under etching patch width (W) and length (L) by 2 mm on a 896 MHz RMPA.

Each of the next three design chapters is concerned with the first three of the design methodologies. In chapter five, the analytical starting point is established and evaluated using simulation. Chapter six uses a predominantly optimization approach to tune the antenna to the appropriate resonant frequency. Chapter seven is comprised of both analytics and optimization in order to finalize the working MPA model for fabrication. Chapter eight contains the measurement component of the methodology.

## 4.2 Modelling

According to Howell [3], “no theory exists to predict [MPA] input impedance.” This certainly agrees chronologically with MPA research and development. However, in this very early MPA work, Howell does apply some basic analytical notions to design a square MPA. The patch dimension is calculated as

$$L = \frac{\lambda_d}{2},$$

where  $\lambda_d$  is the wavelength of the resonant frequency in the dielectric substrate. Subsequently, a design approach is described measuring the impedance of the fabricated patch at the resonant frequency and then implementing a microstrip feed line impedance matching network to transform the impedance to 50 ohms for a match with the coaxial cable. This work constitutes one of the first forays into an analytical approach for developing MPAs.

### 4.2.1 Transmission line model

The first model proposed for the analysis of MPAs was by Munson [5]. Munson used a transmission line circuit model in order to determine the impedances of various S-band parallel network fed MPAs with varying dielectric height. The transmission line model was subsequently refined by Derneryd [19], [20]. Derneryd formalizes the model by identifying a radiating element as two slots separated by a transmission line

of low characteristic impedance. Using this model, Derneyrd determines the radiation pattern, conductance, capacitance, directivity and bandwidth using the equivalent network of a microstrip radiating element. The transmission model forms the basis for the analytical formulae utilized for the design of the control MPA in Chapter Five. A general discussion relating to the transmission line model for MPAs can be found in [11], [15], [110]. This model is examined in greater detail and extended in [16].

### 4.2.2 Cavity model

The cavity model, sometimes referred to as the modal method, characterizes an MPA as a two dimensional region bounded above and below by electric conductors and bounded on the perimeter by magnetic walls. The origins of this model are in Lo *et al* [21]. The cavity model has increased complexity when compared to the transmission line and has been shown to be more accurate and versatile. The cavity model is a planar two dimensional model, whereas the transmission line model was just in one dimension. It acknowledges the radiation from all four sides of the patch, not just the two major radiating edges, resulting in a greater appreciation of the mutual coupling of radiation between edges and thereby improving results. Further reading on this subject can be found in [11], [15] and is covered extensively in [16].

### 4.2.3 Multi-port network model

The multi-port network model is an extension of the cavity model which models the electromagnetic fields above and below, and outside the patch separately. Around the periphery of the cavity or two dimensional planar network are a series of ports which correspond to incremental widths of the patch and address the field effects on these incremental sections. The range of MPA geometries that can be modelled using this method is superior to either of the previous model types because it is possible to model many patches as an amalgam of port-connected simpler geometries. A thorough treatment of this subject can be found in [16].

### 4.2.4 Full-wave models

There are several types of modelling techniques that are based on the electric current distribution on the patch conductor and ground plane as opposed to being based on equivalent magnetic current distribution around the patch edges as is the case in the first three analytical modelling methods [110]. These former approaches are numerically oriented and utilized for higher accuracy computer simulated MPA analysis. Examples of full-wave analysis techniques include the method of moments, the finite-element method, the spectral domain technique, the finite-difference time domain method and the mixed-potential integral equation analysis. These methods of MPA modelling and analysis are covered in [15], [110]. Such modelling techniques form the backbone of the computer simulation analysis and optimization utilized in this thesis.

## Chapter 5

# Basic Rectangular MPA with Coplanar Microstrip Feed Line

The design process is conducted in several stages. The common design specifications and formula from the literature [11], [15], [56] are employed to determine the physical dimensions of a rectangular microstrip antenna. The simple microstrip fed RMPA will be designed to resonate at 900 MHz. The motivation for employing a rectangular design is that its reduced complexity leads to an easier design and fabrication process. Moreover, the addition of design elements and tuning of models via computer simulation is achievable with the resources on hand. The MPA will then be modelled and its parameters evaluated via computer simulation with actual measurements to follow in Chapter Eight. This chapter will be divided into design and simulation sections with the former section being further subdivided into two subsections detailing the ana-

lytical design calculations for the rectangular patch element and the microstrip feed line. The design techniques applied in this chapter are purely analytical. Computer simulation is used as an assessment tool for this analytical approach. The simulation results contained at the end of this chapter suggest that the analytic approach is not completely accurate.

## 5.1 Design

The analytical formulae employed for the design of the control RMPA can be found in [11], [15]. These methods are based on the transmission line and cavity models for MPAs.

### 5.1.1 Rectangular patch

The desired resonant frequency for the MPA is  $f_r = 900$  MHz. This implies a wavelength of measure

$$\lambda = \frac{c}{f_r} = \frac{2.998 \times 10^8 \text{ m/s}}{900 \times 10^6 \text{ Hz}} = 0.3331 \text{ m}, \quad (5.1)$$

where  $c$  is the speed of light in free space. As previously mentioned, the dielectric substrate that will be used is FR-4. A relative dielectric constant of  $\epsilon_r = 4.4$  is assumed with a physical thickness  $h = 1.524$  mm. The width,  $W$ , of the radiating

rectangular patch element is given by

$$W = \frac{c}{2f_r} \sqrt{\frac{2}{\epsilon_r + 1}} \quad (5.2)$$

and for the particular  $f_r$  and  $\epsilon_r$  here,  $W = 10.14$  cm.

The effective dielectric constant,  $\epsilon_{re}$ , is the dielectric value of the substrate when being driven at a given frequency. It is a function of both the physical thickness of the substrate and the frequency of operation and takes the form

$$\epsilon_{re} = \frac{\epsilon_r + 1}{2} + \frac{\epsilon_r - 1}{2} \left( 1 + 12 \frac{h}{W} \right)^{-\frac{1}{2}}. \quad (5.3)$$

Here,  $\epsilon_{re} = 4.265$ .

The patch has an effective or electrical length which is longer than its physical length. The difference between the two,  $\Delta L$ , is due to the electrical field propagating between the patch and the ground layers beyond the physical edges of the patch as shown in Figure 5-1. It is possible to calculate the difference via the following equation

$$\frac{\Delta L}{h} = \frac{\xi_1 \xi_3 \xi_5}{\xi_4} \quad (5.4)$$

where

$$\xi_1 = (0.434907) \left( \frac{\epsilon_{re}^{0.81} + 0.26}{\epsilon_{re}^{0.81} - 0.189} \right) \left( \frac{\left(\frac{W}{h}\right)^{0.8544} + 0.236}{\left(\frac{W}{h}\right)^{0.8544} + 0.87} \right), \quad (5.5)$$

$$\xi_2 = 1 + \frac{\left(\frac{W}{h}\right)^{0.371}}{2.358\epsilon_r + 1}, \quad (5.6)$$

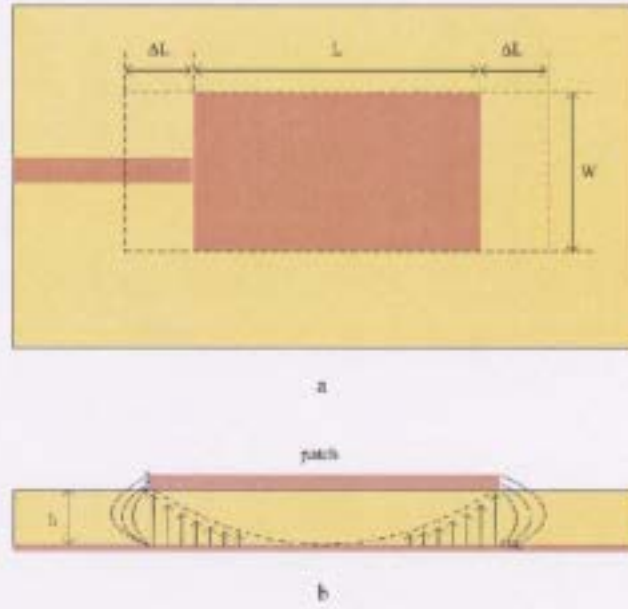


Figure 5-1: (a) Physical and electrical lengths of MPA from top view. (b) Electric field lines in MPA cross section.

$$\xi_3 = 1 + \frac{0.5274 \arctan \left[ 0.084 \left( \frac{W}{h} \right)^{\frac{1.0413}{\epsilon_r}} \right]}{\epsilon_{re}^{0.9236}}, \quad (5.7)$$

$$\xi_4 = 1 + 0.0377 \arctan \left[ 0.067 \left( \frac{W}{h} \right)^{1.456} \right] \times \{ 6 - 5e^{[0.036(1-\epsilon_r)]} \}, \quad (5.8)$$

$$\xi_5 = 1 - 0.218e^{(-7.5 \frac{W}{h})}. \quad (5.9)$$

It has been verified in [15] that the above equations yield an accuracy of at least 0.2% when  $0.01 \leq \frac{W}{h} \leq 100$  and  $\epsilon_r \leq 128$ . Note that for the proposed MPA design the width-to-height ratio is 66.54 and  $\epsilon_r = 4.4$ ; hence the above formulae can be applied in this context. equations (5.5) to (5.9) are evaluated to give  $\xi_1 = 0.4904$ ,  $\xi_3 = 1.2118$ ,  $\xi_4 = 1.0914$  and  $\xi_5 = 1$ . Substituting this data and  $h = 1.524 \times 10^{-3}$  m in equation (5.4) gives  $\Delta L = 8.298 \times 10^{-4}$  m. It is now possible to determine the physical

length of the rectangular patch element via

$$L = \frac{c}{2f_r\sqrt{\epsilon_{re}}} - 2\Delta L = 7.899 \text{ cm.}$$

### 5.1.2 Microstrip feed line

The feed line will be centred on the edge of the patch as shown in Figure 5-1 (a). It is necessary to match the line to a  $50\Omega$  coaxial connection. There are many microstrip impedance calculators available on the World Wide Web; however, the method found in [14] will be used to determine the length and width of the feed line. The width to height ratio is given by

$$\frac{w}{h} = \begin{cases} \frac{8e^A}{e^{2A}-2}, & \text{for } \frac{w}{h} \leq 2 \\ \frac{2}{\pi} \left\{ B - 1 - \ln(2B - 1) + \frac{\epsilon_r - 1}{2\epsilon_r} \left[ \ln(B - 1) + 0.39 - \frac{0.61}{\epsilon_r} \right] \right\}, & \text{for } \frac{w}{h} > 2 \end{cases}, \quad (5.10)$$

where

$$\begin{aligned} A &= \frac{Z_0}{60} \sqrt{\frac{\epsilon_r + 1}{2}} + \frac{\epsilon_r - 1}{\epsilon_r + 1} \left( 0.23 + \frac{0.11}{\epsilon_r} \right), \\ B &= \frac{377\pi}{2Z_0\sqrt{\epsilon_r}}. \end{aligned} \quad (5.11)$$

Assuming that  $w \leq 3.048$  mm, substitution of  $A = 1.530$  from equation (5.11) into equation (5.10) gives  $w = 2.914$  mm.

In order to determine the physical length,  $\ell$ , of the feed line it is noted that the

phase shift equals the product of the propagation constant,  $\beta$ , and  $\ell$ , where

$$\beta = \sqrt{\epsilon_{re}}k_0 \quad (5.12)$$

and  $k_0$  is the wave number given by

$$k_0 = \frac{2\pi f_r}{c}. \quad (5.13)$$

For  $\phi = 90^\circ = \beta\ell$  and from equations (5.12) and (5.13) it follows that

$$\ell = 90^\circ \left( \frac{\pi}{180^\circ} \right) \frac{c}{2\pi f_r \sqrt{\epsilon_{re}}},$$

and here  $\ell = 4.563$  cm. The MPA model is now complete and pictured in Figure 5-2.

## 5.2 Simulation

Computer simulation of the model is done with the Ansoft Designer Version 3.5.0 Suite [111]. It utilizes the method of moments approach in order to determine performance parameters of the modelled antenna [112]. Simulated results of pertinent parameters will be presented in this section and a compilation of additionally generated results is contained in the Appendices.

The model resulting directly from the design equations of the previous section is captured in Figure 5-3. Graphical results for certain antenna parameters from the

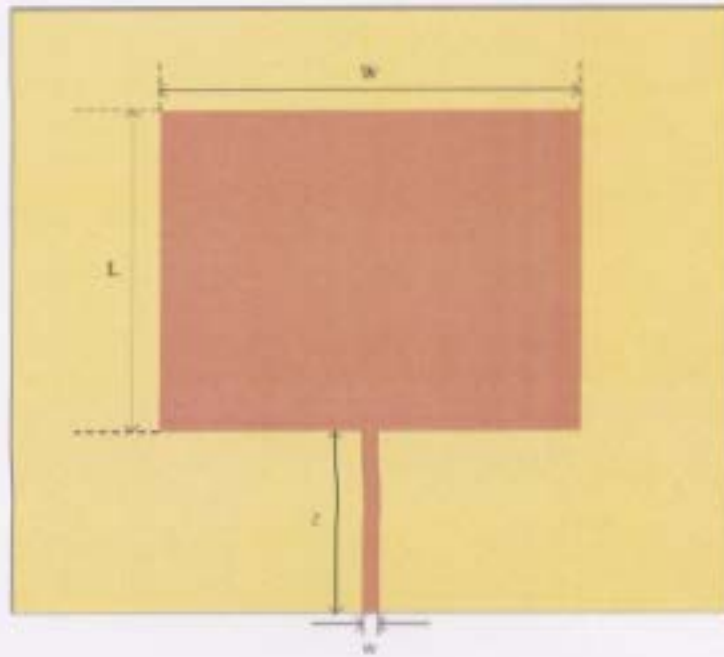


Figure 5-2: Rectangular MPA with single centred microstrip feedline:  $W = 10.14$  cm,  $L = 7.899$  cm,  $w = 2.914$  mm and  $l = 4.563$  cm.

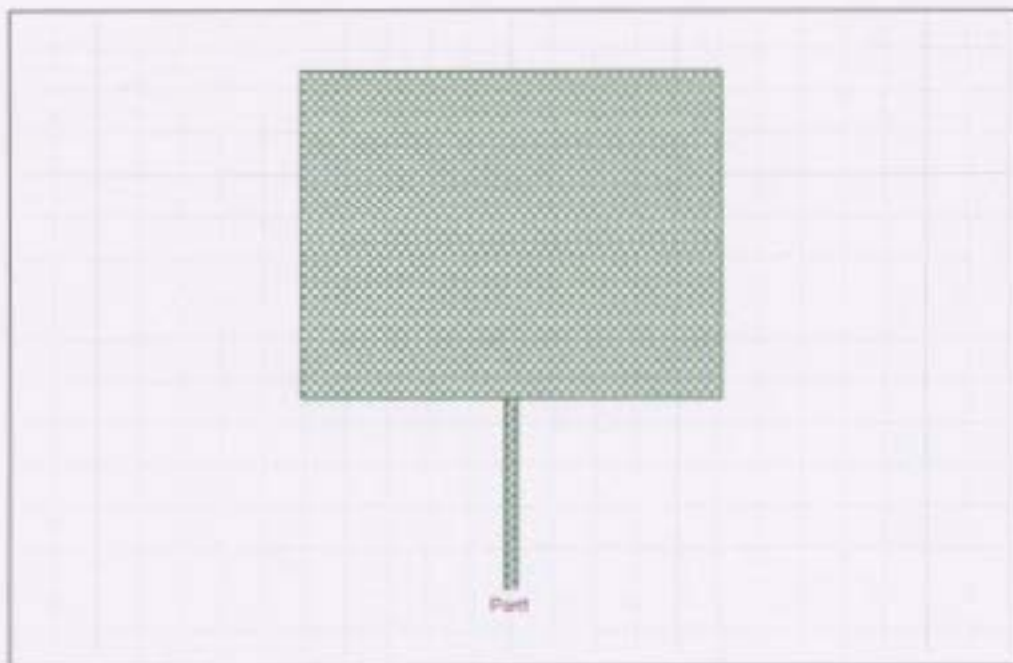


Figure 5-3: Untuned RMPA computer model designed to resonate at 900 MHz.

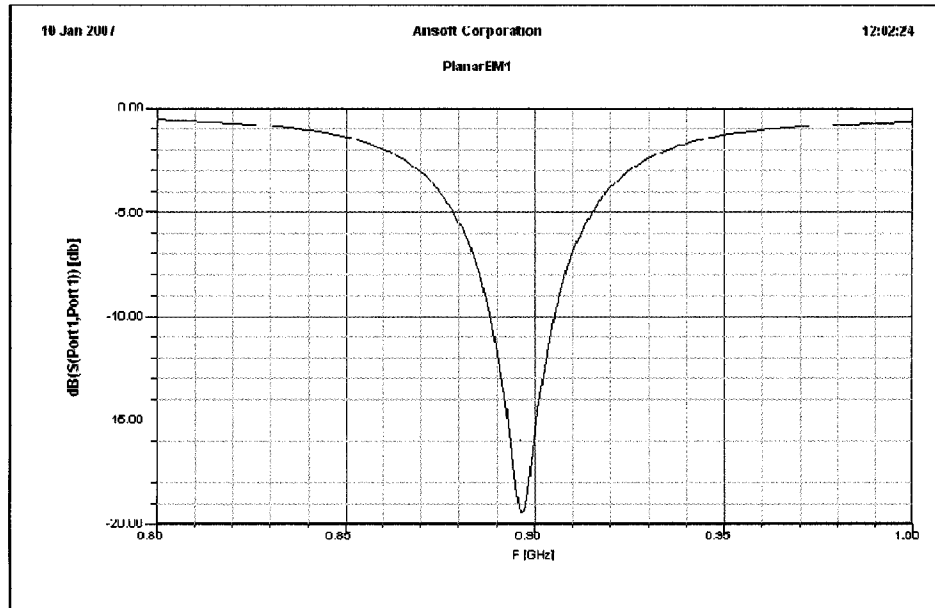


Figure 5-4: Control RMPA: Return loss plot versus frequency (GHz).

simulation are given in Figures 5-4 to 5-7. According to the simulated return loss plot, the control antenna does not resonate at precisely 900 MHz, but rather at a slightly lower frequency of 896 MHz. Moreover, Figure 5-4 also shows that the return loss level is slightly above the -20 dB level. This is confirmed by the results contained in Table 5.1.

It is possible to determine the bandwidth from simulated return loss Table 5.1. It is necessary to determine the frequencies for either side of the band at the -10 dB level. Let  $f_L$  be the lower frequency of the band at -10 dB and  $f_U$  be the higher frequency. In order to determine  $f_L$  we first determine the parameters for the linear

Frequency [MHz]	S(Port1,Port1) [dB]
883	-6.740778
884	-7.248796
885	-7.811885
886	-8.438017
887	-9.136708
888	-9.919338
889	-10.799427
890	-11.792638
891	-12.915769
892	-14.182736
893	-15.591932
894	-17.091023
895	-18.496745
896	-19.404393
897	-19.363983
898	-18.403061
899	-16.987846
900	-15.503470
901	-14.117023
902	-12.873818
903	-11.773076
904	-10.800253
905	-9.938513
906	-9.172337
907	-8.488383
908	-7.875443
909	-7.324154
910	-6.826678

Table 5.1: Simulated return loss for control RMPA

regression line in slope-y intercept form

$$m_L = \frac{(-9.919338) - (-10.799427)}{888 - 889} = -.880089,$$

$$b_L = -9.919338 - (-.880089)(888) = 771.5997.$$

Therefore,

$$f_L = \frac{-10 - 771.5997}{(-.880089)} = 888.1 \text{ MHz.}$$

Similarly for the higher frequency

$$m_U = \frac{(-10.800253) - (-9.938513)}{904 - 905} = .86174,$$

$$b_U = -9.938513 - (.86174)(905) = -789.8132.$$

Therefore

$$f_U = \frac{-10 - (-789.8132)}{.86174} = 904.9 \text{ MHz.}$$

The bandwidth can be calculated via equation (2.2)

$$B = \frac{904.9 - 888.1}{896} = 0.0187.$$

The bandwidth for the control RMPA is 1.87%. Recall that this falls within the aforementioned range of MPA bandwidth according to specialists in the field such as Pozar [7].

The quality factor for the control RMPA can be determined from Table 5.1 via equation (2.3) by first determining the higher and lower frequencies at the  $-7$  dB level, respectively  $f_U$  and  $f_L$ . Then it is possible to calculate the quality factor directly.

$$m_L = \frac{(-6.740778) - (-7.248796)}{883 - 884} = -.5080180,$$

$$b_L = -6.740778 - (-.5080180)(883) = 441.8391.$$

Therefore,

$$f_L = \frac{-7 - 441.8391}{(-.5080180)} = 883.5 \text{ MHz.}$$

Similarly for the higher frequency

$$m_U = \frac{(-7.324154) - (-6.826678)}{909 - 910} = .4974760,$$

$$b_U = -7.324154 - (.4974760)(909) = -459.5298.$$

Therefore,

$$f_U = \frac{-7 - (-459.5298)}{.4974760} = 909.7 \text{ MHz.}$$

Hence, the quality factor for the control RMPA, as determined from equation (2.3)

with  $f_1 = f_L$  and  $f_2 = f_U$  is

$$Q = \frac{896}{909.7 - 883.5} = 34.1985.$$

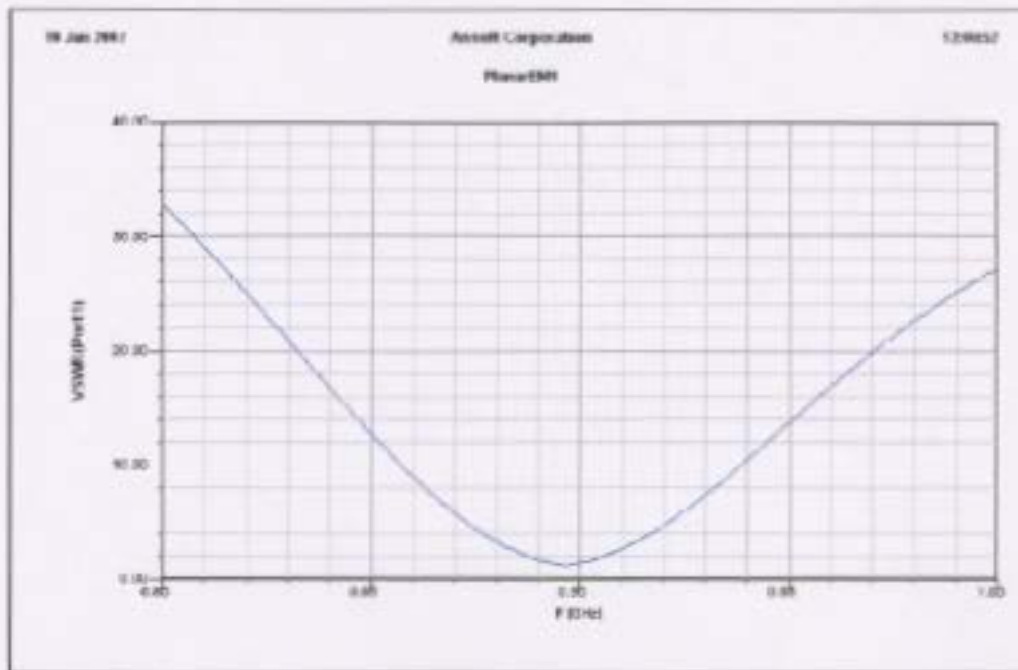


Figure 5-5: Control RMPA: VSWR plot versus frequency (GHz).

The simulated VSWR plot in Figure 5-5 shows that the RMPA resonates optimally at 896 MHz and should perform adequately in the range of 886 MHz to 904 MHz. It can also be noted that the antenna does resonate relatively symmetrically about its centre or resonate frequency.

Figure 5-6 displays the accepted gain measured in dB for the control RMPA in the elevation and azimuthal planes when being driven at 900 MHz. The symmetry in the azimuthal plane (blue) corresponds to the horizontal geometrical symmetry of the antenna. The slight lack of symmetry in the elevation (red) plane results from the lack of vertical geometrical symmetry of the RMPA. It bears mentioning that beyond  $\pm 90^\circ$  there is no measured accepted gain in the simulation. This is because

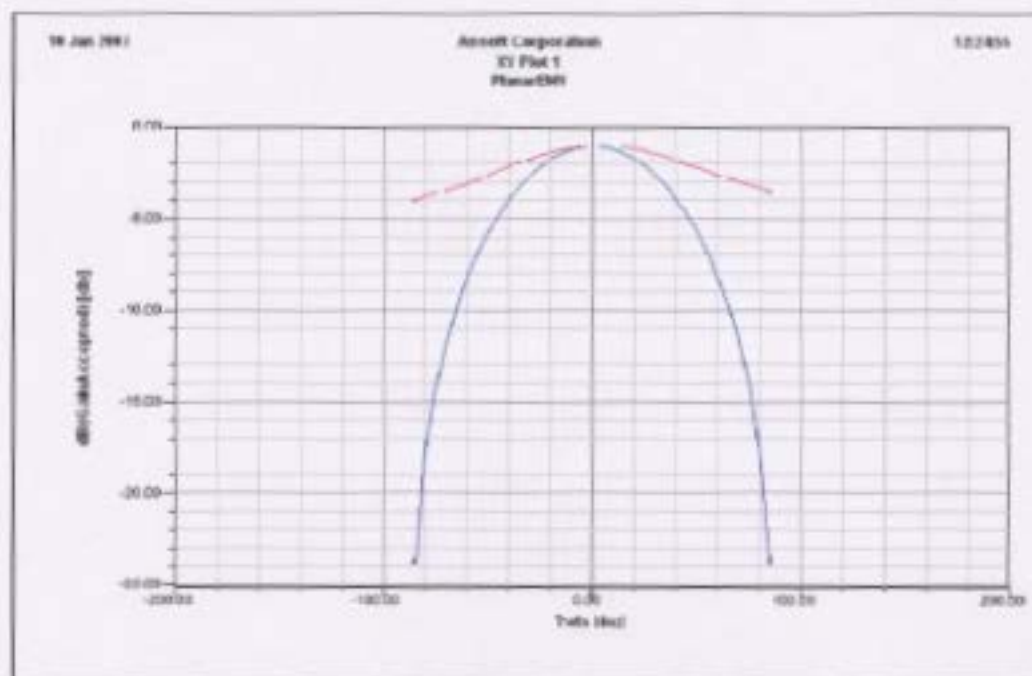


Figure 5-6: Control RMPA: Accepted gain (dB) plot versus angle @ 900 MHz with elevation in red and azimuthal in blue.

the simulator utilizes an infinite ground plane for simulations which agrees with the ideal supposition that MPAs tend to be highly directional and resonate only in the half space above the ground plane. However, in practice there will be slight fringing effects which can be minimized by increasing the dimensions of the ground plane.

Figure 5-7 is a representation of the radiation pattern in polar coordinates. The polar plot relays a good sense of the shape of the beam pattern emanating from the MPA. The front plane radiation is quite evident and it is possible to appreciate how the radiation is reduced in the back plane. Furthermore, the beamwidth in the elevation plane is noticeably wider than the beamwidth in the azimuthal. Additional simulation results for the control RMPA are located in the Appendix A.

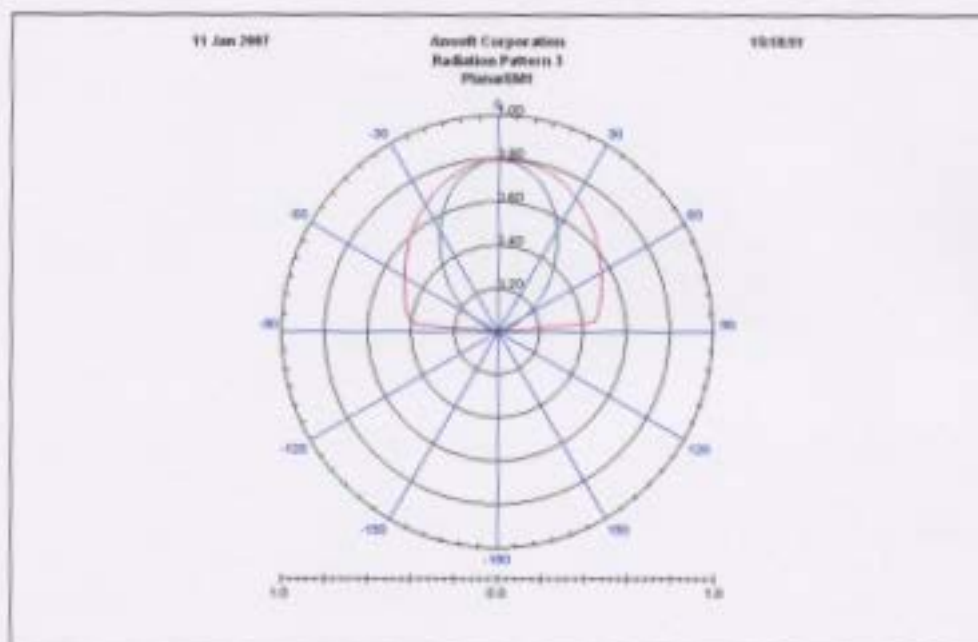


Figure 5-7: Control RMPA: Accepted gain plot versus angle @ 900 MHz with elevation in red and azimuthal in blue.

## Chapter 6

# Coplanar Gap-coupled Parasitic Elements

In order to tune the MPA such that it resonates optimally at the desired frequency of 900 MHz, a pair of parallel coplanar capacitively gap coupled parasitic elements are added to the existing rectangular MPA model. The technique of coupling parasitic elements to resonators in order to affect impedance and alter bandwidth was identified relatively early in MPA research and development [113].

Parasitic element integration and its effects have been studied by a host of researchers and in varying manifestations. Stacking parasitic elements in different layers is a popular theme [44], [58], [114]-[117]. Coplanar gap-coupling has been examined in detail in multiple contexts as well. There are several arrangements one can consider; however, each is a special case or slight generalization of the design presented

in [118]-[120]. In that construction the authors place four elements of comparable size to the directly fed rectangular resonator. These elements are placed along each side of the main element, that is, along its radiating and non-radiating edges. In [122], [125] the authors use a design which is composed of multiple strips coupled to a main strip resonator separated by a small gap. This type of MPA is mentioned by Kumar and Ray [110]. The technique which is to be applied in this thesis is described in [16], mentioned in [9], and studied in minor detail in [121], [123], [124].

The design techniques employed in this chapter differ from those used in the previous chapter. Computer simulation is relied upon in order to satisfy the prescribed design specifications of a  $-9.54$  dB maximum return loss level at 900 MHz.

## 6.1 Design

The method of placing two narrow strips parallel to the non radiating edges of the patch cannot be handled analytically in a simple manner. Popular models, including transmission line and cavity, cannot reliably predict the coupling between the parasitic elements and the patch [123]. It is possible to use an integral method of moments to characterize results as in [123], but there are no works in the literature which allow one to calculate the dimension and location for parasitic elements in order to satisfy the desired antenna parameter criteria. Instead, it is necessary to employ what the authors of [125] call experimental iteration in order to obtain optimal results. That said, there are certain loose design specifications which can be utilized. It is known

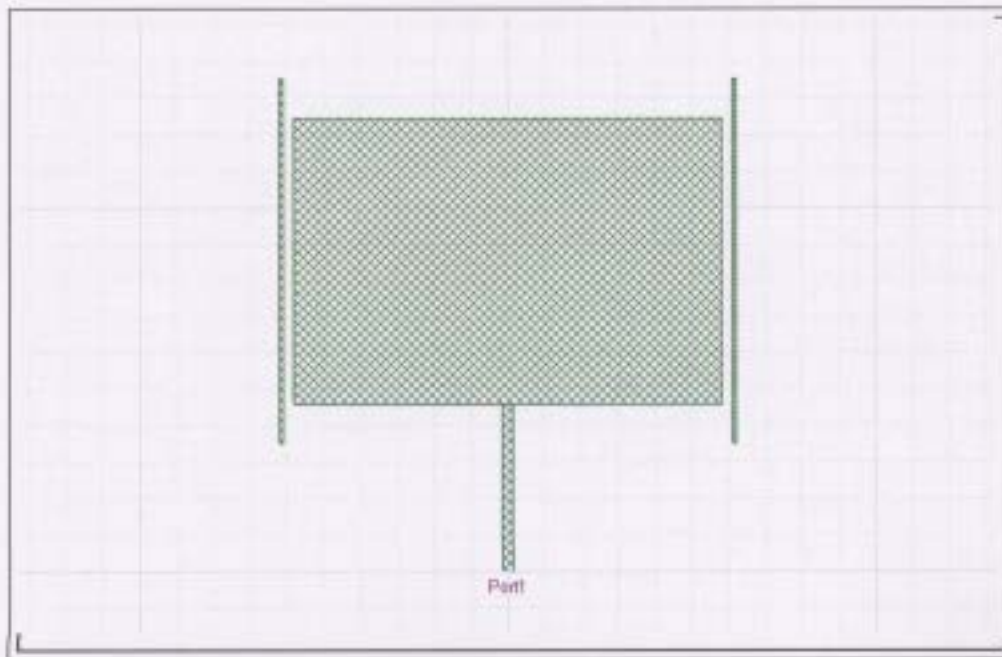


Figure 6-1: Tuned RMPA computer model with parasitic coupling strips designed to resonate at 900 MHz.

that optimal performance tends to occur when the segments are slightly longer than the patch [16]. The gap distance is also a major contributor to frequency modification in this context. A separation distance in the range of 2.5 to 3 times that of the substrate height is recommended.

The initial proposed parasitic strips will have dimension  $l = 97$  by  $w = 3$  mm and be separated from the patch resonator by a distance of 3.8 mm as a starting point for simulation optimization.

## 6.2 Simulation

It has been shown that relying solely on analytic formula to design a MPA for a prescribed resonant frequency operation is not advisable according to the previous simulation results at the end of chapter three. The Ansoft simulation package is used to tune the antenna to a desired resonant frequency of 900 MHz. The parasitic side strips are inserted into the previous model along the non-radiating edges of the RMPA. The simulation will optimize the dimension and placement of these coupling strips in order to satisfy the design criteria.

The model resulting from the optimizing simulation process is captured in Figure 6-1. Graphical results for certain antenna parameters of interest from the simulation are given in Figures 6-2 to 6-5.

Figure 6-2 shows that the return loss has been improved not only with respect to centre frequency but also in terms of resonance. The tuned RMPA with couplers resonates at 900 MHz and at a level of approximately  $-28$  dB.

It is possible to determine the bandwidth and quality factor from Table 6.1. The  $f_L$  and  $f_U$  are determined in the same manner as in the previous chapter and the bandwidth is calculated via equation (2.2). It is determined to be 1.81%. This bandwidth is very close to the 1.87% of the control RMPA. It has been reduced by 3.21%. The quality factor for the tuned RMPA is determined by equation (2.3) and found to be  $Q = 36.4344$ . As expected, there is a minor increase of 6.52% in the quality factor for the tuned RMPA over the control RMPA.

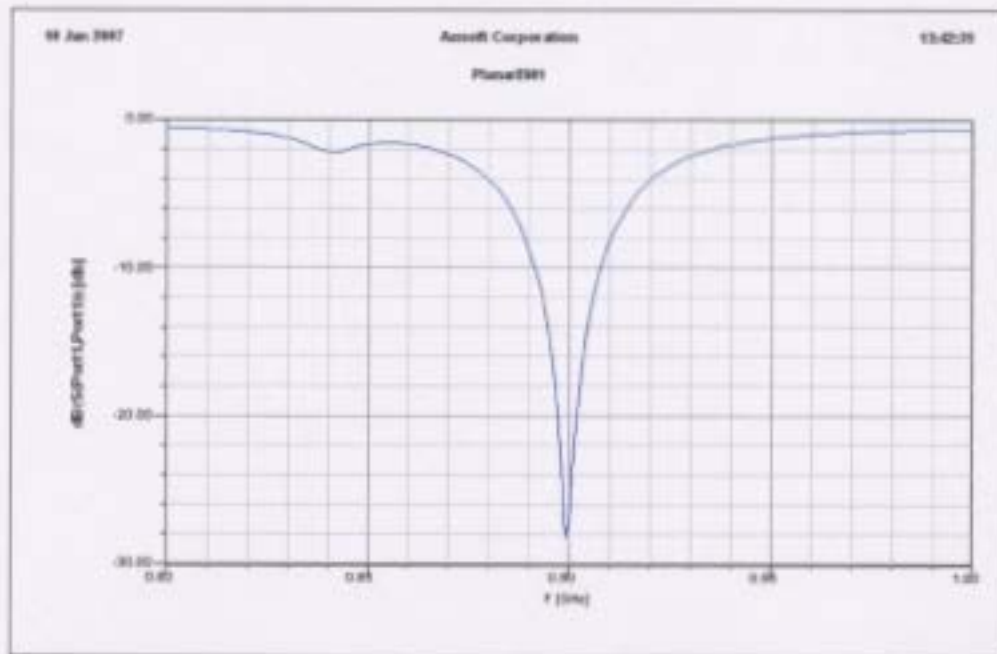


Figure 6-2: Tuned RMPA: Return loss plot versus frequency (GHz).

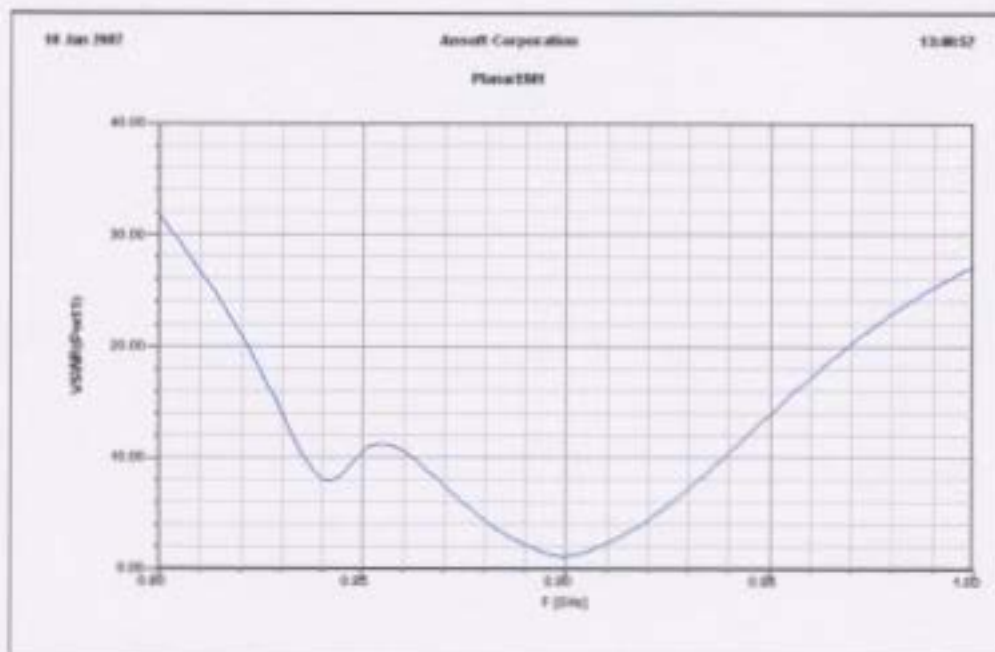


Figure 6-3: Tuned RMPA: VSWR plot versus frequency (GHz).

Frequency [MHz]	S(Port1,Port1) [dB]
887	-6.793286
888	-7.376212
889	-8.033983
890	-8.780707
891	-9.634801
892	-10.621045
893	-11.774059
894	-13.144452
895	-14.810437
896	-16.901284
897	-19.646321
898	-23.445343
899	-28.101850
900	-27.071476
901	-22.415902
902	-18.943136
903	-16.409670
904	-14.459434
905	-12.894318
906	-11.600785
907	-10.508897
908	-9.572717
909	-8.760443
910	-8.049098
911	-7.421487
912	-6.864366

Table 6.1: Simulated return loss for tuned RMPA with coupling strips



Figure 6-4: Tuned RMPA: Accepted gain (dB) plot versus angle @ 900 MHz with elevation in red and azimuthal in blue.

The simulated VSWR plot in Figure 6-3 shows that the antenna should resonate well in the range of approximately 890 MHz to 910 MHz. It also shows that the tuned antenna should operate optimally at the desired frequency of 900 MHz. The antenna's bandwidth is symmetric about the centre frequency in the range of 860 MHz to 940 MHz. Outside of this range, the bandwidth is still generally symmetrical. Despite the fact that the VSWR plot in Figure 6-3 suggests mild asymmetry, one can refer to Figure 6-2 to see that bandwidth of the tuned RMPA is generally symmetric in the range of interest from 800 MHz to 1 GHz.

Figure 6-4 displays the accepted gain measured in dB for the tuned RMPA in the elevation and azimuthal planes when being driven at 900 MHz. The result is

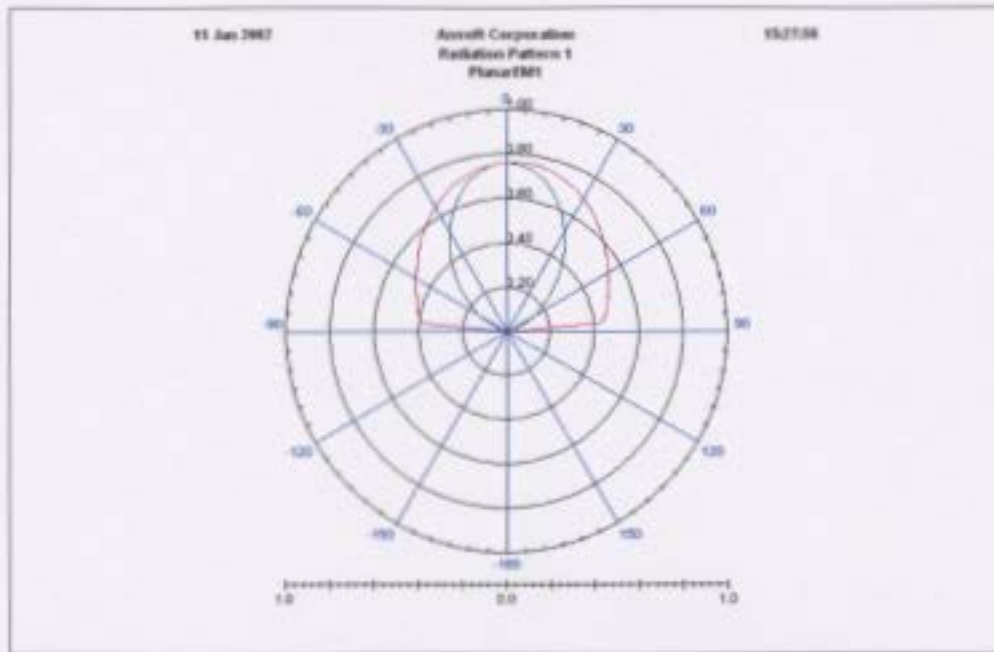


Figure 6-5: Tuned RMPA: Accepted gain plot versus angle @ 900 MHz with elevation in red and azimuthal in blue.

similar to that shown in Figure 5-6. The introduction of the parasitic elements in the tuned RMPA model has not resulted in notable changes in the radiation pattern from the control RMPA, although there is a slight reduction in peak VSWR value. The same pattern attributes pertaining to symmetry hold in the tuned RMPA radiation pattern as those exhibited by the control RMPA radiation pattern. Figure 6-5 is a representation of the radiation pattern in polar coordinates. Naturally, it closely resembles the pattern exhibited by the control RMPA in Figure 5-7.

Another simulation result that will be utilized in the next section in the design of the impedance matching network is the input impedance of the tuned RMPA. At a

frequency of 900 MHz the input impedance of the antenna is

$$Z_0 = 47.591022 + j3.52320.$$

Thus the antenna resistance for the tuned RMPA is  $R_0 = 47.59\Omega$ .

Additional simulation results for the tuned RMPA are located in the Appendix A.

# Chapter 7

## Impedance Matching Feed Line Network

A hybrid design approach will be used for this final stage. A balance of analytical and computer simulation is applied to achieve design goals. The analytical formulae provide a solid starting point for RMPA model modification. Then the computer simulation can be engaged to realize a suitable model for fabrication. The question might be posed, "Why use at all during this stage of the design process?" After all, why not let the computer simulation do all the work to implement the necessary design additions and refine the model according to specifications? Relying solely on the computer simulation to achieve these goals is not realistic in all cases. The incorporation of analytics at the front end of this last design stage saves a great deal of time and permits the computer simulation to start at a more advanced point

for optimization, thereby saving time. Moreover, it decreases the likelihood that the computer optimization process will converge on a non optimal or unsatisfactory solution.

## 7.1 Design

The motivation for introducing an impedance matching network is twofold. Firstly, it will widen the bandwidth of the antenna in proximity to the desired resonant frequency. Secondly, the network can effectively split the band surrounding the resonant frequency. The design intention is that by introducing dual frequency band operation there would be an increased likelihood of a proper resonance at the desired frequency post fabrication. The impedance matching network theory being applied to reach this goal originates in [10] and is based on a three-element modified Chebychev network first proposed in a broadband matching theory by Fano [126]. A higher order network would be significantly more complex and be cumbersome to simulate. The impedances parameter arrangement of the feed line segments and tuning stubs is in Figure 7-1.

It is necessary to ensure that the patch model from the previous chapter is resonant at the centre frequency of its band. This has been achieved via the simulation tuning process. The antenna model parameters  $f_r$ ,  $Q_t$  and  $R_0$  (antenna's resonant resistance) are determined from the previous tuned model. Pues and Van de Capelle recommend establishing these parameter values by accurate measurements, but com-

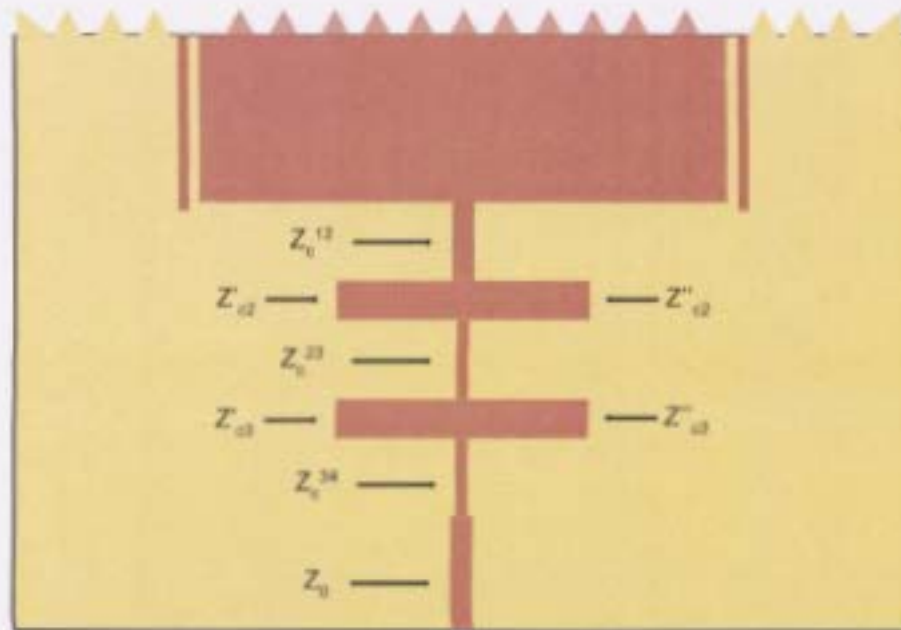


Figure 7-1: Impedance matching network for rectangular MPA with intermediary resonator and segment impedances.

puter simulation will be relied upon here. The designer must choose a bandwidth improvement factor,  $B$ , and the order (number of stubs),  $n$ , of the impedance matching network. Those values are fixed at  $B = 0.1$  and  $n = 3$  for this work in order to ensure the problem is computable. Increasing these values increases the complexity of the overall problem.

Next the  $g_i$  parameters are determined by first establishing the value of intermediary parameters

$$\Lambda = \tan\left(\frac{\pi}{2}B\right)$$

and

$$\delta = \frac{\pi}{2\Lambda Q}$$

Then it is possible to find  $g_i$  design parameters given by  $g_0 = 1$ ,  $g_1 = 1/\delta$  and using Figure 7-2 to find  $g_2$ ,  $g_3$  and  $g_4$ .

In Figure 7-1, the network is composed of three main elements: the rectangular resonator and two parallel stub resonators. The resonators are connected (with no discontinuities) by a series of coplanar microstrip feed line segments of varying impedances. In order to determine the appropriate impedances of the network, one must consider a set of recursive equations outlined in [10]. These equations involve the admittances,  $Y_{ci}$ , of the different segments and a set of parameters known as admittance inverters. The set of general equations to be solved is

$$\begin{aligned} J_{12} &= \sqrt{\frac{\Lambda Y_{c2}}{R_0 g_2}}, \\ J_{i,j+1} &= \Lambda \sqrt{\frac{Y_{ci} Y_{c,j+1}}{g_i g_{i+1}}}, \quad i = 2, 3, \dots, n-1, \\ J_{n,n+1} &= \sqrt{\frac{\Lambda Y_{cn}}{g_n g_{n+1} Z_0}}. \end{aligned}$$

Equivalently, the following equations are to be satisfied for  $i = 2, \dots, n$  :

$$\begin{aligned} Y_c^{i,j+1} &= J_{i,j+1} \cos\left(\frac{\pi}{4} B\right), \\ Y'_{ci} &= [Y_{ci} \Lambda - (Y_c^{i-1,j} + Y_c^{i,j+1}) \Gamma] \frac{a_i - \beta^2}{(1 + a_i) \beta}, \\ Y''_{ci} &= a_i Y'_{ci}, \end{aligned}$$

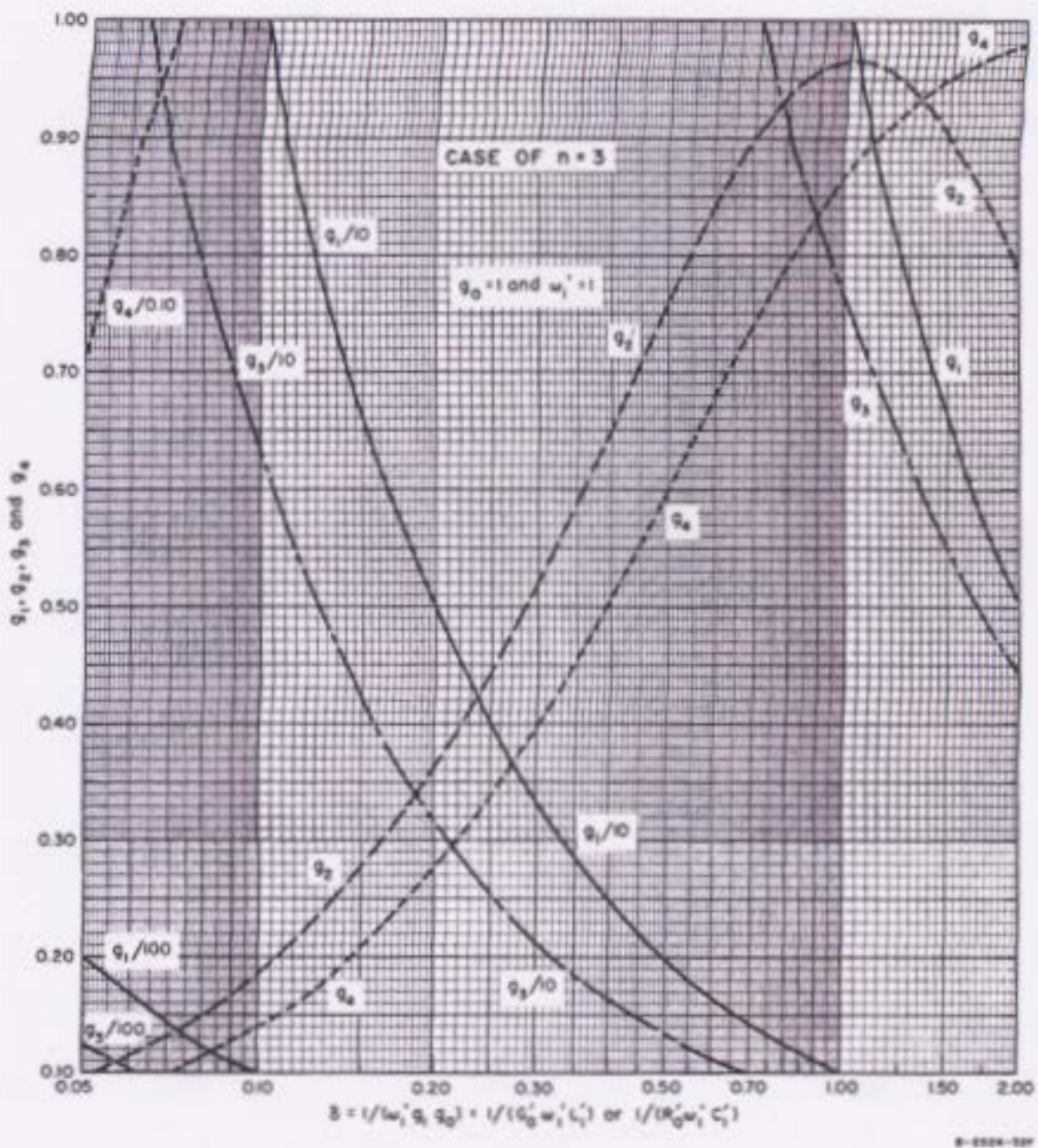


FIG. 4.09-7 ELEMENT VALUES vs.  $\delta$  FOR CHEBYSHEFF IMPEDANCE-MATCH NETWORKS THAT MINIMIZE  $(L_A)_{max}$

Figure 7-2: Chart for  $g_i$  parameters from [127].

Network parameter	Impedance ( $\Omega$ )
$Z_c^{12}$	53.2977
$Z_c^{23}$	130
$Z_c^{34}$	72.1050
$Z'_{c2}$	26.064
$Z''_{c2}$	26.064
$Z'_{c3}$	24.5105
$Z''_{c3}$	24.5105
$Z_0$	50

Table 7.1: Parameters for impedance matching network

where

$$\beta = \tan\left(\frac{\pi}{4}B\right).$$

The values calculated for the different impedances are given in Table 7.1 and are the starting point for the simulation model. By definition the admittance,  $Y$  is the reciprocal of the impedance,  $Z$ .

## 7.2 Simulation

Once the impedance matching network was inserted into the tuned RMPA model, a computer simulation was used to manipulate the model dimensions in order to satisfy the design specifications. The model as depicted in Figure 7-3 is the result of a lengthy optimization process. It is consistent with the model of Pues and Van de Capelle [10]. The return loss for the modified model is given in Figure 7-4. The band has been effectively widened and split about the 900 MHz frequency. The modified RMPA resonates at 864 MHz and 939 MHz. The design intention is that any shift

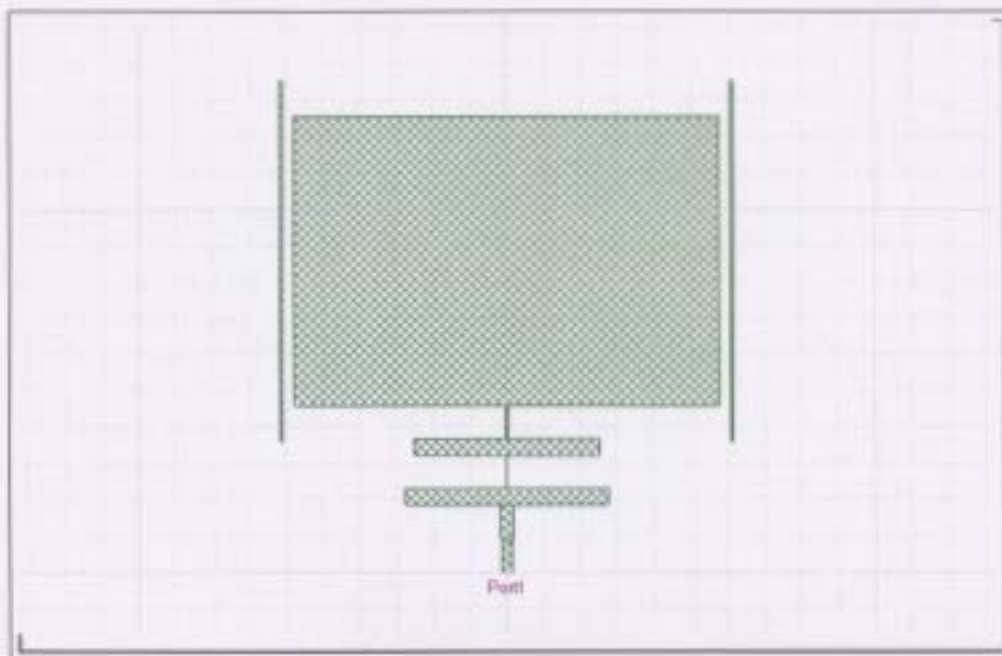


Figure 7-3: Modified RMPA computer model with gap coupled parastic strips and impedance matching network.



Figure 7-4: Modified RMPA: Return loss plot versus frequency ( GHz).

Frequency [MHz]	S(Port1,Port1) [dB]
846	-9.382516
847	-10.296952
854	-20.609119
855	-21.750429
856	-22.078892
857	-21.798249
858	-21.358005
859	-21.076503
860	-21.104645
861	-21.504100
862	-22.280038
863	-23.323712
864	-24.204313
865	-24.054445
866	-22.515305
867	-20.329029
874	-10.040227
875	-9.248159
932	-9.688767
933	-10.681982
939	-20.932458
940	-20.890676
946	-10.316881
947	-9.277360

Table 7.2: Simulated return loss for modified RMPA

in poles due to variants encountered in the fabrication process are equally likely to cover the desired resonant frequency of 900 MHz. Table 7.2 has been abbreviated to include values necessary to calculate the bandwidth for the modified RMPA. The table consists of those points of interest at the limits of both frequency bands as well as data points below the  $-20$  dB level for both resonant frequencies. The complete set of points for the 800 MHz to 1 GHz is available in the Appendix A.

The bandwidth for the modified RMPA can be quantified about each resonant fre-

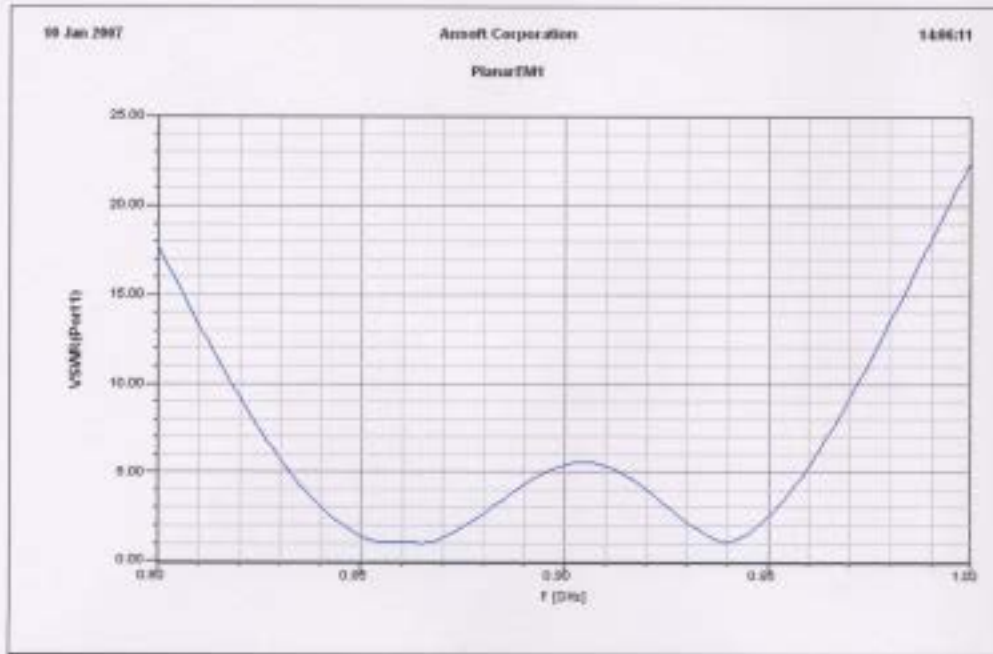


Figure 7-5: Modified RMPA: VSWR plot versus frequency (GHz).

quency. The bandwidth as determined about the lower resonant frequency of 860 MHz via equation (2.2) is 3.17%. The bandwidth about the higher resonant frequency of 939 MHz is calculated as 1.49% which is more than half the bandwidth of the lower pole. According to the simulations, the available bandwidth in the frequency range of interest has more than doubled. Only actual measurement can determine if this is sufficient to overcome post fabrication frequency shifts. These measurement results are found in the following chapter. The VSWR for the modified RMPA is given in Figure 7-5. The general symmetry of the dual frequency operation about 900 MHz is good. The antenna radiation pattern for the modified RMPA is given in Figure 7-6 and differs insignificantly from the previous radiation patterns for the control and tuned RMPA models, respectively Figures 5-6 and 6-4. There is a minor drop in

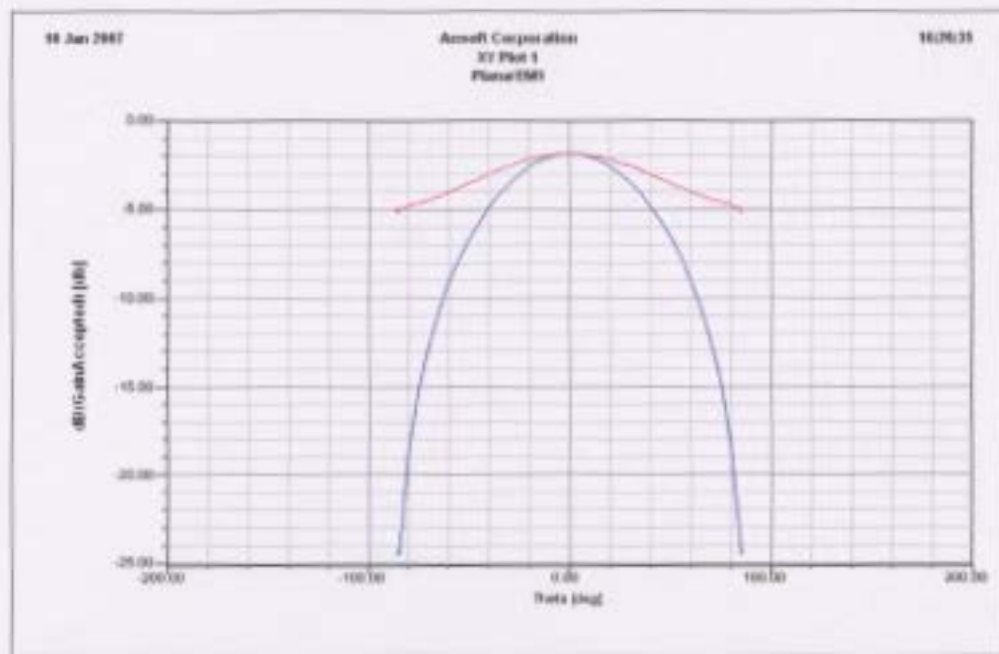


Figure 7-6: Modified RMPA: Accepted gain (dB) plot versus angle @ 900 MHz with elevation in red and azimuthal in blue.

accepted gain exhibited at peak value. Similar to the pattern for the tuned RMPA, the radiation intensity is slightly reduced to the  $-2$  dB level likely due to increased energy loss in the impedance matching network. More notable however, is that the simulated radiation pattern has greater symmetry in the azimuthal plane than either the control or tuned RMPA models. This is likely due to the radiation from the impedance matching network overcoming the lack of vertical geometric symmetry of the model. Comparison of the radiation pattern of the modified RMPA of Figure 7-7 to the previous gain polar plots of the control and tuned RMPA (Figures 5-7 and 6-5) shows that the overall radiation pattern intensity is slightly less in the front half plane.

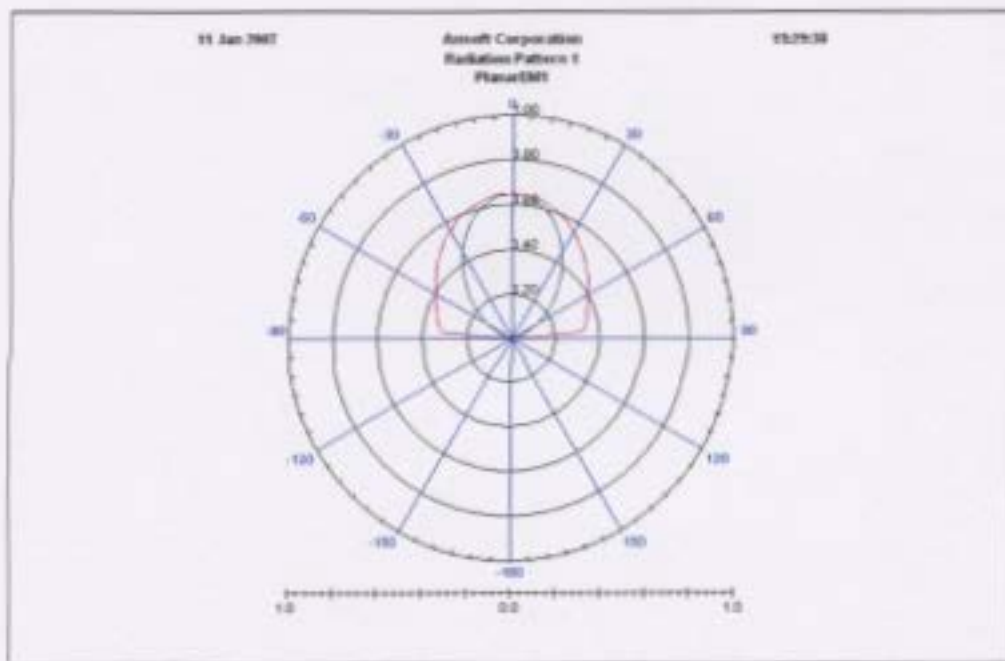


Figure 7-7: Modified RMPA: Accepted gain plot versus angle @ 900 MHz with elevation in red and azimuthal in blue.

# Chapter 8

## Measurements and Discussion

There are two separate test procedures to measure certain antenna parameters of interest.

The first set of test procedures examines the radiation properties for the RMPAs. Each RMPA is placed in an anechoic chamber and probed with a transmitting antenna. Radiation levels are observed and the radiation pattern is determined for the RMPAs in the azimuthal and elevation planes. It is not possible to compare the real radiation patterns results quantitatively with the simulation results because there are no calibrated sources for measuring antenna radiation patterns available at Memorial University of Newfoundland. A qualitative analysis of the actual radiation data is made and it is possible to objectively comment on the shape of the real observed pattern versus the simulated RMPA radiation patterns.

The purpose of the second series of tests is to ascertain the actual return loss

measurements, reconcile the result with the expected simulation results and decide whether the RMPAs perform satisfactorily according to the design specifications. The fabricated RMPAs were connected to a Vector Network Analyzer in order to evaluate their respective reflection coefficients. Using this information it is possible to calculate the return loss and VSWR of the fabricated RMPAs and compare these numbers to the pre-fabrication simulation results on the RMPA models.

## **8.1 Radiation pattern measurements**

### **8.1.1 General setup**

The measurements were conducted inside a  $2.5\text{ m} \times 2.5\text{ m} \times 4.25\text{ m}$  RF anechoic chamber located in the Faculty of Engineering's Thermal Laboratory. The RF anechoic chamber is designed to suppress reflected electromagnetic waves from sources inside the chamber. The specially designed foam wall tiles are radiation absorbent and are neither a good conductor nor a good insulator. The inside of the chamber can be seen in Figure 8-1.

The basic configuration for the radiation pattern set of measurements is captured in Figure 8-2. The connection of the antennas to the hardware instruments was with  $50\Omega$  coaxial cable. The hardware instruments were located outside of the anechoic chamber for these tests, otherwise the devices would interfere with electromagnetic wave propagation and taint the radiation pattern of the RMPAs.



Figure 8-1: Inside the RF anechoic chamber, Tx antenna in background and Rx antenna in foreground.

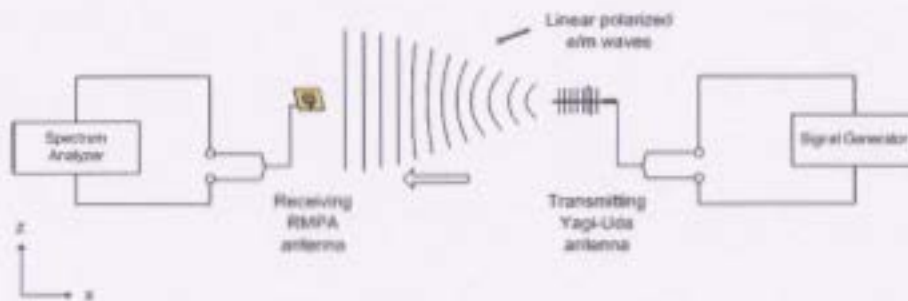


Figure 8-2: General setup for antennas and hardware for RMPA radiation pattern measurements.



Figure 8-3: Transmitting antenna: 7-element Yagi-Uda array in Anechoic chamber oriented for RMPA azimuthal angle measurements.

The transmitting device, a seven element Yagi-Uda antenna array, was mounted on a wooden stand in the centre of one side of the chamber such that the individual array elements were perpendicular to the ground as shown in Figure 8-3. This linearly polarized Yagi-Uda antenna is an ideal candidate for a transmitting device because of its highly directional nature, designed optimal operating frequency of approximately 880 MHz, and overall dimensions. Given the desired transmission frequency of 900 MHz and the Yagi-Uda length of  $D = 46$  cm then it follows by equation (2.1) that the far-field range of the Yagi-Uda array begins at a distance of

$$\frac{2D^2}{\lambda} = \frac{2(.46)^2}{\left(\frac{299.8}{900}\right)} = 1.27 \text{ m.}$$

The transmitting antenna is connected to a Hewlett Packard 8656B Synthesized Signal Generator with a coaxial cable. The signal generator is configured to a driving frequency of 900 MHz and a signal amplitude of  $-17$  dBm.



Figure 8-4: Receiving antenna: Control RMPA in Anechoic chamber oriented azimuthal angle measurements in ( $\theta = 0^\circ$  position).

The RMPA is connected via a coaxial cable to an Advantest R4131A Spectrum Analyzer and was placed in a circular wooden stand that permits rotation of the RMPA a full  $360^\circ$  with measurement divisions at  $5^\circ$  increments. The mounting apparatus is pictured in Figure 8-4. The largest dimension on the RMPAs measures 14 cm. The far-field range for the RMPA antennas is less than that for the Yagi Uda

$$\frac{2D^2}{\lambda} = \frac{2(.14)^2}{\left(\frac{299.8}{900}\right)} = 0.18 \text{ m.}$$

The transmitting and receiving antennas are placed a distance of 2.02 m apart to measure the far-field radiation pattern of the RMPAs. Since this separation distance is greater than the far field range for the transmitting and receiving antennas, we can be satisfied that the far-field radiation pattern measurements are indeed in the far field for both antennas. An illustration showing the RMPA orientation for these azimuthal plane measurements is found in Figure 8-5. In this case, the angle  $\Phi = \theta$

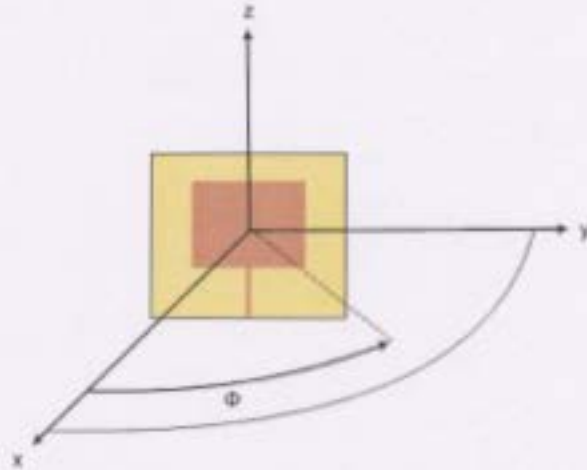


Figure 8-5: RMPA orientation for azimuthal plane radiation pattern measurements.

where  $\theta$  is from Figure 2-2.

### 8.1.2 Azimuthal plane results

The results of the measurements for the azimuthal plane are included in Figures 8-6 to 8-12. The azimuthal plane radiation pattern measurements are plotted separately in Figures 8-6 to 8-8. The data plots give the received signal amplitude as a function of the angle of rotation of the RMPA. It is possible to compare these plots to the simulated accepted gain plots for the control, tuned and modified RMPAs, respectively the azimuthal (blue) trace in Figures 5-6, 6-4, and 7-6.

The traces in the rectangular azimuthal plots are highly symmetrical and quite comparable to the symmetrical nature of the simulation prediction. These plots also show that most of the received signal is focused in the front half of the plane. In each case, the received signal is above the  $-80$  dBm level in the  $-90^\circ$  to  $90^\circ$  range.

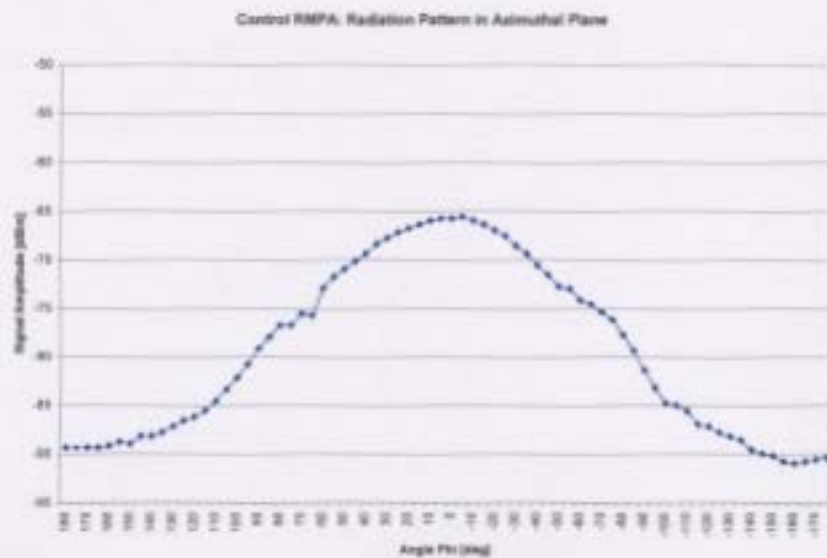


Figure 8-6: Control RMPA: Signal amplitude (dBm) as a function of azimuthal angle.

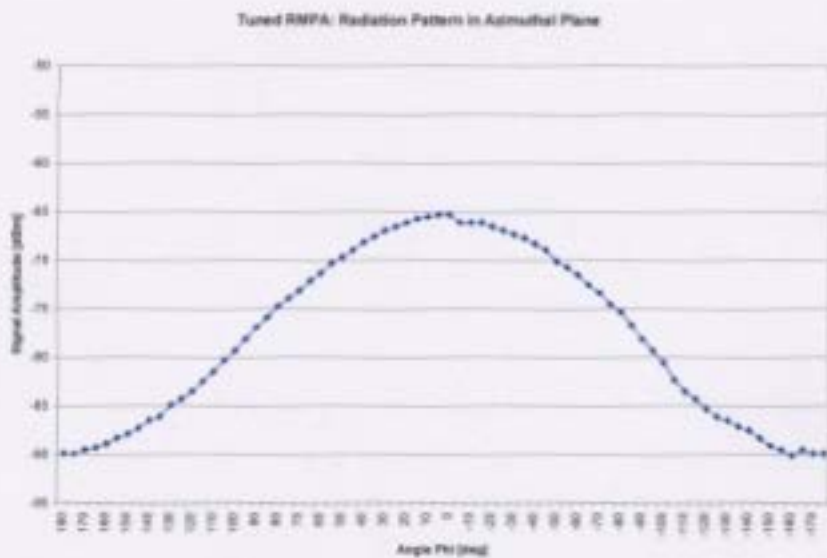


Figure 8-7: Tuned RMPA: Signal amplitude (dBm) as a function of azimuthal angle.

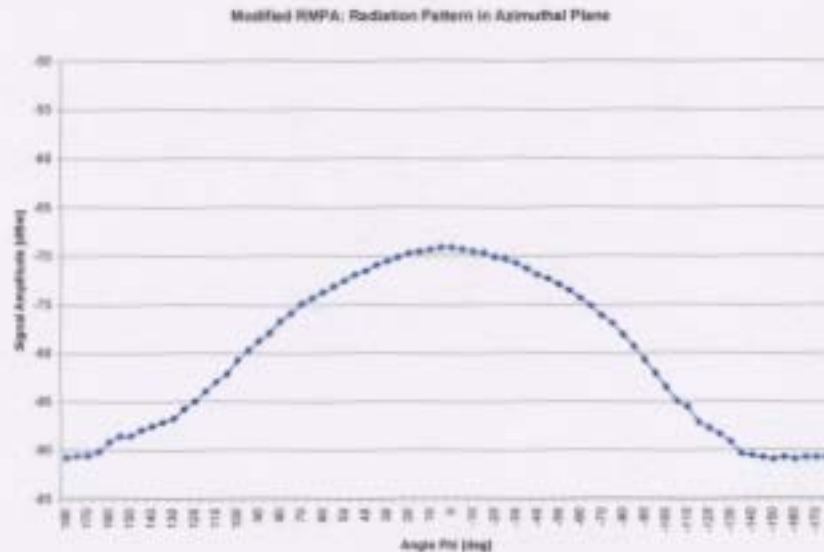


Figure 8-8: Modified RMPA: Signal amplitude (dBm) as a function of azimuthal angle.

There is signal received in the backplane which differs from the simulated results, but it is not entirely unexpected because simulation uses an infinite ground plane for calculations. Therefore, some fringing and radiation outside of the  $-90^{\circ}$  to  $90^{\circ}$  range is anticipated. In fact, once the plots are filtered for background noise, the azimuthal plane radiation pattern results are in closer agreement with the simulation results. Figure 8-9 is a plot of the azimuthal radiation pattern of all three RMPAs with signal below  $-88.5$  dBm treated as measurement noise.

Examination of the relative peak values (at approximately the  $\theta = 0^{\circ}$ ) of the three traces in Figure 8-9 shows close agreement with the simulation results. The simulated peak accepted gain values for the control, tuned and modified from Figures 5-6, 6-4, and 7-6 are approximately  $-1$  dB,  $-1.2$  dB, and  $-2$  dB respectively. That

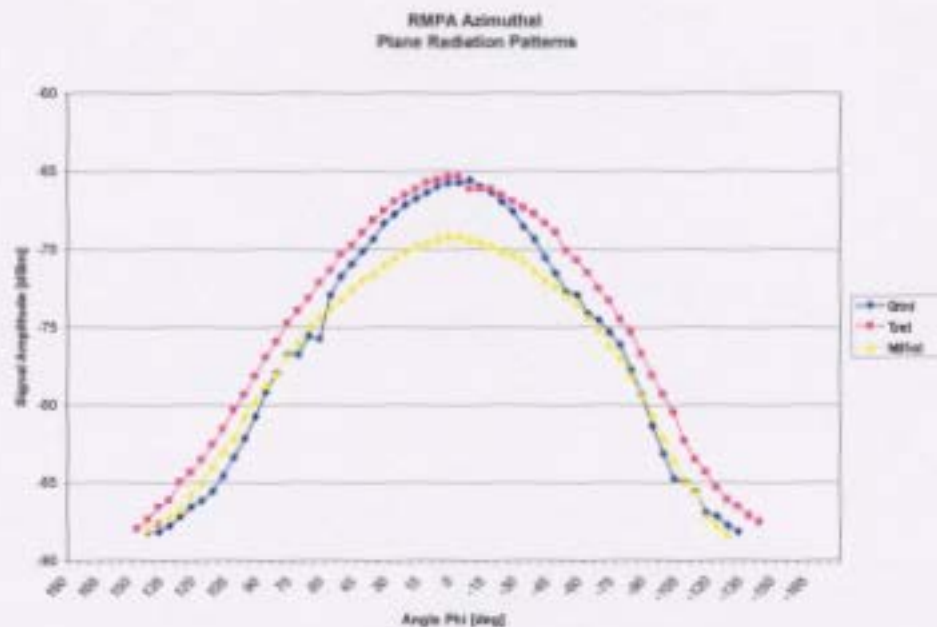


Figure 8-9: RMPAs: Cleaned signal amplitude (dBm) as a function of azimuthal angle with noise reduction.

is, the accepted gain values for the control and tuned RMPA models are very close, and the peak value for the modified RMPA model being noticeably less. In Figure 8-9 the same trend can be seen. The actual peak values for the control and tuned RMPA measurements are very close together, whereas the peak value for the signal amplitude of the modified RMPA is appreciably lower.

Polar representations of the real azimuthal data for each RMPA is given in Figures 8-10 to 8-12. Note that for the polar plots of these measurements the reference position of  $\theta = 0^\circ$  is at the 6 o'clock position whereas the polar plots for the simulated radiation pattern were given with  $0^\circ$  in the 12 o'clock position. The polar plot of the azimuthal data can be compared to the azimuthal (blue) trace in Figures 5-7, 6-5

Control RMPA: Azimuthal Plane Radiation Pattern

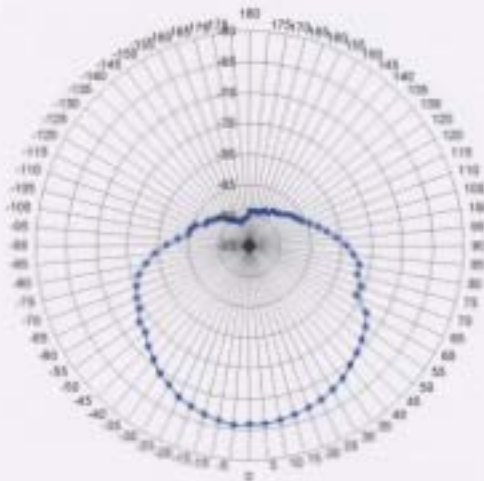


Figure 8-10: Control RMPA: Signal amplitude (dBm) as a function of azimuthal angle in polar coordinates.

Tuned RMPA: Azimuthal Plane Radiation Pattern

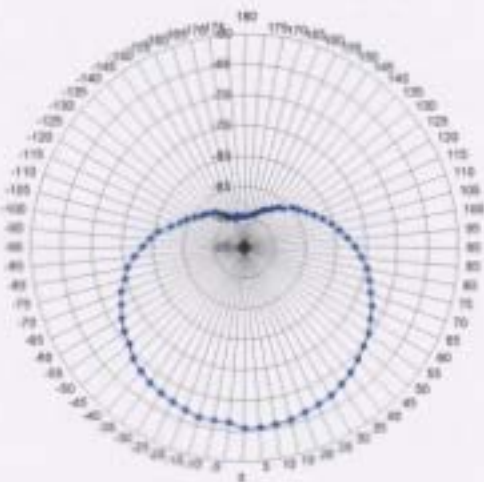


Figure 8-11: Tuned RMPA: Signal amplitude (dBm) as a function of azimuthal angle in polar coordinates.

Modified RMPA: Azimuthal Plane Radiation Pattern

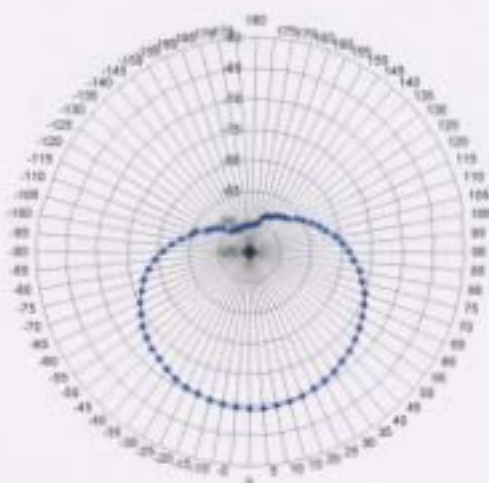


Figure 8-12: Modified RMPA: Signal amplitude (dBm) as a function of azimuthal angle in polar coordinates.

and 7-7. Naturally, the real measured data for the polar plots compare well with the simulated azimuthal polar plots for all three RMPA models. The plots in this format allow the reader to better appreciate the magnitude of the radiation in the front half plane when compared to radiation into the back plane beyond  $\pm 90^\circ$ .

### 8.1.3 Elevation plane results

In order to measure the radiation patterns for the RMPAs in the elevation plane it was necessary to reconfigure the measurements set up slightly due to a possible polarization mismatch. The Yagi-Uda array was rotated  $90^\circ$  so that the array elements were parallel to the ground. The RMPAs were likewise rotated by  $90^\circ$  and placed on their side in the mounting apparatus. The images in Figures 8-13 and 8-14 reflect



Figure 8-13: Yagi-Uda array in Anechoic chamber oriented for RMPA elevation angle measurements.



Figure 8-14: Receiving antenna: Control RMPA oriented in elevation angle measurements position ( $\phi = 90^\circ$ ).

the configurations for the transmit and receive antennas for elevation plane radiation pattern measurements. The RMPA reference orientation for these measurements is given in Figure 8-15. In that diagram  $\Phi = 90^\circ - \phi$  where  $\phi$  is from Figure 2-2.

The rectangular plots of the radiation pattern for the elevation plane of three RMPAs is in Figures 8-16 to 8-18. These can be compared with the elevation (red) trace in 5-6, 6-4, and 7-6. It should be pointed out that there is a slight discrepancy in the actual data points for the peak value of the azimuthal and elevation measured

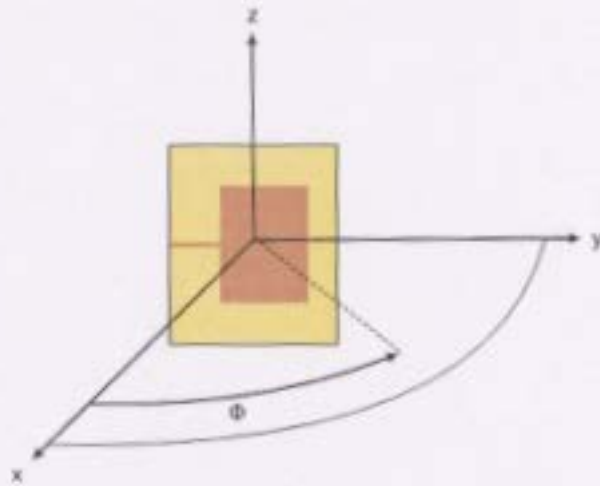


Figure 8-15: RMPA orientation for elevation plane,  $\phi$ , radiation pattern measurements.

in the reference position. This is likely due to the orientation of the RMPA with respect to the transmitting Yagi-Uda antenna. Despite deliberate attempts to align the centre of the RMPAs with the Yagi-Uda for each measurement set, there was some slight offset resulting in minor variability in the RMPAs orientation with respect to the transmitting device.

There are some minor differences between the elevation plane plots in Figures 8-16 to 8-18 and the previous set of azimuthal plane plots (Figures 8-6 to 8-8). Most noticeably, there is a more pronounced parabolic shape to the data points for the azimuthal data when compared to the elevation data. The received signal strength decreases rapidly as the angle spread increases in the radiation pattern in the front plane for elevation versus azimuthal. Table 8.1 captures the relative incremental received amplitude drop-off for both the simulated model and real RMPAs. Based on

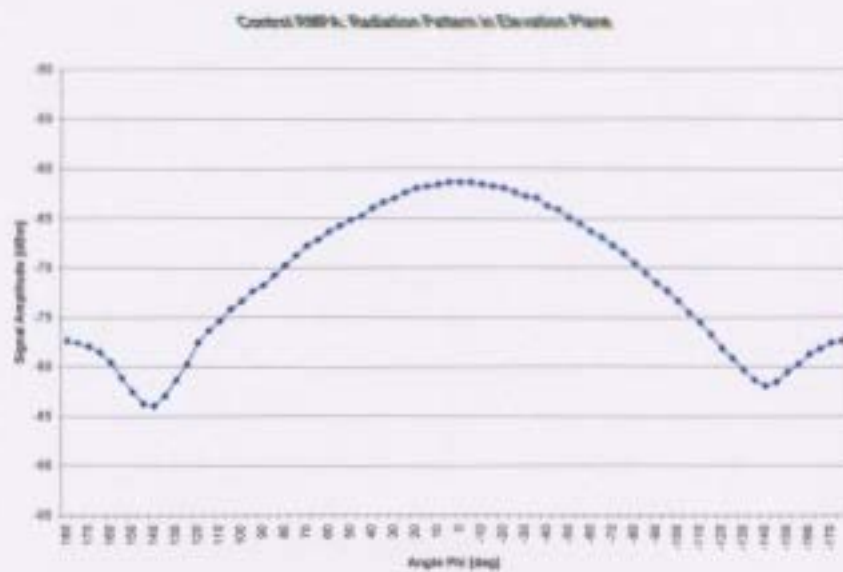


Figure 8-16: Control RMPA: Signal amplitude (dBm) as a function of elevation angle.

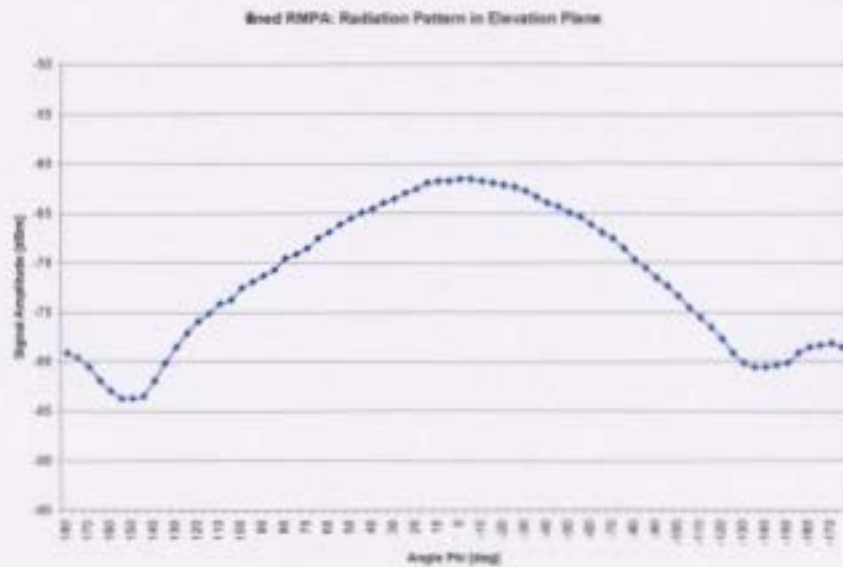


Figure 8-17: Tuned RMPA: Signal amplitude (dBm) as a function of elevation angle.

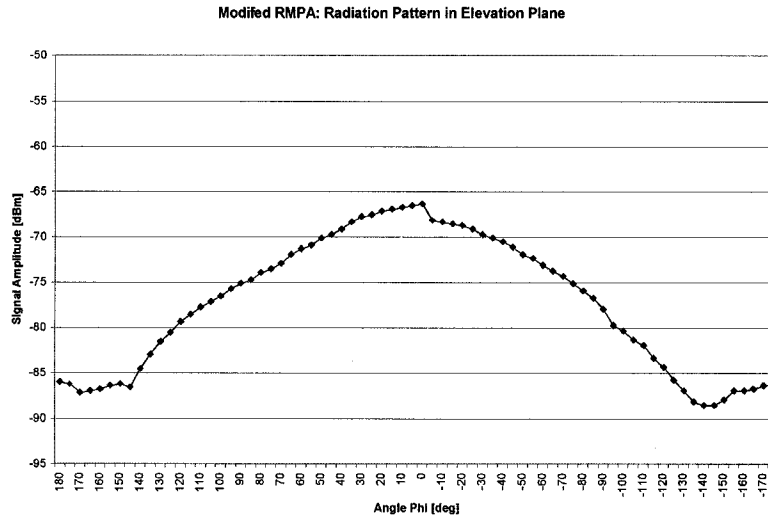


Figure 8-18: Modified RMPA: Signal amplitude (dBm) as a function of elevation angle.

the numbers in this table, it can be seen that the elevation plane measurements tend to be flatter than the azimuthal plane measurements. There is good agreement between the simulated and actual measured data points on this matter. However, there is notably more radiation into the backplane for the elevation pattern measurements. This is somewhat evident in the rectangular plots and very identifiable in the polar plots.

Similar to Figure 8-9, the traces of the control, tuned and modified RMPAs in Figure 8-19 show the same relationship at their respective peak values. The separation between the control, tuned and modified RMPAs is consistent with their modelled simulation results.

Polar plots of the elevation plane radiation pattern measurements are in Figures

Angle Azim.	Control		Tuned		Modified	
	model (dB)	RMPA (dBm)	model (dB)	RMPA (dBm)	model (dB)	RMPA (dBm)
-90°	22.616	15.8	22.61	12.8	22.347	11.6
-45°	3.820	6	3.942	3.6	3.813	3.2
45°	3.760	4.6	3.748	3.6	3.813	2.8
90°	22.683	13.6	22.61	11.6	22.347	9.6
Elev.						
-90°	2.983	10.2	2.977	10	3.103	11.6
-45°	1.301	2.8	1.423	2.8	1.421	4.8
45°	0.979	3.4	1.040	3.4	1.421	3.4
90°	2.466	10.4	2.461	9.8	3.103	8.8

Table 8.1: Received amplitude drop-off from peak

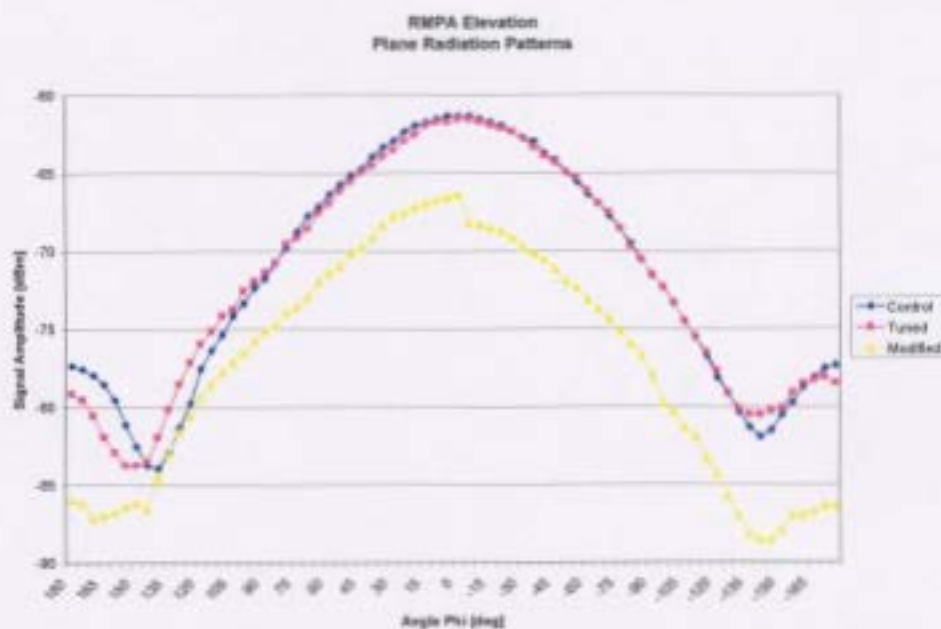


Figure 8-19: RMPAs: Signal amplitude (dBm) as a function of elevation angle.

Control RMPA: Elevation Plane Radiation Pattern

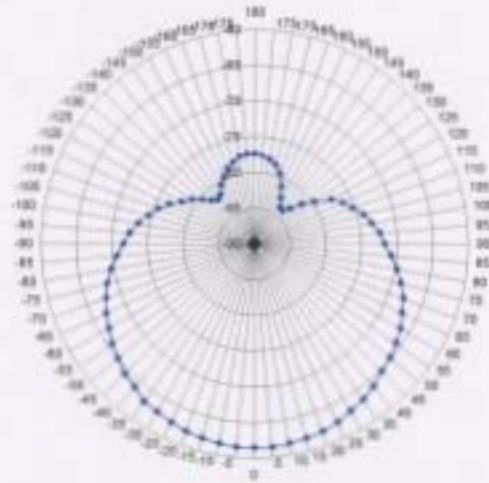


Figure 8-20: Control RMPA: Signal amplitude (dBm) as a function of elevation angle in polar coordinates.

8-20 to 8-22. The back plane radiation mentioned earlier is especially evident in the polar plots. A contributing factor of this radiation might be the orientation for the elevation plane measurements. The non-symmetrical placement of the RMPAs for these measurements coupled with the ground plane deficit at the base of the feed line compared to the other three sides of the RMPA likely result in some backplane radiation. However for the most part, the radiation pattern for the elevation plane agrees with the elevation (red) trace in Figures 5-7, 6-5, and 7-7 in that most of the antennas radiation occurs in the front half plane and the amount of back plane radiation is noticeably less.

Tuned RMPA: Elevation Plane Radiation Pattern

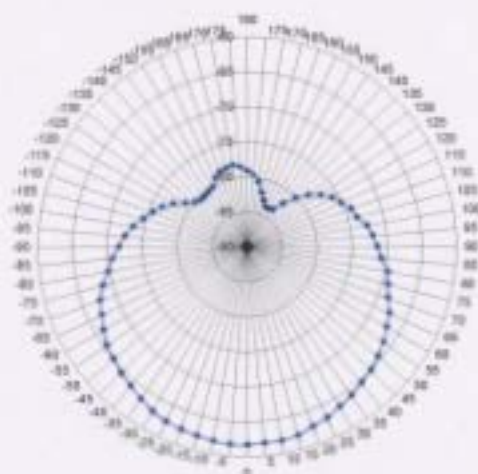


Figure 8-21: Tuned RMPA: Signal amplitude (dBm) as a function of elevation angle in polar coordinates.

Modified RMPA: Elevation Plane Radiation Pattern

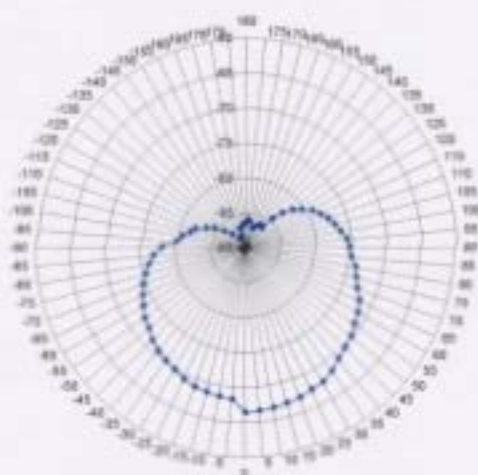


Figure 8-22: Modified RMPA: Signal amplitude (dBm) as a function of elevation angle in polar coordinates.

## 8.2 Return loss and VSWR measurements

This component of the RMPA testing was conducted at Superior Modular Products in North Carolina, USA. To measure the associated parameters of the reflection coefficient: return loss and VSWR, the three RMPAs were connected to an Agilent E5070B Vector Network Analyzer.

Measurements were made for each RMPA at various driving frequencies in the range of 1 MHz to 3 GHz. Although for the purposes of this work, only the measurements in the 800 MHz to 1 GHz range are presented and considered.

### 8.2.1 Control RMPA results

The actual measurements for the control RMPA are comparable to the simulation results for the control model in the sense that the plots are presented on a similar horizontal (frequency) scale. The simulation results in Figures 5-4 and 5-5 can be directly compared to real reflection coefficient related measurements in this section. Figure 8-23 is a plot of the real return loss for the control RMPA. The control RMPA resonates optimally at a frequency of 907 MHz at a level of  $-13.1$  dB. In simulation, the control model has resonate frequency of 896 MHz at the  $-19.4$  dB level. There is a frequency upshift of 11 MHz and a reduction of the level of resonance by 6.3 dB.

Using Table 8.2 it is possible to calculate the frequency bandwidth for the fabricated control RMPA. Using equation (2.2), the bandwidth is determined to be 1.40%. This bandwidth is approximately 25% less than the 1.88% of the control RMPA in

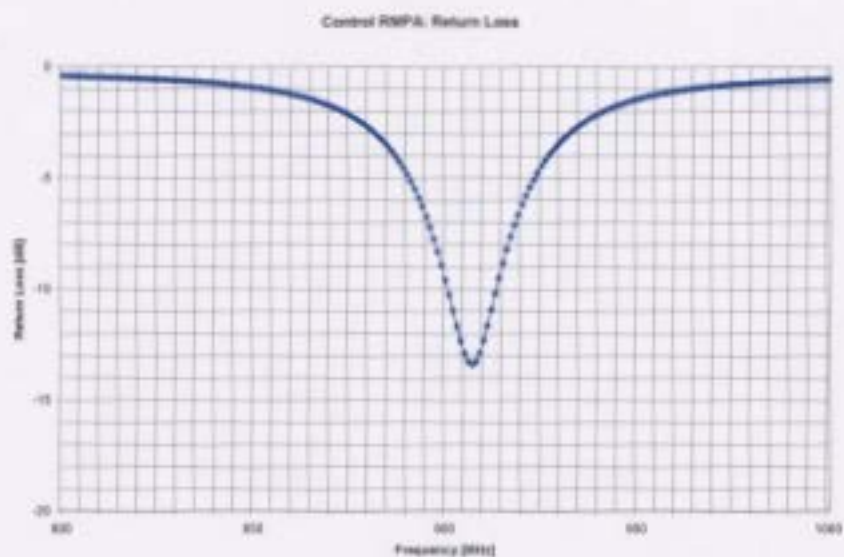


Figure 8-23: Control RMPA: Return Loss (dB) as a function of frequency ( MHz).

Frequency [MHz]	Return Loss [dB]
900	-9.594
901	-10.279
902	-10.987
903	-11.692
904	-12.351
905	-12.905
906	-13.281
907	-13.410
908	-13.266
909	-12.881
910	-12.315
911	-11.643
912	-10.926
913	-10.205
914	-9.497

Table 8.2: Real return loss for control RMPA

Frequency [MHz]	Return Loss [dB]
895	-6.746
896	-7.227
918	-7.123
919	-6.645

Table 8.3: Real return loss for control RMPA quality factor

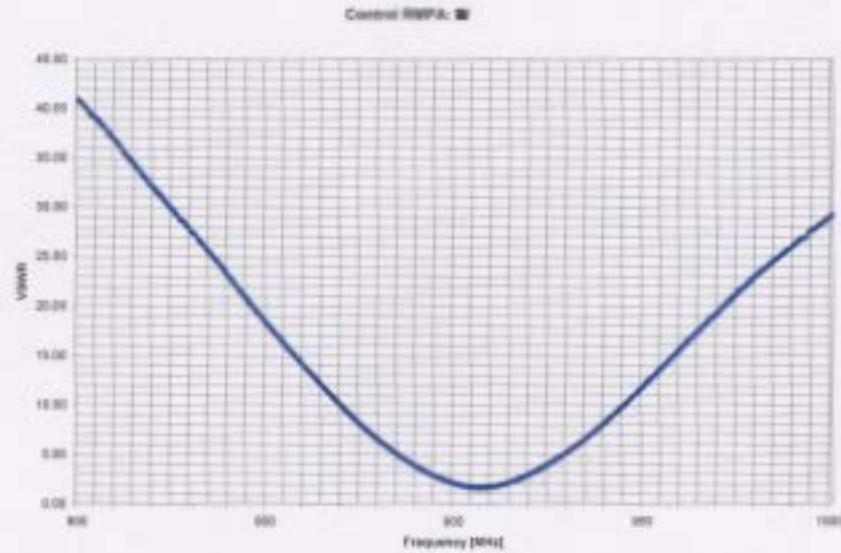


Figure 8-24: Control RMPA: VSWR as a function of frequency (MHz).

simulation.

The quality factor for the control RMPA is calculated using Table 8.3 and equation (2.3). It is determined to be  $Q = 39.9046$ . This value compares to  $Q = 34.199$  for the control antenna in simulation. The higher quality signifies that the actual control RMPA has more losses than in its modelled counterpart in simulation. The real VSWR for the control RMPA in Figure 8-24 exhibits a similar general symmetry to the simulated VSWR for the control RMPA model in Figure 5-5. However, the real VSWR realizes a minimum of 1.543 compared 1.240 for the simulated control RMPA.

As well, the real VSWR values increase faster as the distance (frequency shift) from the minimum grows. These comparisons naturally agree with the inferior resonance level and bandwidth of the real control RMPA.

Most importantly though, is that the upshift in frequency is significant enough such that the control RMPA is barely suitable for operation at the 900 MHz frequency. At this frequency the RMPA resonates at a level of  $-9.594$  dB and has a VSWR of 1.991. Such values indicate that the control RMPA is a satisfactory device for operation at the 900 MHz frequency, although it only just meets specifications and may not be tolerant to variation in electrical properties.

### **8.2.2 Tuned RMPA results**

The real measurements for the tuned RMPA compare to Figures 6-2 and 6-3. There is a general agreement with the simulation, but a similar resonant frequency pole shift and reduction in resonance level is encountered as was with the control RMPA. The actual return loss measurements for the tuned RMPA display a resonant frequency shift upwards to 917 MHz. The tuned RMPA resonates better than the control RMPA; it operates at  $-20.7$  dB. Although in simulation, the tuned RMPA resonates optimally at the  $-28.1$  dB level for an operating frequency of 899 MHz. There is an overall frequency upshift of 18 MHz and reduction in the level of resonance by 7.4 dB.

The bandwidth for the tuned RMPA is calculated using Table 8.4 and equation (2.2). The actual tuned RMPA has a bandwidth of 1.58%. This is an improvement

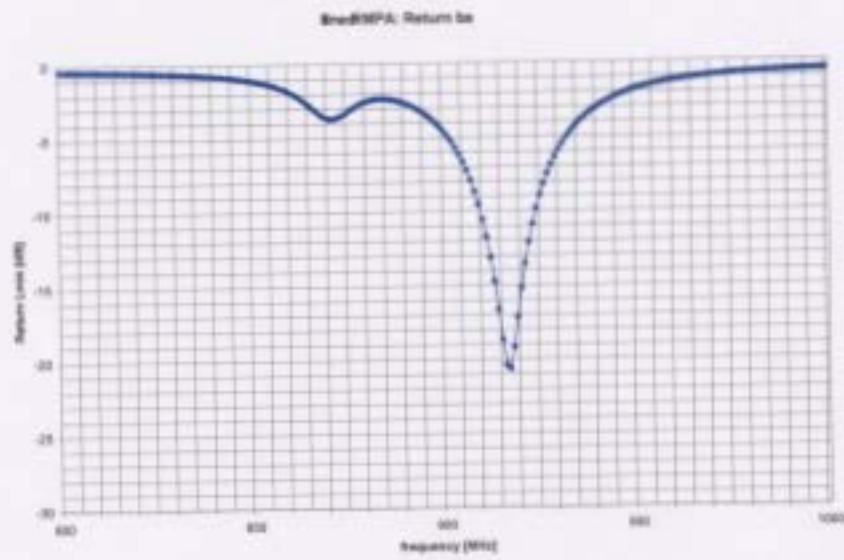


Figure 8-25: Tuned RMPA: Return Loss (dB) as a function of frequency (MHz).

Frequency [MHz]	Return Loss [dB]
909	-9.594
910	-10.606
911	-11.782
912	-13.156
913	-14.775
914	-16.664
915	-18.734
916	-20.451
917	-20.700
918	-19.235
919	-17.190
920	-15.246
921	-13.567
922	-12.144
923	-10.939
924	-9.897

Table 8.4: Real return loss for tuned RMPA

Frequency [MHz]	Return Loss [dB]
905	-6.704
906	-7.293
927	-7.541
928	-6.940

Table 8.5: Real return loss for tuned RMPA quality factor

over the control RMPA real bandwidth by approximately 13%. However, it falls short of the tuned RMPA simulated bandwidth by roughly the same amount of 13%. In terms of performance, independent of frequency, the tuned RMPA surpasses the control RMPA. The former has a superior level of resonance and larger bandwidth; however, the tuned RMPA experiences a greater frequency shift than the control RMPA compared to their respective simulation results. The tuned RMPA shift is 7 MHz over its control RMPA counterpart. This is approximately a 64 % increase in frequency shift. Perhaps the added geometrical complexity accounts for this increase in the frequency shift.

Next, the quality factor for the tuned RMPA can be found using Table 8.5 and equation (2.3). The quality factor for the actual tuned RMPA is  $Q = 40.9417$ . This compares to a quality factor of  $Q = 36.434$  for the tuned RMPA model in simulation.

The real VSWR plot for the tuned RMPA in Figure 8-26 has a similar pattern as the simulated VSWR for the tuned RMPA model in Figure 6-3. There is a local minimum to the left of the global minimum. The minimum is 4.678 at 871 MHz and is lower than the simulated VSWR local minimum of 7.904 at 841 MHz. Notice that the frequency shift in the local minimum is not the same as the frequency shift of

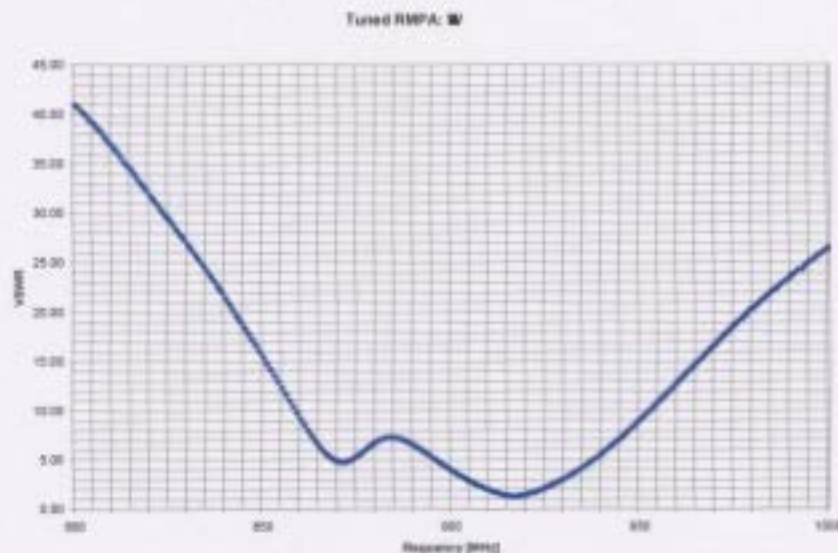


Figure 8-26: Tuned RMPA: VSWR as a function of frequency ( MHz).

the global minimum. It is a 30 MHz shift compared to 18 MHz. A possible reason for this may be the sensitivity of the dielectric constant to changes in frequency and that this susceptibility to frequency variation might not lead to a linear relationship in the horizontal frequency shift between the simulation and the actual return loss measurements. As well, it is possible the FR-4 may not be of the same production batch, resulting in different electrical properties ( $\epsilon_r$  and  $\tan \delta$ ).

At the intended operation frequency of 900 MHz, the tuned RMPA is unable to function adequately. It performs less satisfactorily at the desired 900 MHz frequency than the control RMPA. This notably contradicts the expectations based on the simulation results. The tuned RMPA manages a 3.836 VSWR and  $-4.636$  dB level at the 900 MHz frequency mark. These values do not meet the operational specification

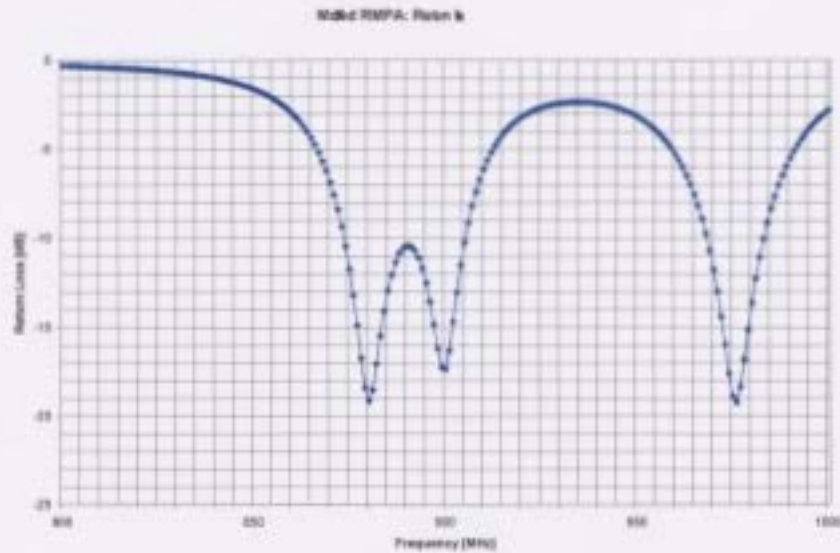


Figure 8-27: Modified RMPA: Return Loss (dB) as a function of frequency ( MHz).

because they are above the  $-9.54$  dB level established in Subsection 2.2.7.

### 8.2.3 Modified RMPA results

The actual measurements for the modified RMPA compare to Figures 7-4 and 7-5. Similarly to the previous parameter measurement sets for the control and tuned RMPAs, the actual measurements of the modified RMPA generally agree well with trends in the simulation. There is a consistency in the overall shape of the data. Also, the same general upward frequency shift occurs, but to an even greater extent in this case.

Figure 8-27 displays the actual measured return loss plot for the modified RMPA. Immediately note that at 900 MHz the level of resonance is  $-17.403$  dB. Therefore,

Frequency [MHz]	Return Loss [dB]
968	-9.767
969	-10.706
970	-11.785
971	-13.022
972	-14.442
973	-16.024
974	-17.656
975	-18.955
976	-19.276
977	-18.397
978	-16.849
979	-15.190
980	-13.655
981	-12.299
982	-11.113
983	-10.079
984	-9.167

Table 8.6: Real return loss for modified RMPA - upper pole

the modified RMPA build is suitable for operation at this frequency and appreciably surpasses the performance of the previous antenna builds.

The upper pole at 976 MHz resonates at the  $-19.276$  dB level. This compares to a  $-20.932$  dB level at 939 MHz for the simulated return loss. Thus, there is a frequency upshift of 37 MHz for the upper pole coupled with only a minimal drop in resonance level of 1.7 dB. The bandwidth for this higher frequency pole is calculated via Table 8.6 and equation (2.2). The upper pole for the modified RMPA has a bandwidth of 1.52%. This is a marginal increase over the bandwidth for the upper pole in the simulation results which was 1.49%.

The return loss points for the lower pole are in Table 8.7. The bandwidth for

Frequency [MHz]	Return Loss [dB]
873	-9.372
874	-10.478
879	-18.457
880	-19.215
881	-18.576
898	-16.253
899	-17.302
900	-17.403
901	-16.360
905	-10.274
906	-9.168

Table 8.7: Real return loss for modified RMPA - lower pole

this pole is calculated in a modified manner. Firstly,  $f_L$  and  $f_U$  are determined to be  $f_L = 873.5678$  MHz and  $f_U = 905.2441$  MHz. In the lower pole, there appear to be two peaks at 880 MHz and 900 MHz. For this reason, it is difficult to compare the measured results of the modified RMPA to the simulated results about the lower pole. An effort to rectify the actual and simulated measurements for this pole is made by using the centre frequency for the band in lieu of resonant frequency. The centre frequency,  $f_c$ , is employed in this instance unlike previous calculations which utilized the resonant frequency to determine the bandwidth because there is no definite resonant frequency for this band. That is  $f_c$  replaces  $f_r$  in equation (2.2) where

$$\begin{aligned}
 f_c &= f_L + \frac{f_U - f_L}{2} \\
 &= \frac{f_U + f_L}{2}.
 \end{aligned} \tag{8.1}$$

So

$$f_c = \frac{905.2441 + 873.5678}{2} = 889.4060 \text{ MHz},$$

therefore

$$B = \frac{905.2441 - 873.5678}{889.4060} = 0.0356.$$

This 3.56% bandwidth is a notable improvement over the simulation result of 3.19 %. In the case of the lower pole from the simulated data for the modified RMPA (Figure 7-4) it is possible to isolate two peaks. This was not done earlier because there is a much smaller spread in the frequency for that lower pole in the simulated return loss and replacing  $f_r$  with  $f_c$  is not that significant. If the two peaks of the lower pole are isolated then we have the first peak at a level of  $-22.079$  dB for 856 MHz and a lower peak at the  $-24.204$  dB level for 866 MHz. If these two peaks correspond to the 880 MHz and 900 MHz peaks for the lower pole then we see there is a 24 MHz upshift and 2.864 dB drop for the first peak and a 34 MHz frequency shift and 6.801 dB drop in resonance. The centre frequency for the lower pole in simulation is 846.7 MHz (by way of equation (8.1) and the bandwidth calculations for this pole). Hence there is frequency upshift measuring 42.704 MHz

In simulation for the modified RMPA, there is a frequency spread of 92.3 MHz between the upper pole's resonant frequency and the centre frequency for the lower pole. This compares to frequency spread of 86.59 MHz between the upper pole and lower pole centre frequency for the measured return loss. The frequency spread between the

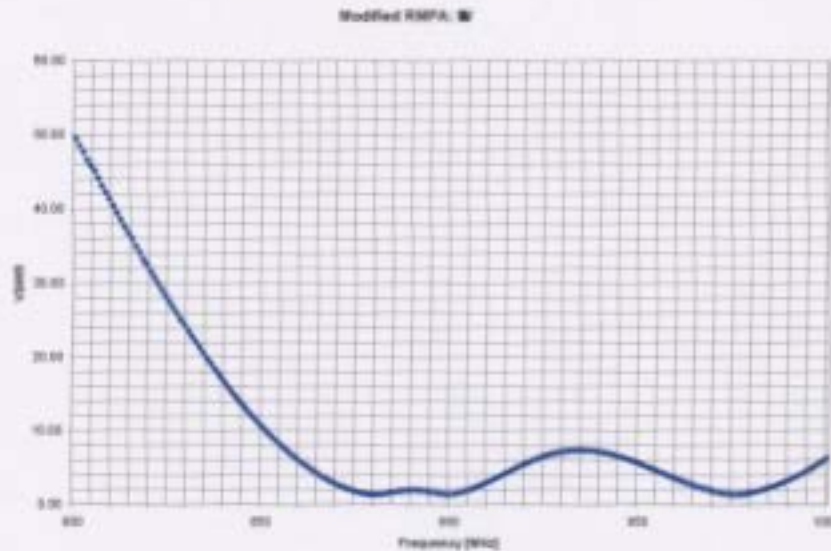


Figure 8-28: Modified RMPA: VSWR as a function of frequency ( MHz).

two poles is fairly consistent in magnitude between the simulated and actual return loss for this antenna.

The VSWR plot for the actual measurements in Figure 8-28 has the same general pattern as the simulated VSWR for the modified RMPA with a noticeable frequency upshift and tendency toward rapid VSWR increase as the frequency spread from the local minima increases.

#### 8.2.4 Summary statistics

Parameter values related to return loss from simulation and actual measurements are provided in table format for comparison purposes.

Table 8.8 contains the resonant frequency, return loss level at resonant frequency,

RMPA	Control		Tuned		Modified			
	sim.	actual	sim.	actual	sim.		actual	
Pole					low	high	low	high
$f_r$ (MHz)	896	907	899	917	864	939	889.4	976
$RL$ (dB)	-19.40	-13.41	-28.10	-20.70	-24.02	-20.93	$\sim -18$	-19.28
$B$	1.87%	1.40%	1.81%	1.58%	3.17%	1.49%	3.56%	1.52%
$Q$	34.20	39.91	36.43	40.94	<i>n/a</i>	<i>n/a</i>	<i>n/a</i>	<i>n/a</i>

Table 8.8: Parameters of interest: simulation versus actual

RMPA	Control	Tuned	Modified		
			low		high
Freq. Shift	11 MHz	18 MHz	24 MHz	34 MHz	37 MHz
Reduction	6.3 dB	7.4 dB	2.9 dB	6.8 dB	1.7 dB

Table 8.9: Frequency shifts and pole reductions

bandwidth and quality factor for each RMPA model from the simulation and the actual post fabrication measurements. In the case of the actual measurements for the modified RMPA, the centre frequency replaces the resonant frequency and an approximate return loss level for the lower pole. Also, note that no quality factor is given for the modified RMPA in simulation and actual measurements for either the lower or higher poles. This is because the method of calculation employed for this parameter does not support the dual band nature of this MPA.

Table 8.9 is a summary of Table 8.8 which captures the upward shift in frequency between the RMPA models in simulation and post fabrication. The table highlights the reduction in the level of resonance for the resonant poles pre and post fabrication as well.

# Chapter 9

## Conclusion

The original design criteria to fabricate a microstrip patch antenna with sufficient bandwidth to overcome manufacturing variability ( $\epsilon_r$ ,  $\tan \delta$  and etching variance) and achieve a specified level of operability at a given frequency have been satisfied. This goal has been achieved in a cost effective manner by using only an inexpensive dielectric substrate material and without adding active hardware components to the fabricated MPA, but rather modifying a basic design with several coplanar design elements to affect impedance and thereby influence frequency bandwidth. This end goal was achieved using a course of simulation and one fabrication only. That is, there was no second revision component employed as part of satisfying specifications. Moreover, the novel modified design presented in this thesis performed comfortably according to specification, whereas the control MPA designed according to purely analytic means barely satisfied specification and the tuned antenna designed using

simulated frequency tuning methods did not achieve a suitable level of operability at the desired frequency. In terms of return loss, the modified RMPA is a noticeable improvement over the control RMPA and successfully satisfies the design goals.

## 9.1 Summary

The RMPAs fabricated were determined to perform according to the generally accepted radiation attributes for this type of antenna technology. The actual MPA radiation pattern measurements agree well with simulation predictions. Radiation through the ground is at acceptable levels and the fabricated RMPAs clearly display the characteristic radiation pattern of MPAs. Based on this component of the measurements it is possible to conclude that the MPA fabrication process at Memorial University of Newfoundland's Technical Services is fundamentally sound and capable of producing quality MPA hardware builds that can satisfy basic specifications. Therefore, the facilities and resources on hand permit further MPA research.

The consistency in peak radiation pattern for the control, tuned and modified RMPAs compared with their respective models and their relative drop off from peak values in terms of azimuthal and elevation plane measurements confirm the utility of simulation in predicting radiation pattern characteristics for RMPAs. Furthermore, the near perfect symmetries in the azimuthal plane measurements for all three RMPAs signify the quality of the radiation pattern measurements test configuration in the anechoic chamber environment. These latter results confirm the choice of transmitting

device at 900 MHz as a sensible option and verify the current quality of the Thermal Lab's anechoic chamber environment for test at this frequency. If there was significant energy reflection it likely would have been noticed in the azimuthal plane patterns. The directional nature of the transmission antenna may have masked some reflected energies, but not all.

The return loss and VSWR measurements display a general trend toward a frequency upshift from simulation which was mentioned in the literature. In addition to this upshift, a slight increase (worsening) in the level of resonance for poles is suggestive that perhaps the dielectric substrate actually had  $\epsilon_r < 4.4$  and  $\tan \delta < 0.02$ . The measurements confirm that each of MPA builds is operable (resonates at less than  $-10$  dB) at some frequency in the 800 MHz to 1 GHz range. The measured return loss exhibited a nonlinear relationship in the frequency shift between simulation and actual results. This is not surprising given the dynamic nature of antenna design and the propensity of MPAs to be very reactive to even minor variations. In the case of most poles, there was also a minor drop in the measured level of resonance between simulation and the corresponding poles, post fabrication.

Futhermore, this exercise confirms the utility of simulation as an MPA design tool. However, it was shown that an understanding of the physical nature of a problem is essential. In the context of this work, it was shown that improving a model via simulation can actually worsen the fabrication result. The control RMPA displayed greater functionality at the 900 MHz frequency than the tuned RMPA ( $-9.59$  dB

versus  $-4.64$  dB). It is inadvisable to depend on simulation blindly for this type of work. Indeed, it was the expectation of some sort of frequency shifting and a subsequent splitting of the frequency band in simulation that resulted in a successful modified RMPA fabrication according to specification. A combination of simulation for electromagnetic behavioural tendencies and experience results in the best overall design process.

## 9.2 Original contributions

The individual design elements employed to realize specifications are not novel; however, combining both elements in the same MPA design is an original effort. The addition of the coupling strips separates the design of this thesis from the previous work of [10]. As well, study of the radiation patterns is not widely popular in the literature because of a lack of access to an anechoic chamber resource and is an enriching aspect of this work.

## 9.3 Recommendations

Additional fabrication runs and revisions would permit an enhanced understanding of the MPA fabrication process. In this manner, one could loosely quantify an expected frequency shift range based on frequency and MPA design complexity.

If time is a constraint in the manufacturing process then fabrication of several

versions of the same model with slight dimensional variation is a method to achieve satisfactory results. Developing a pre-qualification process to determine  $\epsilon_r$  and  $\tan \delta$  is advisable. Some, if only limited, foreknowledge of frequency shift quality coupled with simulation examination will allow a designer to vary model dimensions sufficiently for specification satisfaction.

The Thermal Laboratory's anechoic chamber environment is an important resource for study of antennas in the UHF band and above. An infrastructure investment in this resource is required for maintenance. The acquisition of appropriate hardware capable of measuring MPA parameters is recommended in order to sustain and stimulate further research in this area. Currently, the in house hardware is only capable of examining radiation patterns up to 990 MHz only.

A vector network analyzer is not available within Memorial University. There is no local capacity to measure the reflection coefficient and its associated parameters. That measurement component of the thesis was outsourced.

## **9.4 Future work**

There are several concepts arising from this thesis which are available for further examination and research. As mentioned in the recommendations, a better understanding of the post fabrication frequency shift is advisable. Exploration of the relationship between frequency and MPA design complexity can be undertaken immediately and could be done, so utilizing the resources used in this thesis. A quantitative assessment

of this shift would be a substantial contribution to the current body of MPA research.

Establishing a comprehensive metric to measure MPA design complexity would be a valuable contribution and novel to the area. It may be possible to assign a numeric value or apply a grading scale to MPA configurations based on feed technique, and layering and geometrical considerations such as dimension, area and number of edges.

A microscopic study of the physical MPA footprint and slight geometrical variations resulting from etching orientation would be of interest. For instance, if etching is done perpendicular to an edge or parallel to an edge, then is there a measurable effect on MPA parameters? Also, a quantitative study of etching errors and their effect on resonance levels and frequency shifts would be novel.

# Bibliography

- [1] G. Deschamps and W. Sichak, "Microstrip microwave antennas," *Proc. 3<sup>rd</sup> Symposium on the USAF Antenna Research and Development Program*, Oct. 1953.
- [2] H. Gutton and G. Baissinot, "Flat aerial for ultra high frequencies," French Patent No. 703113, 1955.
- [3] J. Howell, "Microstrip antennas," *Antennas Propag. Soc. Int. Symp.*, 1972, pp. 177-180.
- [4] J. Howell, "Microstrip antennas," *IEEE Trans. Antennas Propag.*, vol. 23, no. 1, pp. 90-93, Jan. 1975.
- [5] R. Munson, "Conformal microstrip arrays and microstrip phased arrays," *IEEE Trans. Antennas Propag.*, vol. 22, no. 1, pp. 74-78, Jan. 1974.
- [6] J. James, P. Hall, and C. Wood, *Microstrip Antenna - Theory and Design*, London, UK: Peter Peregrinus Ltd., 1981.

- [7] D. Pozar, "Microstrip antennas," *Proc. IEEE*, vol. 80, no. 1, pp. 79-91, Jan. 1992.
- [8] W. Kahn, ed. *IEEE Trans. Antennas Propag.*, vol. 29, no. 1, Jan. 1981.
- [9] J. Zürcher and F. Gardiol, *Broadband Patch Antennas*, Boston, MA: Artech House, 1995.
- [10] H. Pues and A Van de Capelle, "An impedance-matching technique for increasing the bandwidth of microstrip antennas," *IEEE Trans. Antennas Propag.*, vol. 37, no. 11, pp. 1345-1354, Nov. 1989.
- [11] C. Balanis, *Antenna Theory - Analysis and Design*, 2<sup>nd</sup> ed., New York, NY: John Wiley and Sons, 1997.
- [12] W. Stutzman and G. Thiele, *Antenna Theory and Design*, 2<sup>nd</sup> ed., New York, NY: John Wiley and Sons, 1998.
- [13] "IEEE Standard Definitions of Terms for Antennas," Std 145-1983, pp. 1-29. June 22, 1983.
- [14] D. Pozar, *Microwave Engineering*, 3<sup>rd</sup> ed., New York, NY: John Wiley and Sons, 2005.
- [15] R. Garg, P. Bhartia, I. Bahl and A. Ittipiboon, *Microstrip Antenna Design Handbook*, Boston, MA: Artech House, Inc., 2001.

- [16] J. James and P. Hall, "Introduction" in *Handbook of Microstrip Antennas*, vol. 1, J. James and P. Hall, Ed., London: UK, Peter Peregrinus Ltd., 1989.
- [17] H. An, B. Nauwelaers and A. Van de Capelle, "Matching network design of microstrip antennas with simplified real frequency technique," *IEEE Electron. Lett.*, vol. 27, no. 24, pp. 2295-2297, Nov. 1991.
- [18] R. Munson, "Microstrip phased array antennas," *Proc. 22<sup>nd</sup> Symposium on the USAF Antenna Research and Development Program*, Oct. 1972.
- [19] A. Derneryd, "Linearly polarized microstrip antennas," *IEEE Trans. Antennas Propag.*, vol. 24, no. 6, pp. 846-851, Nov. 1976.
- [20] A. Derneryd, "A theoretical investigation of the rectangular microstrip antenna element," *IEEE Trans. Antennas Propag.*, vol. 26, no. 4, pp. 532-535, Jul. 1978.
- [21] Y. Lo, D. Soloman and W. Richards, "Theory and experiment on microstrip antennas," *IEEE Trans. Antennas Propag.*, vol. AP-27, no. 2, pp. 137-145, Mar. 1979.
- [22] J. Bernhard, P. Mayes, D. Schaubert and R. Mailloux, "A commemoration of Deschamps' and Sichak's 'Microstrip microwave antennas': 50 years of development, divergence, and new directions," *Proc. 2003 Antenna Application Symposium*, Sep. 2003.

- [23] J. Kerr, "Microstrip polarization techniques," *Proc. 1978 Antenna Application Symposium*, Sep. 1978.
- [24] W. Richards, Y. Lo and D. Harrison, "An improved theory for microstrip antennas and applications," *IEEE Trans. Antennas Propag.*, vol. AP-29, no. 1, pp. 38-46, Jan. 1981.
- [25] W. Richards, Y. Lo and P. Simon, "Design and theory of circularly polarized microstrip antennas," *IEEE Antennas Propag. Soc. Int. Symposium*, vol. 17, Jun. 1979, pp. 117-120.
- [26] J. Row, "The design of a squarer-ring slot antenna for circular polarization," *IEEE Trans. Antennas Propag.*, vol. 53, no. 6, pp. 1967-1972, Jun. 2005.
- [27] Y. Lo, B. Engst and R. Lee, "Simple design formulas for circularly polarised microstrip antennas," *IEE Proc. H Microw, Antennas Propag.*, vol. 135, no. 3, Jun. 1988, pp. 213-215.
- [28] R. Dearnley and A. Barel, "A comparison of models to determine the resonant frequencies of a rectangular microstrip antenna," *IEEE Trans. Antennas Propag.*, vol. 37, no. 1, pp. 114-118, Jan. 1989.
- [29] H. Jones, D. Schaubert and F. Reggia, "A conformal, dielectric filled edge-slot antenna for bodies of revolution," *Proc. 1977 Antenna Application Symposium*, Apr. 1977.

- [30] D. Schaubert, F. Farrar, A. Sindoris and S. Hayes, "Frequency agile microstrip antennas," *IEEE Antennas Propag. Soc. Int. Symposium*, vol. 18, Jun. 1980, pp. 601-604.
- [31] D. Schaubert, F. Farrar, A. Sindoris and S. Hayes, "Microstrip antennas with frequency agility and polarization diversity," *IEEE Trans. Antennas Propag.*, vol. 29, no. 1, pp. 118-123, Jan. 1981.
- [32] L. Xiu-zhen, F. Shao-jun and T. Ke-jun, "Analysis and optimization design of compact microstrip patch antennas loaded with shorting pins," *IEEE IWAT 2005: Small Antenna and Novel Metamaterials*, Mar. 2005, pp. 529-533.
- [33] J. Kerr, "Other microstrip antennas applications," *Proc. 1977 Antenna Application Symposium*, Apr. 1977.
- [34] D. Schaubert, F. Farrar, A. Sindoris and S. Hayes, "Post-tuned microstrip antennas for frequency-agile and polarization-diverse applications," US Army Electron. Research and Development Report, HDL-TM-81-8, Mar. 1981.
- [35] D. Sanchez-Hernandez and I. Robertson, "Analysis and design of a dual-band circularly polarized microstrip patch antenna," *IEEE Trans. Antennas Propag.*, vol. 43, no. 2, pp. 201-205, Feb. 1995.
- [36] K. Tong, K. Luk, K. Lee and R. Lee, "A broad-band U-slot rectangular patch antenna on a microwave substrate," *IEEE Trans. Antennas Propag.*, vol. 48, no. 6, pp. 954-960, Jun. 2000.

- [37] S. Weigand, G. Huff, K. Pan and J. Bernhard, "Analysis and design of broadband single-layer rectangular U-slot microstrip patch antennas," *IEEE Trans. Antennas Propag.*, vol. 51, no. 3, pp. 457–468, Mar. 2003.
- [38] B. Ooi, "A double- $\Pi$  stub proximity feed U-slot patch antenna," *IEEE Trans. Antennas Propag.*, vol. 52, no. 9, pp. 2491–2496, Sep. 2004.
- [39] J. Lu, "Bandwidth enhancement design of single-layer slotted circular microstrip antennas," *IEEE Trans. Antennas Propag.*, vol. 51, no. 5, pp. 1126–1129, May 2003.
- [40] J. Lu, C. Tang and K. Wong, "Single-feed slotted equilateral-triangular microstrip antenna for circular polarization," *IEEE Trans. Antennas Propag.*, vol. 47, no. 7, pp. 1174–1178, Jul. 1999.
- [41] R. Lelaratne and R. Langley, "Dual-band patch antenna for mobile satellite systems," *IEE Proc. Microw, Antennas Propag.*, vol. 147, no. 6, Dec. 2000, pp. 427–430.
- [42] R. Lelaratne and R. Langley, "Compact mobile communication antennas," *IEE 11th Int. Conf. Antennas Propag.*, vol. 1, Apr. 2001, pp. 340–343.
- [43] C. Sim, K. Lin and J. Row, "Design of an annular-ring microstrip antenna for circular polarization," *IEEE Antennas Propag. Soc. Int. Symposium*, vol. 1, Jun. 2004, pp. 471–474.

- [44] H. Ohmine, Y. Sunahara, M. Matsunaga and S. Mano, "Car-top annular-ring microstrip antenna," *IEEE Antennas Propag. Soc. Int. Symposium*, vol. 3, May. 1990, pp. 1136–1139.
- [45] H. Ohmine, Y. Sunahara and M. Matsunaga, "An annular-ring microstrip antenna fed by a co-planar feed circuit for mobile satellite communication use," *IEEE Trans. Antennas Propag.*, vol. 45, no. 6, pp. 1001–1008, Jun. 1997.
- [46] S. Onat, L. Alatan and S. Demir, "Design of triple-band reconfigurable microstrip antenna employing RF-MEMS switches," *IEEE Antennas Propag. Soc. Int. Symposium*, vol. 2, Jun. 2004, pp. 1812–1815.
- [47] J. Kuo and C. Huang, "Novel design concept of gain enhancement circularly polarized microstrip antennas," *IEEE IWAT 2005: Small Antenna and Novel Metamaterials*, Mar. 2005, pp. 230-233.
- [48] J. Lu, H. Yu and K. Wong, "Compact circular polarisation design for equilateral-triangular microstrip antenna with spur lines," *IEEE Electron. Lett.*, vol. 34, no. 21, pp. 1989-1990, Oct. 1998.
- [49] S. Palit and A. Hamadi, "Design and development of wideband and dual-band microstrip antennas," *IEE Proc. Microw, Antennas Propag.*, vol. 146, no. 1, Feb. 1999, pp. 35–39.

- [50] A. Shackelford, K. Lee and K. Luk, "Design of a small-size wide-bandwidth microstrip-patch antennas," *IEEE Antennas Propag. Mag.*, vol. 45, no.1, pp. 75-83, Feb. 2003.
- [51] G. Oh and Y. Kim, "A design of asymmetric double T-type microstrip dipole antennas," *Int. Symposium of Commun. Inf. Tech.*, Oct. 2004, pp. 720-725.
- [52] K. Loi, S. Uysal and M. Leong, "Design of a wideband microstrip bowtie patch antenna," *IEE Proc. Microw, Antennas Propag.*, vol. 145, no. 2, Apr. 1998, pp. 137-140.
- [53] H. Choo and H. Ling, "Design of multiband microstrip antennas using a genetic algorithm," *IEEE Microw. Guided Wave Lett.*, vol. 12, no. 9, pp. 345-347, Sep. 2002.
- [54] D. Guha, "Microstrip and printed antennas : recent trends and developments," *6th Int. Conf. Telecommun. in Modern Sat. Cable Broadcasting Service (TEL-SIKS 2003)*, vol. 1, Oct. 2003, pp. 39-44.
- [55] P. Grajek, B. Schoenlinner and G. Rebeiz, "A 24-GHz high-gain Yagi-Uda antenna array," *IEEE Trans. Antennas Propag.*, vol. 52, no. 5, pp. 1257-1261, May 2004.
- [56] Z. Dafalla, W. Kuan, A. Rahman and S. Shudakar, "Design of a rectangular microstrip patch antenna at 1 GHz," *IEEE Proc. RF Microw.*, Oct. 2004, pp. 145-149.

- [57] P. Hall, J. Dahele and J. James, "Design principles of sequentially fed, wide bandwidth, circularly polarised microstrip antennas," *IEE Proc. H Microw, Antennas Propag.*, vol. 136, no. 5, Oct. 1989, pp. 381-389.
- [58] J. Yun, H. Noh, S. Jeon and C. Kim, "Design and analysis of TX/RX dual microstrip antenna using FDTD at Ku-band" *IEEE Electron. Lett.*, vol. 39, no. 17, pp. 1228-1230, Aug. 2003.
- [59] H. Kim, Y. Lee, C. Won and H. Lee, "Design of compact dual-band microstrip patch antenna for GPS/K-PCS operation," *IEEE Antennas Propag. Soc. Int. Symposium*, vol. 4, Jun. 2004, pp. 3529-3532.
- [60] B. Lim, E. Korolkiewicz and S. Scott, "Optimised design of corner microstrip fed nearly square patch antenna for circular polarisation," *IEEE Electron. Lett.*, vol. 32, no. 7, pp. 610-612, Mar. 1996.
- [61] S. Lee, A. Sambell, E. Korolkiewicz, S. Ooi and Q. Yi, "Design of a circular polarized nearly square microstrip patch antenna with offset feed," *High Frequency Postgraduate Student Colloquim*, Sep. 2004, pp. 61-66.
- [62] Q. Yi, E. Lim and E. Korolkiewicz, "Design of microstrip offset feed circular polarised nearly square patch antenna operating at 2.45 GHz," *IEEE Electron. Lett.*, vol. 38, no. 16, pp. 844-845, Aug. 2002.

- [63] M. Niroojazi and M. Azarmanesh, "Practical design of single feed truncated corner microstrip antenna," *Proc. 2<sup>nd</sup> Conf. Commun. Netw. Services Research*, May 2004, pp. 25–29.
- [64] G. Kirov, A. Abdel-Rahman, G. Nadim and A. Omar, "Impedance matching improvement for a class of wideband antennas," *IEEE Antennas Propag. Mag.*, vol. 46, no.6, pp. 98-101, Dec. 2004.
- [65] D. Kurup, A. Rydberg and M. Himdi, "Compact microstrip-T coupled patch antenna for dual polarisation and active antenna applications," *IEEE Electron. Lett.*, vol. 38, no. 21, pp. 1240-1241, Oct. 2002.
- [66] Y. Sung and Y. Kim, "An improved design of microstrip patch antennas using compact microstrip resonant cell," *IEEE Antennas Propag. Soc. Int. Symposium*, vol. 1, Jun. 2004, pp. 966–969.
- [67] Y. Sung and Y. Kim, "An improved design of microstrip patch antennas using photonic bandgap structure," *IEEE Trans. Antennas Propag.*, vol. 53, no. 5, pp. 1799–1804, May 2005.
- [68] H. Oltman and D. Huebner, "Electromagnetically coupled microstrip dipoles," *IEEE Trans. Antennas Propag.*, vol. 29, no. 1, pp. 151–157, Jan. 1981.
- [69] P. Katehi and N. Alexopoulos, "On the modeling of electromagnetically coupled microstrip antennas—the printed strip dipole," *IEEE Trans. Antennas Propag.*, vol. 32, no. 11, pp. 1179–1186, Nov. 1984.

- [70] R. Cock and C. Christodoulou, "Design of a two-layer, capacitively coupled, microstrip patch antenna element for broadband applications," *IEEE Antennas Propag. Soc. Int. Symposium*, vol. 25, Jun. 1987, pp. 936–939.
- [71] H. Iwasaki, "A circularly polarized rectangular microstrip antenna using single-fed proximity-coupled method," *IEEE Trans. Antennas Propag.*, vol. 43, no. 8, pp. 895–897, Aug. 1995.
- [72] H. Iwasaki, "A circularly polarized small-size microstrip antenna with a cross slot," *IEEE Trans. Antennas Propag.*, vol. 44, no. 10, pp. 1399–1401, Oct. 1996.
- [73] S. Duffy, "An enhanced bandwidth design technique for electromagnetically coupled microstrip antennas," *IEEE Trans. Antennas Propag.*, vol. 48, no. 2, pp. 161–164, Feb. 2000.
- [74] D. Pozar, "A microstrip antenna aperture coupled to a microstrip line," *IEEE Electron. Lett.*, vol. 21, pp. 49–50, Jan. 1985.
- [75] P. Sullivan and D. Schaubert, "Analysis of an aperture coupled microstrip antenna," *IEEE Trans. Antennas Propag.*, vol. 34, no. 8, pp. 977–984, Aug. 1986.
- [76] G. Gronau and I. Wolff, "Aperture-coupling of a rectangular microstrip resonator," *IEEE Electron. Lett.*, vol. 22, pp. 554–556, May 1986.

- [77] D. Pozar, "An update on microstrip antenna theory and design including some novel feeding techniques," *IEEE Antennas Propag. Soc. Newsletter*, vol. 28, no. 5, pp. 4–9, Oct. 1986.
- [78] T. Vlasits, E. Korolkiewicz, A. Sambell and B. Robinson, "Performance of a cross-aperture coupled single feed circularly polarised patch antenna," *IEEE Electron. Lett.*, vol. 32, no. 7, pp. 612-613, Mar. 1996.
- [79] T. Vlasits, E. Korolkiewicz and A. Sambell, "Analysis of cross-aperture coupled patch antenna using transmission line model," *IEEE Electron. Lett.*, vol. 32, no. 21, pp. 1934-1935, Oct. 1996.
- [80] C. Huang, J. Wu and K. Wong, "Cross-slot-coupled microstrip antenna and dielectric resonator antenna for circular polarization," *IEEE Trans. Antennas Propag.*, vol. 47, no. 4, pp. 605–609, Apr. 1999.
- [81] B. Al-Jibouri, T. Viasits, E. Korolkiewicz, S. Scott and A. Sambell, "Transmission-line modelling of the cross-aperture-coupled circular polarised microstrip antenna," *IEE Proc. Microw, Antennas Propag.*, vol. 147, no. 2, Apr. 2000, pp. 82–86.
- [82] D. Pozar and S. Targonski, "Improved coupling for aperture coupled microstrip antennas," *IEEE Electron. Lett.*, vol. 27, no. 13, pp. 1129-1131, Jun. 1991.

- [83] P. Mayes and M. Thomas, "A broad-band, unidirectional, two-port microstrip patch antenna," *IEEE Trans. Antennas Propag.*, vol. 38, no. 5, pp. 760–763, May 1990.
- [84] S. Targonski and D. Pozar, "Design of wideband circularly polarized aperture-coupled microstrip antennas," *IEEE Trans. Antennas Propag.*, vol. 41, no. 2, pp. 214–220, Feb. 1993.
- [85] S. Gao, L. Li, M. Leong and T. Yeo, "A broad-band dual-polarized microstrip patch antenna with aperture coupling," *IEEE Trans. Antennas Propag.*, vol. 51, no. 4, pp. 898–900, Apr. 2003.
- [86] X. Liang Y. Zhang, S. Zhong and W. Wang, "Design of dual-polarized microstrip patch antennas with excellent polarization purity," *Proc. 3rd Int. Conf. Computational Electromagnetics Appl. (ICCEA 2004)*, Nov. 2004, pp. 197–199.
- [87] J. Xiao and M. Zhu, "Design of a compact and wideband microstrip antenna array," *Proc. 3rd Int. Conf. Computational Electromagnetics Appl. (ICCEA 2004)*, Nov. 2004, pp. 171–173.
- [88] K. Wong, H. Tung and T. Chiou, "Broadband dual-polarized aperture-coupled patch antennas with modified H-shaped coupling slots," *IEEE Trans. Antennas Propag.*, vol. 50, no. 2, pp. 188–191, Feb. 2002.

- [89] T. Chiou and K. Wong, "A compact dual-band dual-polarized patch antenna for 900/1800-MHz cellular systems," *IEEE Trans. Antennas Propag.*, vol. 51, no. 8, pp. 1936–1940, Aug. 2003.
- [90] K. Wong and T. Chiou, "Broadband dual-polarized patch antennas fed by capacitively coupled feed and slot-coupled feed," *IEEE Trans. Antennas Propag.*, vol. 50, no. 3, pp. 346–351, Mar. 2002.
- [91] K. Lau and K. Luk, "A novel wide-band circularly polarized patch antenna based on L-probe and aperture-coupling techniques," *IEEE Trans. Antennas Propag.*, vol. 53, no. 1, pp. 577–582, Jan. 2005.
- [92] J. Litva, C Wu, Z. Bi and K. Wu, "Some considerations for microstrip coplanar-waveguide antennas," *IEEE Antennas Propag. Soc. Int. Symposium*, vol. 1, Jul. 1992, pp. 491–494.
- [93] J. Greisler, "Coplanar stripline antenna," *Microw J.*, pp. 47-49, Oct. 1976.
- [94] M. Aksun, S. Chuang and Y. Lo, "Coplanar waveguide-fed microstrip antennas," *Microw. Opt. Tech. Lett.*, vo. 4, no. 8, pp. 292-295, Jul. 1991.
- [95] S. Deng, M. Wu and P. Hsu, "Analysis of coplanar waveguide-fed microstrip antennas," *IEEE Trans. Antennas Propag.*, vol. 43, no. 7, pp. 734–737, Jul. 1995.

- [96] R. Simmons and R. Lee, "Coplanar waveguide aperture coupled patch antennas with ground plane/substrate of finite extent," *IEEE Electron. Lett.*, vol. 28, no. 1, pp. 75-76, Jan. 1992.
- [97] W. Menzel and W. Grabherr, "A microstrip patch antenna with coplanar feed line," *Microw. Guided Wave Lett.*, vol. 1, no. 11, pp. 340-342, Nov. 1991.
- [98] S. Deng, M. Wu and P. Hsu, "Impedance characteristics of microstrip antennas excited by coplanar waveguides with inductive or capacitive coupling slots," *Microw. Guided Wave Lett.*, vol. 5, no. 11, pp. 391-393, Nov. 1995.
- [99] A. Suzuki and M. Haneishi, "A broadband microstrip antenna fed by a coplanar waveguide with dogbone slot," *IEEE Antennas Propag. Soc. Int. Symposium*, vol. 3, Jul. 2001, pp. 494-497.
- [100] A. Omar, "Coplanar waveguide-fed-dual band microstrip patch antenna," *IEEE Antennas Propag. Soc. Int. Symposium*, vol. 4, Jun. 2003, pp. 568-571.
- [101] C. Huang and K. Wong, "Coplanar waveguide-fed circularly polarized microstrip antenna," *IEEE Trans. Antennas Propag.*, vol. 48, no. 2, pp. 328-329, Feb. 2000.
- [102] R. Lee and R. Simons, "Coplanar-waveguide aperture-coupled microstrip patch antenna," *Microw. Guided Wave Lett.*, vol. 2, no. 4, pp. 138-139, Apr. 1991.

- [103] S. Hudson and D. Pozar, "Grounded coplanar waveguide-fed aperture-coupled cavity-backed microstrip antenna," *IEEE Electron. Lett.*, vol. 36, no. 12, pp. 1003-1005, Jun. 2000.
- [104] R. Simons, R. Lee, K. Shalkhausere, J. Owens, J. Demarco, J. Leen, and D. Sturzebecher, "Finite width coplanar waveguide patch antenna with vertical fed through interconnect," *IEEE Antennas Propag. Soc. Int. Symposium*, vol. 2, Jul. 1996, pp. 1338-1341.
- [105] R. Smith and J. Williams, "Coplanar waveguide feed for microstrip patch antennas," *IEEE Electron. Lett.*, vol. 28, no. 25, pp. 2272-2274, Dec. 1992.
- [106] H. Iwasaki, "A back-to-back rectangular-patch antenna fed by a CPW," *IEEE Trans. Antennas Propag.*, vol. 46, no. 10, pp. 1527-1530, Oct. 1998.
- [107] D. Jahagirdar and R. Stewart, "Non-leaky conductor-backed coplanar waveguide-fed microstrip patch antenna," *High Frequency Postgraduate Student Colloquim*, Sep. 1997, pp. 94-99.
- [108] K. Wong, *Compact and Broadband Microstrip Antennas*, New York, NY: John Wiley and Sons, 2002.
- [109] D. Sanchez-Hernandez and I. Robertson, "A survey of broadband microstrip patch antennas," *Microw J.*, pp. 1-10, Sept. 1996.

- [110] G. Kumar and K. Ray, *Broadband Microstrip Antennas*, Boston, MA: Artech House, Inc., 2003.
- [111] Ansoft Designer Version 3.5. Pittsburgh, PA, Ansoft Corporation, 2006.
- [112] E. Newman and P. Tulyathan, "Analysis of microstrip antennas using moment methods," *IEEE Trans. Antennas Propag.*, vol. 29, no. 1, pp. 47–53, Jan. 1981.
- [113] D. Schaubert and F. Farrar, "Some conformal, printed circuit antenna design," *Proc. Workshop Print. Circuit Antenna Tech.*, Oct. 1979, pp. 5.1-5.21.
- [114] S. Egashira and E. Nishiyama, "Stacked microstrip antenna with wide bandwidth and high gain," *IEEE Trans. Antennas Propag.*, vol. 44, no. 11, pp. 1533–1534, Nov. 1996.
- [115] S. Bokhari, J. Zurcher, J. Mosig and F. Gardiol, "A small microstrip patch antenna with a convenient tuning option," *IEEE Trans. Antennas Propag.*, vol. 44, no. 11, pp. 1521–1528, Nov. 1996.
- [116] Z. Li, P. Papalambros and J. Volakis, "Designing broad-band patch antennas using the sequential quadratic programming method," *IEEE Trans. Antennas Propag.*, vol. 45, no. 11, pp. 1689–1692, Nov. 1997.
- [117] Z. Liu, P. Kooi, L. Li, M. Leong and T. Yeo, "A method for designing broad-band microstrip antennas in multilayered planar structures," *IEEE Trans. Antennas Propag.*, vol. 47, no. 9, pp. 1416–1420, Sep. 1999.

- [118] G. Kumar and K. Gupta, "Broadband microstrip antennas using coupled resonators," *IEEE Antennas Propag. Soc. Int. Symposium*, vol. 21, May. 1983, pp. 67–70.
- [119] G. Kumar and K. Gupta, "Broad-band microstrip antennas using additional resonators gap-coupled to the radiating edges," *IEEE Trans. Antennas Propag.*, vol. 32, no. 12, pp. 1375–1379, Dec. 1984.
- [120] G. Kumar and K. Gupta, "Nonradiating edges and four edges gap-coupled multiple resonator broad-band microstrip antennas," *IEEE Trans. Antennas Propag.*, vol. 33, no. 2, pp. 173–178, Feb. 1985.
- [121] C. Aanandan, P. Mohanan and K. Nair, "Theoretical analysis of compact and broad-band microstrip antenna with gap-coupled parasitic elements along the non-radiating edges," *IEEE Antennas Propag. Soc. Int. Symposium*, vol. 1, Jun. 1989, pp. 463–466.
- [122] R. Garg and V. Reddy, "A broad-band coupled-strips microstrip antenna," *IEEE Trans. Antennas Propag.*, vol. 49, no. 9, pp. 1344–1345, Sep. 2001.
- [123] J. Mosig and F. Gardiol, "The effect of parasitic elements on microstrip antennas," *IEEE Antennas Propag. Soc. Int. Symposium*, vol. 23, Jun. 1985, pp. 397–400.

- [124] C. Wu and K. Wong, "Broadband microstrip antenna with directly coupled and parasitic patches," *Microw. Opt. Tech. Lett.*, vo. 22, no. 5, pp. 348-349, Sep. 1999.
- [125] C. Aanandan and K. Nair, "Compact broadband microstrip antenna," *IEEE Electron. Lett.*, vol. 22, no. 20, pp. 1064-1065, Sep. 1986.
- [126] R. Fano, "Theoretical limitations on the broadband matching of arbitrary impedances," *J. Franklin Inst.*, vol. 249, no. 1-2, pp. 139-154, Jan.-Feb. 1950.
- [127] G. Matthaei, L. Young and E. Jones, *Microwave Filters, Impedance-Matching Networks, and Coupling Structures*, Boston, MA: Artech House, Inc., 1964.

# Appendix A

## Simulation Results

### A.1 Data

#### A.1.1 Control RMPA return loss

F (GHz)	RL (dB)	F (GHz)	RL (dB)	F (GHz)	RL (dB)
0.800	-0.53088	0.808	-0.58442	0.816	-0.65333
0.801	-0.53690	0.809	-0.59209	0.817	-0.66332
0.802	-0.54309	0.810	-0.60000	0.818	-0.67366
0.803	-0.54947	0.811	-0.60817	0.819	-0.68438
0.804	-0.55605	0.812	-0.61661	0.820	-0.69548
0.805	-0.56282	0.813	-0.62533	0.821	-0.70700
0.806	-0.56980	0.814	-0.63435	0.822	-0.71895
0.807	-0.57700	0.815	-0.64368	0.823	-0.73135

F (GHz)	RL (dB)	F (GHz)	RL (dB)	F (GHz)	RL (dB)
0.824	-0.74422	0.843	-1.12411	0.862	-2.12190
0.825	-0.75759	0.844	-1.15471	0.863	-2.21337
0.826	-0.77149	0.845	-1.18687	0.864	-2.31123
0.827	-0.78594	0.846	-1.22070	0.865	-2.41605
0.828	-0.80097	0.847	-1.25631	0.866	-2.52846
0.829	-0.81662	0.848	-1.29384	0.867	-2.64915
0.830	-0.83292	0.849	-1.33341	0.868	-2.77891
0.831	-0.84990	0.850	-1.37517	0.869	-2.91858
0.832	-0.86760	0.851	-1.41928	0.870	-3.06912
0.833	-0.88606	0.852	-1.46591	0.871	-3.23160
0.834	-0.90534	0.853	-1.51525	0.872	-3.40720
0.835	-0.92546	0.854	-1.56749	0.873	-3.59725
0.836	-0.94649	0.855	-1.62287	0.874	-3.80325
0.837	-0.96848	0.856	-1.68163	0.875	-4.02687
0.838	-0.99149	0.857	-1.74403	0.876	-4.26999
0.839	-1.01557	0.858	-1.81036	0.877	-4.53476
0.840	-1.04080	0.859	-1.88095	0.878	-4.82359
0.841	-1.06725	0.860	-1.95613	0.879	-5.13924
0.842	-1.09499	0.861	-2.03631	0.880	-5.48487

F (GHz)	RL (dB)	F (GHz)	RL (dB)	F (GHz)	RL (dB)
0.881	-5.86410	0.901	-14.11702	0.921	-3.55291
0.882	-6.28111	0.902	-12.87382	0.922	-3.37943
0.883	-6.74078	0.903	-11.77308	0.923	-3.21874
0.884	-7.24880	0.904	-10.80025	0.924	-3.06969
0.885	-7.81189	0.905	-9.93851	0.925	-2.93124
0.886	-8.43802	0.906	-9.17234	0.926	-2.80248
0.887	-9.13671	0.907	-8.48838	0.927	-2.68257
0.888	-9.91934	0.908	-7.87544	0.928	-2.57077
0.889	-10.79943	0.909	-7.32415	0.929	-2.46639
0.890	-11.79264	0.910	-6.82668	0.930	-2.36884
0.891	-12.91577	0.911	-6.37642	0.931	-2.27755
0.892	-14.18274	0.912	-5.96777	0.932	-2.19204
0.893	-15.59193	0.913	-5.59597	0.933	-2.11185
0.894	-17.09102	0.914	-5.25692	0.934	-2.03656
0.895	-18.49675	0.915	-4.94707	0.935	-1.96581
0.896	-19.40439	0.916	-4.66333	0.936	-1.89926
0.897	-19.36398	0.917	-4.40303	0.937	-1.83658
0.898	-18.40306	0.918	-4.16380	0.938	-1.77751
0.899	-16.98785	0.919	-3.94355	0.939	-1.72179
0.900	-15.50347	0.920	-3.74047	0.940	-1.66916

F (GHz)	RL (dB)	F (GHz)	RL (dB)	F (GHz)	RL (dB)
0.941	-1.61943	0.961	-1.01317	0.981	-0.75937
0.942	-1.57238	0.962	-0.99518	0.982	-0.75094
0.943	-1.52785	0.963	-0.97794	0.983	-0.74279
0.944	-1.48565	0.964	-0.96139	0.984	-0.73491
0.945	-1.44563	0.965	-0.94551	0.985	-0.72729
0.946	-1.40766	0.966	-0.93025	0.986	-0.71992
0.947	-1.37160	0.967	-0.91559	0.987	-0.71279
0.948	-1.33732	0.968	-0.90151	0.988	-0.70589
0.949	-1.30473	0.969	-0.88796	0.989	-0.69921
0.950	-1.27370	0.970	-0.87492	0.990	-0.69274
0.951	-1.24416	0.971	-0.86238	0.991	-0.68647
0.952	-1.21600	0.972	-0.85030	0.992	-0.68040
0.953	-1.18915	0.973	-0.83867	0.993	-0.67452
0.954	-1.16352	0.974	-0.82746	0.994	-0.66882
0.955	-1.13906	0.975	-0.81666	0.995	-0.66330
0.956	-1.11568	0.976	-0.80624	0.996	-0.65794
0.957	-1.09334	0.977	-0.79619	0.997	-0.65274
0.958	-1.07197	0.978	-0.78649	0.998	-0.64770
0.959	-1.05151	0.979	-0.77714	0.999	-0.64281
0.960	-1.03193	0.980	-0.76810	1.000	-0.63806

### A.1.2 Tuned RMPA with coupling strips return loss

F (GHz)	RL (dB)	F (GHz)	RL (dB)	F (GHz)	RL (dB)
0.800	-0.54748	0.818	-0.78278	0.836	-1.80058
0.801	-0.55659	0.819	-0.80489	0.837	-1.91143
0.802	-0.56586	0.820	-0.82885	0.838	-2.01660
0.803	-0.57535	0.821	-0.85489	0.839	-2.10745
0.804	-0.58511	0.822	-0.88331	0.840	-2.17450
0.805	-0.59517	0.823	-0.91443	0.841	-2.20967
0.806	-0.60559	0.824	-0.94863	0.842	-2.20896
0.807	-0.61641	0.825	-0.98635	0.843	-2.17403
0.808	-0.62771	0.826	-1.02809	0.844	-2.11186
0.809	-0.63952	0.827	-1.07444	0.845	-2.03242
0.810	-0.65193	0.828	-1.12605	0.846	-1.94596
0.811	-0.66499	0.829	-1.18364	0.847	-1.86090
0.812	-0.67880	0.830	-1.24799	0.848	-1.78304
0.813	-0.69342	0.831	-1.31986	0.849	-1.71573
0.814	-0.70897	0.832	-1.39993	0.850	-1.66040
0.815	-0.72555	0.833	-1.48863	0.851	-1.61725
0.816	-0.74328	0.834	-1.58585	0.852	-1.58578
0.817	-0.76230	0.835	-1.69063	0.853	-1.56515

F (GHz)	RL (dB)	F (GHz)	RL (dB)	F (GHz)	RL (dB)
0.854	-1.55444	0.873	-2.72906	0.892	-10.62105
0.855	-1.55275	0.874	-2.87578	0.893	-11.77406
0.856	-1.55930	0.875	-3.03596	0.894	-13.14445
0.857	-1.57342	0.876	-3.21097	0.895	-14.81044
0.858	-1.59459	0.877	-3.40240	0.896	-16.90128
0.859	-1.62241	0.878	-3.61206	0.897	-19.64632
0.860	-1.65661	0.879	-3.84201	0.898	-23.44534
0.861	-1.69702	0.880	-4.09461	0.899	-28.10185
0.862	-1.74358	0.881	-4.37260	0.900	-27.07148
0.863	-1.79631	0.882	-4.67912	0.901	-22.41590
0.864	-1.85533	0.883	-5.01784	0.902	-18.94314
0.865	-1.92083	0.884	-5.39304	0.903	-16.40967
0.866	-1.99309	0.885	-5.80979	0.904	-14.45943
0.867	-2.07247	0.886	-6.27411	0.905	-12.89432
0.868	-2.15940	0.887	-6.79329	0.906	-11.60079
0.869	-2.25441	0.888	-7.37621	0.907	-10.50890
0.870	-2.35812	0.889	-8.03398	0.908	-9.57272
0.871	-2.47123	0.890	-8.78071	0.909	-8.76044
0.872	-2.59456	0.891	-9.63480	0.910	-8.04910

F (GHz)	RL (dB)	F (GHz)	RL (dB)	F (GHz)	RL (dB)
0.911	-7.42149	0.930	-2.42315	0.949	-1.28398
0.912	-6.86437	0.931	-2.32172	0.950	-1.25237
0.913	-6.36729	0.932	-2.22728	0.951	-1.22237
0.914	-5.92184	0.933	-2.13924	0.952	-1.19387
0.915	-5.52116	0.934	-2.05705	0.953	-1.16678
0.916	-5.15952	0.935	-1.98023	0.954	-1.14101
0.917	-4.83216	0.936	-1.90835	0.955	-1.11649
0.918	-4.53500	0.937	-1.84101	0.956	-1.09313
0.919	-4.26458	0.938	-1.77784	0.957	-1.07087
0.920	-4.01793	0.939	-1.71853	0.958	-1.04965
0.921	-3.79246	0.940	-1.66278	0.959	-1.02939
0.922	-3.58592	0.941	-1.61032	0.960	-1.01006
0.923	-3.39637	0.942	-1.56091	0.961	-0.99158
0.924	-3.22208	0.943	-1.51433	0.962	-0.97393
0.925	-3.06153	0.944	-1.47038	0.963	-0.95705
0.926	-2.91339	0.945	-1.42886	0.964	-0.94090
0.927	-2.77648	0.946	-1.38961	0.965	-0.92544
0.928	-2.64974	0.947	-1.35247	0.966	-0.91064
0.929	-2.53224	0.948	-1.31730	0.967	-0.89645

F (GHz)	RL (dB)	F (GHz)	RL (dB)	F (GHz)	RL (dB)
0.968	-0.88286	0.979	-0.76475	0.990	-0.68722
0.969	-0.86982	0.980	-0.75632	0.991	-0.68158
0.970	-0.85731	0.981	-0.74821	0.992	-0.67614
0.971	-0.84531	0.982	-0.74040	0.993	-0.67089
0.972	-0.83379	0.983	-0.73287	0.994	-0.66582
0.973	-0.82272	0.984	-0.72562	0.995	-0.66092
0.974	-0.81209	0.985	-0.71863	0.996	-0.65618
0.975	-0.80187	0.986	-0.71188	0.997	-0.65161
0.976	-0.79204	0.987	-0.70538	0.998	-0.64719
0.977	-0.78259	0.988	-0.69911	0.999	-0.64292
0.978	-0.77350	0.989	-0.69306	1.000	-0.63880

### A.1.3 Modified RMPA with coupling strips and impedance

#### matching network return loss data

F (GHz)	RL (dB)	F (GHz)	RL (dB)	F (GHz)	RL (dB)
0.800	-0.97783	0.817	-1.66457	0.834	-3.81179
0.801	-1.00317	0.818	-1.73057	0.835	-4.05761
0.802	-1.02979	0.819	-1.80102	0.836	-4.32772
0.803	-1.05780	0.820	-1.87632	0.837	-4.62521
0.804	-1.08727	0.821	-1.95691	0.838	-4.95368
0.805	-1.11832	0.822	-2.04326	0.839	-5.31731
0.806	-1.15105	0.823	-2.13592	0.840	-5.72095
0.807	-1.18557	0.824	-2.23550	0.841	-6.17027
0.808	-1.22202	0.825	-2.34267	0.842	-6.67194
0.809	-1.26053	0.826	-2.45819	0.843	-7.23382
0.810	-1.30126	0.827	-2.58290	0.844	-7.86520
0.811	-1.34437	0.828	-2.71776	0.845	-8.57708
0.812	-1.39004	0.829	-2.86385	0.846	-9.38252
0.813	-1.43848	0.830	-3.02240	0.847	-10.29695
0.814	-1.48990	0.831	-3.19478	0.848	-11.33837
0.815	-1.54454	0.832	-3.38257	0.849	-12.52695
0.816	-1.60266	0.833	-3.58756	0.850	-13.88314

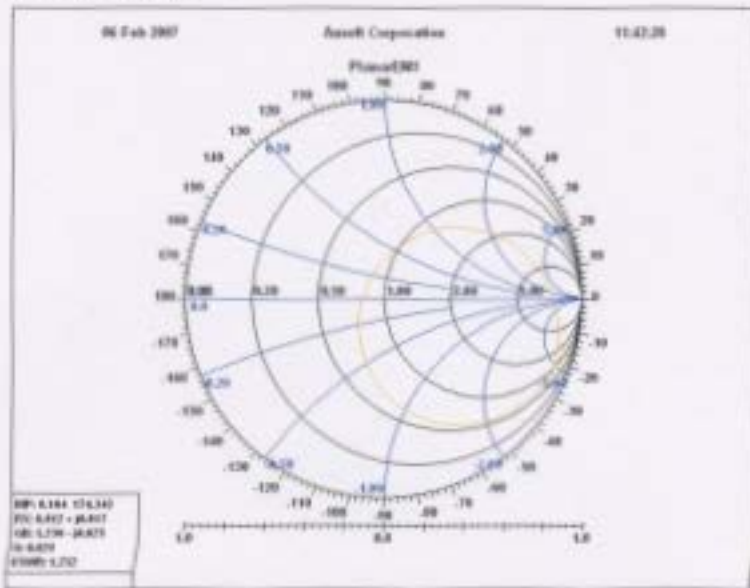
F (GHz)	RL (dB)	F (GHz)	RL (dB)	F (GHz)	RL (dB)
0.851	-15.42129	0.870	-14.60936	0.889	-4.15276
0.852	-17.13175	0.871	-13.20107	0.890	-4.00427
0.853	-18.93655	0.872	-11.99164	0.891	-3.87061
0.854	-20.60912	0.873	-10.94727	0.892	-3.75054
0.855	-21.75043	0.874	-10.04023	0.893	-3.64299
0.856	-22.07889	0.875	-9.24816	0.894	-3.54704
0.857	-21.79825	0.876	-8.55307	0.895	-3.46188
0.858	-21.35801	0.877	-7.94037	0.896	-3.38683
0.859	-21.07650	0.878	-7.39816	0.897	-3.32132
0.860	-21.10465	0.879	-6.91663	0.898	-3.26486
0.861	-21.50410	0.880	-6.48765	0.899	-3.21705
0.862	-22.28004	0.881	-6.10443	0.900	-3.17758
0.863	-23.32371	0.882	-5.76126	0.901	-3.14619
0.864	-24.20431	0.883	-5.45332	0.902	-3.12271
0.865	-24.05445	0.884	-5.17649	0.903	-3.10705
0.866	-22.51531	0.885	-4.92729	0.904	-3.09915
0.867	-20.32903	0.886	-4.70272	0.905	-3.09904
0.868	-18.16829	0.887	-4.50020	0.906	-3.10683
0.869	-16.25465	0.888	-4.31752	0.907	-3.12268

F (GHz)	RL (dB)	F (GHz)	RL (dB)	F (GHz)	RL (dB)
0.908	-3.14684	0.927	-6.43154	0.946	-10.31688
0.909	-3.17962	0.928	-6.91673	0.947	-9.27736
0.910	-3.22143	0.929	-7.47084	0.948	-8.38290
0.911	-3.27276	0.930	-8.10633	0.949	-7.60737
0.912	-3.33422	0.931	-8.83894	0.950	-6.93064
0.913	-3.40652	0.932	-9.68877	0.951	-6.33688
0.914	-3.49050	0.933	-10.68198	0.952	-5.81346
0.915	-3.58715	0.934	-11.85300	0.953	-5.35013
0.916	-3.69762	0.935	-13.24678	0.954	-4.93848
0.917	-3.82327	0.936	-14.91778	0.955	-4.57150
0.918	-3.96564	0.937	-16.90858	0.956	-4.24331
0.919	-4.12656	0.938	-19.13088	0.957	-3.94897
0.920	-4.30815	0.939	-20.93246	0.958	-3.68425
0.921	-4.51290	0.940	-20.89068	0.959	-3.44553
0.922	-4.74369	0.941	-19.01975	0.960	-3.22971
0.923	-5.00392	0.942	-16.74202	0.961	-3.03412
0.924	-5.29761	0.943	-14.69980	0.962	-2.85645
0.925	-5.62948	0.944	-12.97864	0.963	-2.69468
0.926	-6.00520	0.945	-11.53574	0.964	-2.54706

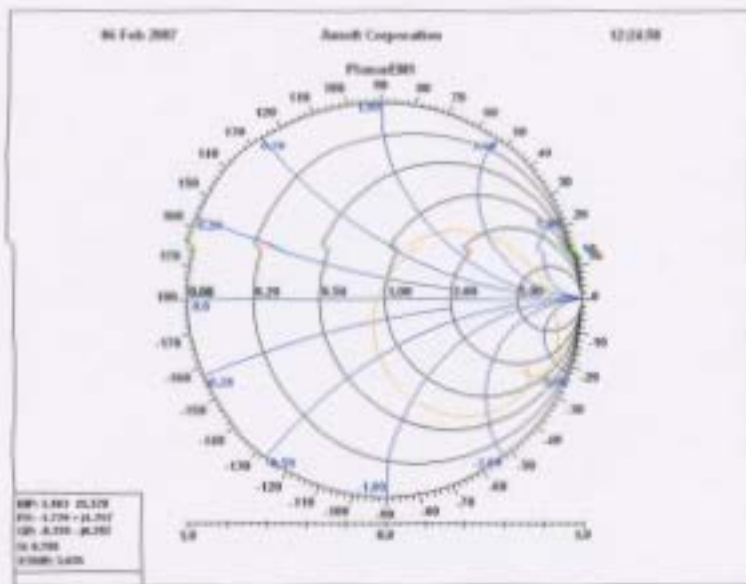
F (GHz)	RL (dB)	F (GHz)	RL (dB)	F (GHz)	RL (dB)
0.965	-2.41207	0.977	-1.41794	0.989	-0.98156
0.966	-2.28837	0.978	-1.36801	0.990	-0.95699
0.967	-2.17478	0.979	-1.32124	0.991	-0.93369
0.968	-2.07027	0.980	-1.27738	0.992	-0.91156
0.969	-1.97394	0.981	-1.23620	0.993	-0.89052
0.970	-1.88498	0.982	-1.19749	0.994	-0.87051
0.971	-1.80268	0.983	-1.16105	0.995	-0.85147
0.972	-1.72641	0.984	-1.12672	0.996	-0.83332
0.973	-1.65562	0.985	-1.09433	0.997	-0.81603
0.974	-1.58979	0.986	-1.06374	0.998	-0.79953
0.975	-1.52850	0.987	-1.03483	0.999	-0.78378
0.976	-1.47133	0.988	-1.00747	1.000	-0.76874

## A.2 Plots

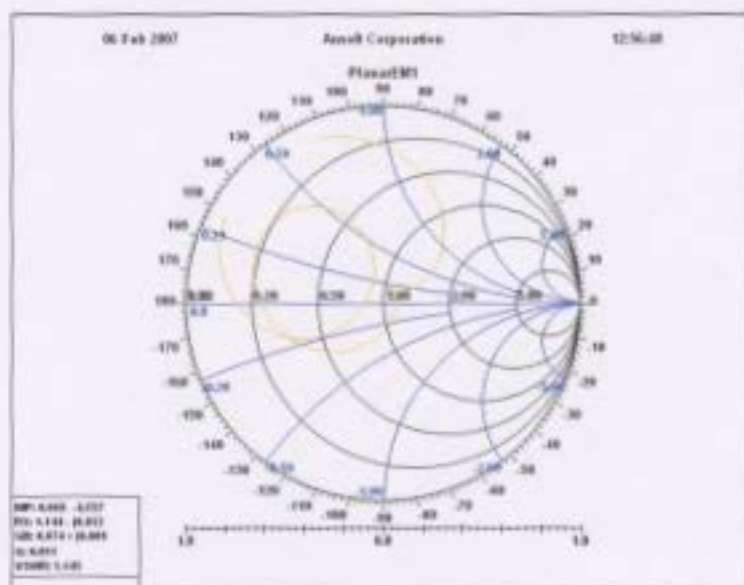
### A.2.1 Smith charts



Control RMPA: Smith chart

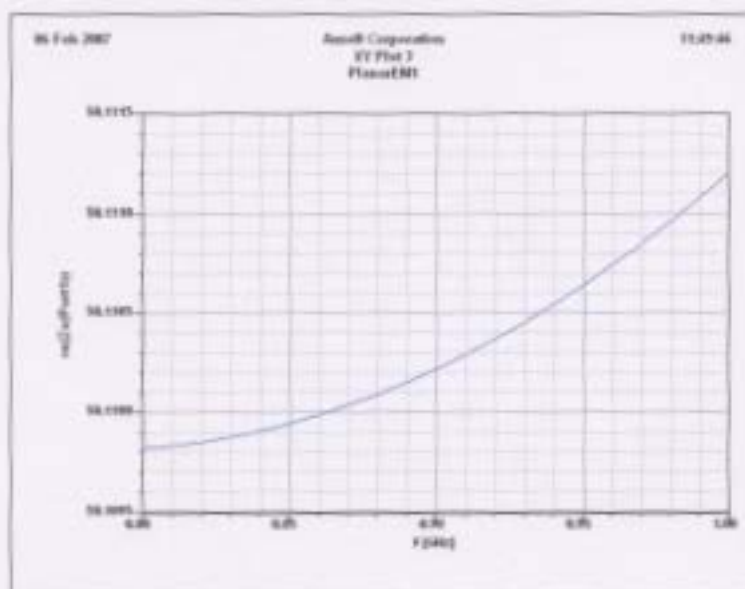


Tuned RMPA: Smith chart



Modified RMPA: Smith chart

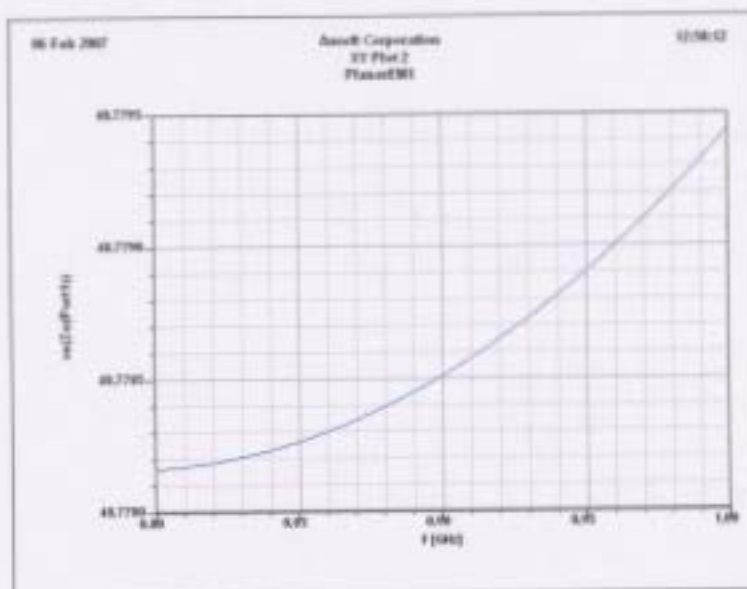
## A.2.2 Characteristic impedance



Control RMPA: Characteristic impedance ( $Z_0$ ) as a function of frequency (GHz)

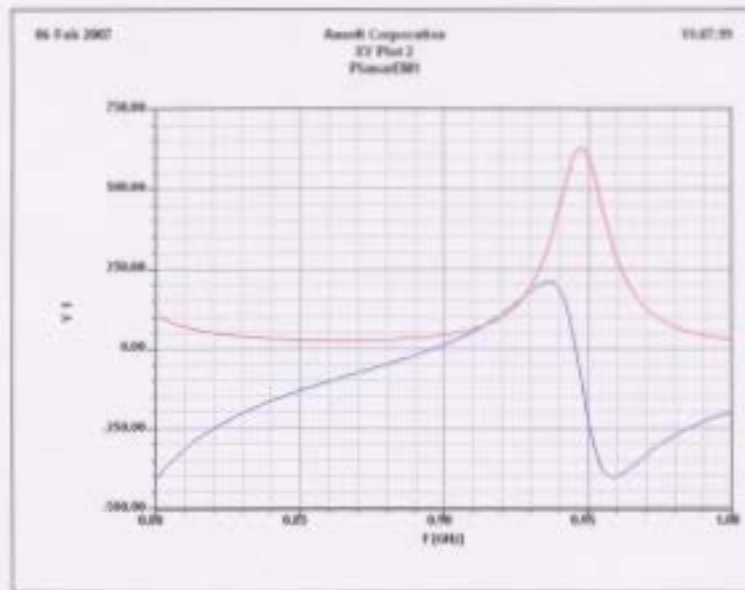


Tuned RMPA: Characteristic impedance ( $Z_0$ ) as a function of frequency (GHz)

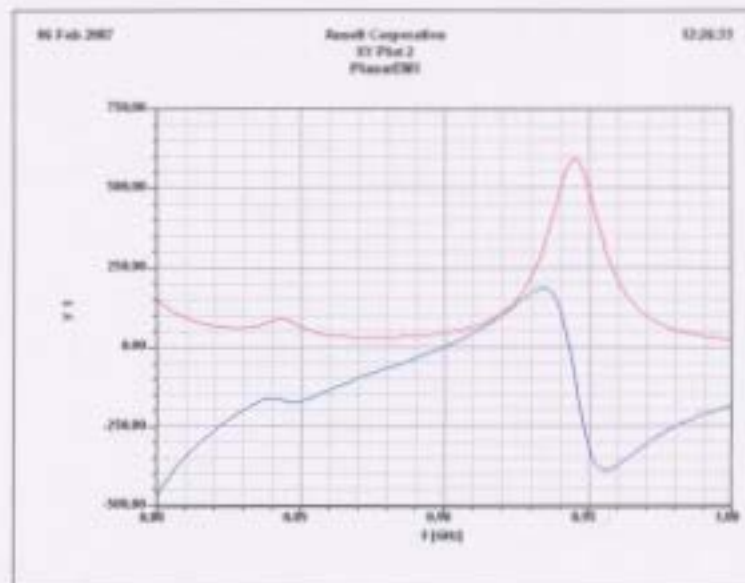


Modified RMPA: Characteristic impedance ( $Z_0$ ) as a function of frequency (GHz)

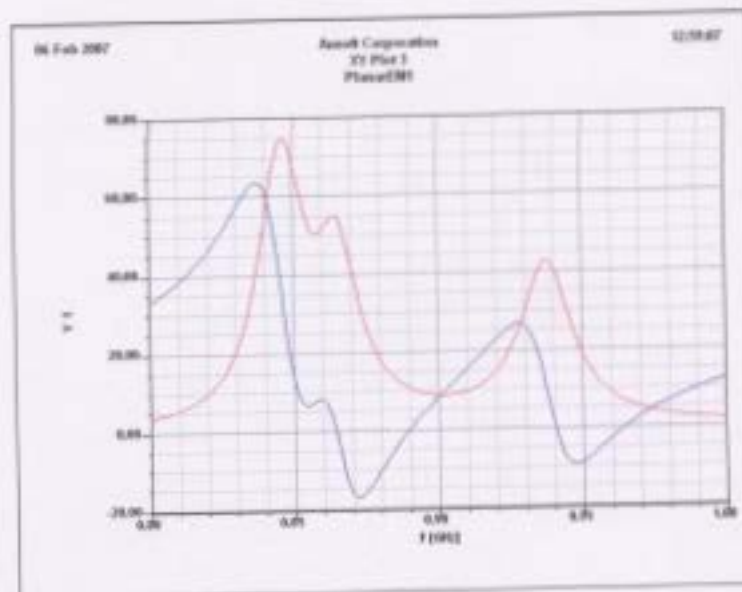
### A.2.3 Real and imaginary impedance



Control RMPA: Real (red) and imaginary (blue) impedance versus frequency ( GHz)

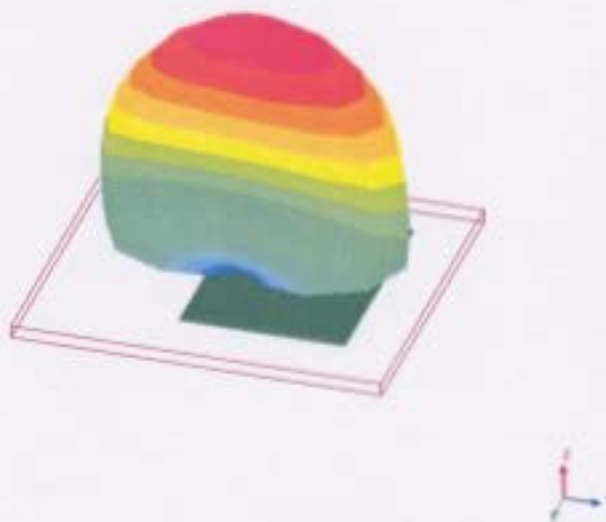


Tuned RMPA: Real (red) and imaginary (blue) impedance versus frequency ( GHz)

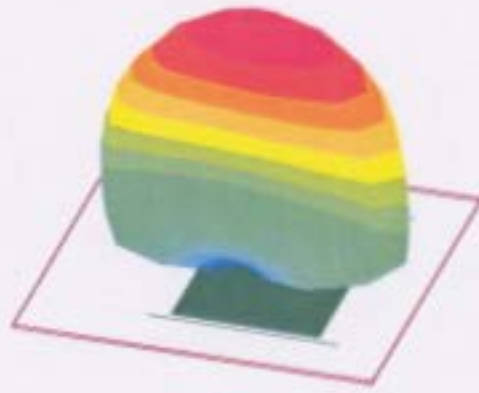


Modified RMPA: Real (red) and imaginary (blue) impedance versus frequency  
 (GHz)

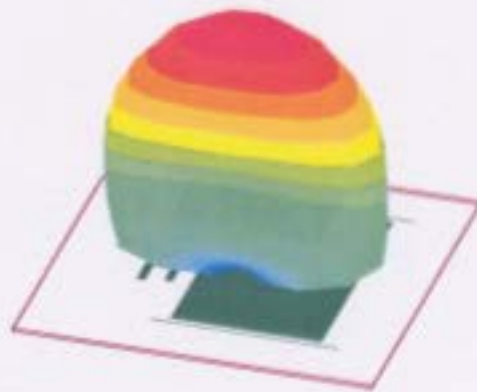
#### A.2.4 Far field radiation



Control RMPA: Far field radiation pattern

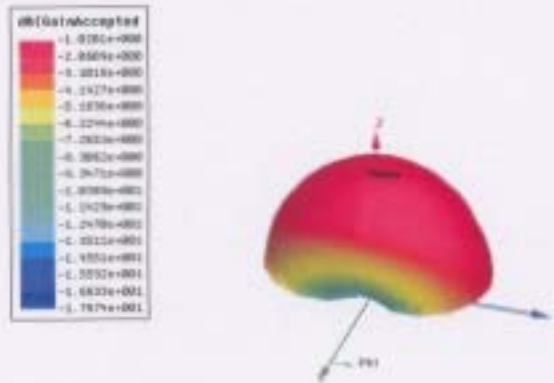


Tuned RMPA: Far field radiation pattern

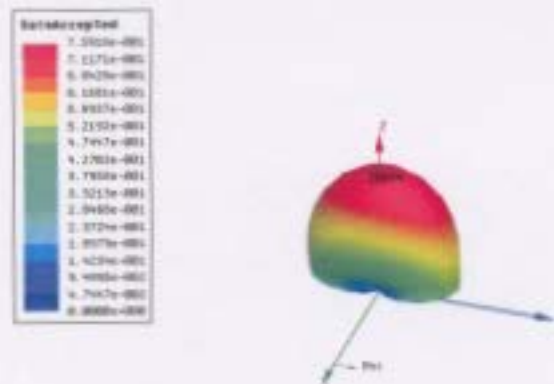


Modified RMPA: Far field radiation pattern

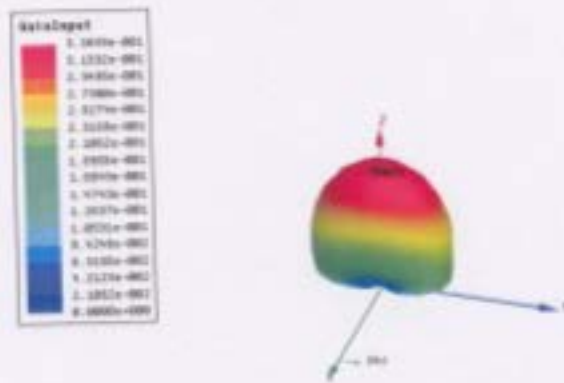
## A.2.5 Accepted gain



Control RMPA: 3D Accepted gain

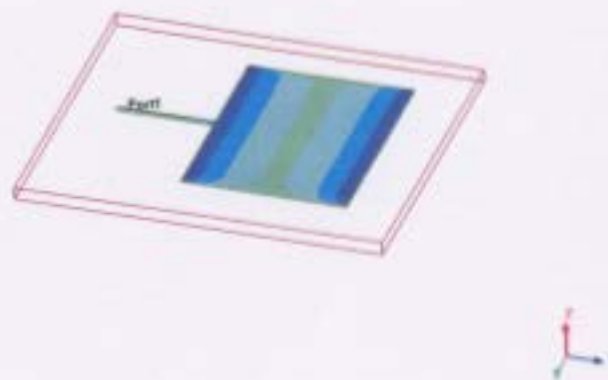


Tuned RMPA: 3D Accepted gain

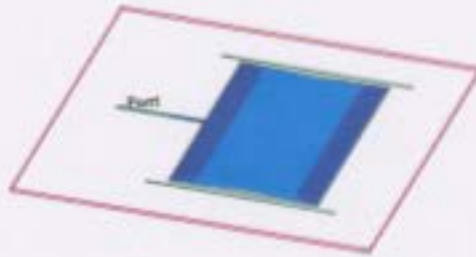


Modified RMPA: 3D Accepted gain

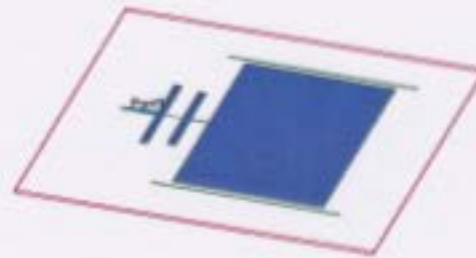
### A.2.6 Current distribution



Control RMPA: Current distribution at 90° phase



Tuned RMPA: Current distribution at  $90^\circ$  phase



Modified RMPA: Current distribution at  $90^\circ$  phase

# Appendix B

## Measurement Results

### B.1 Return loss data

#### B.1.1 Control RMPA

F (MHz)	RL (dB)	F (MHz)	RL (dB)	F (MHz)	RL (dB)
800	-0.426	808	-0.464	816	-0.515
801	-0.429	809	-0.470	817	-0.523
802	-0.434	810	-0.475	818	-0.530
803	-0.440	811	-0.480	819	-0.539
804	-0.444	812	-0.489	820	-0.546
805	-0.448	813	-0.496	821	-0.553
806	-0.453	814	-0.501	822	-0.560
807	-0.457	815	-0.508	823	-0.569

F (MHz)	RL (dB)	F (MHz)	RL (dB)	F (MHz)	RL (dB)
824	-0.578	843	-0.810	862	-1.329
825	-0.586	844	-0.827	863	-1.375
826	-0.595	845	-0.846	864	-1.421
827	-0.606	846	-0.865	865	-1.470
828	-0.611	847	-0.888	866	-1.524
829	-0.622	848	-0.907	867	-1.581
830	-0.634	849	-0.930	868	-1.642
831	-0.640	850	-0.953	869	-1.706
832	-0.654	851	-0.975	870	-1.773
833	-0.664	852	-1.001	871	-1.846
834	-0.676	853	-1.027	872	-1.923
835	-0.688	854	-1.054	873	-2.005
836	-0.700	855	-1.083	874	-2.094
837	-0.712	856	-1.114	875	-2.188
838	-0.727	857	-1.146	876	-2.289
839	-0.742	858	-1.178	877	-2.396
840	-0.759	859	-1.214	878	-2.512
841	-0.773	860	-1.255	879	-2.634
842	-0.791	861	-1.289	880	-2.770

F ( MHz)	RL (dB)	F ( MHz)	RL (dB)	F ( MHz)	RL (dB)
881	-2.912	901	-10.279	921	-5.798
882	-3.066	902	-10.987	922	-5.426
883	-3.230	903	-11.692	923	-5.090
884	-3.406	904	-12.351	924	-4.777
885	-3.600	905	-12.905	925	-4.492
886	-3.809	906	-13.281	926	-4.230
887	-4.036	907	-13.410	927	-3.991
888	-4.284	908	-13.266	928	-3.772
889	-4.556	909	-12.881	929	-3.572
890	-4.852	910	-12.315	930	-3.385
891	-5.171	911	-11.643	931	-3.216
892	-5.516	912	-10.926	932	-3.058
893	-5.893	913	-10.205	933	-2.912
894	-6.301	914	-9.497	934	-2.774
895	-6.746	915	-8.841	935	-2.648
896	-7.227	916	-8.218	936	-2.531
897	-7.754	917	-7.648	937	-2.417
898	-8.326	918	-7.123	938	-2.314
899	-8.938	919	-6.645	939	-2.219
900	-9.594	920	-6.202	940	-2.129

F ( MHz)	RL (dB)	F ( MHz)	RL (dB)	F ( MHz)	RL (dB)
941	-2.042	961	-1.085	981	-0.744
942	-1.963	962	-1.059	982	-0.735
943	-1.888	963	-1.036	983	-0.726
944	-1.816	964	-1.013	984	-0.715
945	-1.756	965	-0.993	985	-0.706
946	-1.690	966	-0.970	986	-0.698
947	-1.631	967	-0.950	987	-0.689
948	-1.577	968	-0.929	988	-0.681
949	-1.521	969	-0.912	989	-0.674
950	-1.474	970	-0.899	990	-0.665
951	-1.426	971	-0.877	991	-0.657
952	-1.383	972	-0.862	992	-0.649
953	-1.343	973	-0.846	993	-0.648
954	-1.305	974	-0.832	994	-0.634
955	-1.268	975	-0.816	995	-0.628
956	-1.234	976	-0.804	996	-0.623
957	-1.202	977	-0.792	997	-0.616
958	-1.172	978	-0.779	998	-0.611
959	-1.141	979	-0.767	999	-0.604
960	-1.112	980	-0.754	1000	-0.598

### B.1.2 Tuned RMPA

F (MHz)	RL (dB)	F (MHz)	RL (dB)	F (MHz)	RL (dB)
800	-0.426	818	-0.532	836	-0.737
801	-0.428	819	-0.539	837	-0.754
802	-0.433	820	-0.549	838	-0.774
803	-0.437	821	-0.557	839	-0.793
804	-0.443	822	-0.566	840	-0.817
805	-0.446	823	-0.576	841	-0.839
806	-0.452	824	-0.585	842	-0.864
807	-0.456	825	-0.594	843	-0.891
808	-0.463	826	-0.604	844	-0.919
809	-0.469	827	-0.616	845	-0.949
810	-0.475	828	-0.626	846	-0.980
811	-0.480	829	-0.637	847	-1.015
812	-0.487	830	-0.651	848	-1.051
813	-0.496	831	-0.663	849	-1.092
814	-0.501	832	-0.677	850	-1.135
815	-0.507	833	-0.690	851	-1.183
816	-0.515	834	-0.705	852	-1.234
817	-0.525	835	-0.720	853	-1.293

F ( MHz)	RL (dB)	F ( MHz)	RL (dB)	F ( MHz)	RL (dB)
854	-1.355	873	-3.632	892	-2.965
855	-1.425	874	-3.486	893	-3.101
856	-1.504	875	-3.313	894	-3.257
857	-1.594	876	-3.137	895	-3.431
858	-1.692	877	-2.971	896	-3.623
859	-1.802	878	-2.822	897	-3.839
860	-1.932	879	-2.696	898	-4.078
861	-2.067	880	-2.597	899	-4.341
862	-2.226	881	-2.520	900	-4.636
863	-2.404	882	-2.467	901	-4.960
864	-2.598	883	-2.436	902	-5.323
865	-2.809	884	-2.427	903	-5.731
866	-3.032	885	-2.438	904	-6.188
867	-3.253	886	-2.464	905	-6.704
868	-3.456	887	-2.507	906	-7.293
869	-3.624	888	-2.568	907	-7.956
870	-3.732	889	-2.644	908	-8.719
871	-3.772	890	-2.736	909	-9.594
872	-3.733	891	-2.840	910	-10.606

F (MHz)	RL (dB)	F (MHz)	RL (dB)	F (MHz)	RL (dB)
911	-11.782	930	-5.937	949	-2.026
912	-13.156	931	-5.516	950	-1.941
913	-14.775	932	-5.138	951	-1.865
914	-16.664	933	-4.797	952	-1.793
915	-18.734	934	-4.489	953	-1.726
916	-20.451	935	-4.208	954	-1.663
917	-20.700	936	-3.954	955	-1.602
918	-19.235	937	-3.721	956	-1.550
919	-17.190	938	-3.507	957	-1.499
920	-15.246	939	-3.314	958	-1.452
921	-13.567	940	-3.134	959	-1.407
922	-12.144	941	-2.970	960	-1.362
923	-10.939	942	-2.817	961	-1.321
924	-9.897	943	-2.676	962	-1.284
925	-9.003	944	-2.547	963	-1.248
926	-8.221	945	-2.432	964	-1.214
927	-7.541	946	-2.317	965	-1.182
928	-6.940	947	-2.213	966	-1.151
929	-6.409	948	-2.116	967	-1.123

F (MHz)	RL (dB)	F (MHz)	RL (dB)	F (MHz)	RL (dB)
968	-1.093	979	-0.866	990	-0.740
969	-1.069	980	-0.857	991	-0.730
970	-1.048	981	-0.842	992	-0.720
971	-1.021	982	-0.827	993	-0.717
972	-0.997	983	-0.816	994	-0.704
973	-0.977	984	-0.803	995	-0.696
974	-0.957	985	-0.791	996	-0.688
975	-0.936	986	-0.781	997	-0.681
976	-0.919	987	-0.769	998	-0.673
977	-0.903	988	-0.758	999	-0.667
978	-0.887	989	-0.751	1000	-0.660

### B.1.3 Modified RMPA

F (MHz)	RL (dB)	F (MHz)	RL (dB)	F (MHz)	RL (dB)
800	-0.352	817	-0.511	834	-0.844
801	-0.358	818	-0.526	835	-0.877
802	-0.365	819	-0.537	836	-0.908
803	-0.373	820	-0.552	837	-0.942
804	-0.380	821	-0.567	838	-0.978
805	-0.386	822	-0.583	839	-1.017
806	-0.395	823	-0.600	840	-1.059
807	-0.404	824	-0.618	841	-1.103
808	-0.412	825	-0.635	842	-1.152
809	-0.421	826	-0.653	843	-1.202
810	-0.430	827	-0.674	844	-1.255
811	-0.441	828	-0.695	845	-1.313
812	-0.452	829	-0.715	846	-1.373
813	-0.463	830	-0.739	847	-1.439
814	-0.474	831	-0.764	848	-1.510
815	-0.484	832	-0.789	849	-1.586
816	-0.499	833	-0.816	850	-1.667

F (MHz)	RL (dB)	F (MHz)	RL (dB)	F (MHz)	RL (dB)
851	-1.755	870	-6.880	889	-10.579
852	-1.852	871	-7.601	890	-10.448
853	-1.957	872	-8.419	891	-10.491
854	-2.067	873	-9.372	892	-10.712
855	-2.193	874	-10.478	893	-11.115
856	-2.326	875	-11.755	894	-11.721
857	-2.474	876	-13.239	895	-12.543
858	-2.637	877	-14.939	896	-13.610
859	-2.817	878	-16.788	897	-14.887
860	-3.016	879	-18.457	898	-16.253
861	-3.232	880	-19.215	899	-17.302
862	-3.474	881	-18.576	900	-17.403
863	-3.748	882	-17.112	901	-16.360
864	-4.052	883	-15.532	902	-14.744
865	-4.393	884	-14.137	903	-13.077
866	-4.779	885	-12.986	904	-11.572
867	-5.213	886	-12.076	905	-10.274
868	-5.701	887	-11.382	906	-9.168
869	-6.251	888	-10.887	907	-8.229

F (MHz)	RL (dB)	F (MHz)	RL (dB)	F (MHz)	RL (dB)
908	-7.426	927	-2.596	946	-2.813
909	-6.745	928	-2.549	947	-2.894
910	-6.162	929	-2.510	948	-2.985
911	-5.659	930	-2.478	949	-3.084
912	-5.226	931	-2.453	950	-3.198
913	-4.848	932	-2.436	951	-3.327
914	-4.517	933	-2.423	952	-3.467
915	-4.231	934	-2.416	953	-3.624
916	-3.978	935	-2.416	954	-3.798
917	-3.755	936	-2.419	955	-3.992
918	-3.554	937	-2.428	956	-4.206
919	-3.388	938	-2.444	957	-4.441
920	-3.234	939	-2.466	958	-4.701
921	-3.102	940	-2.493	959	-4.990
922	-2.987	941	-2.529	960	-5.315
923	-2.890	942	-2.572	961	-5.669
924	-2.796	943	-2.621	962	-6.067
925	-2.719	944	-2.676	963	-6.516
926	-2.652	945	-2.743	964	-7.017

F ( MHz)	RL (dB)	F ( MHz)	RL (dB)	F ( MHz)	RL (dB)
965	-7.582	977	-18.397	989	-5.993
966	-8.224	978	-16.849	990	-5.546
967	-8.943	979	-15.190	991	-5.145
968	-9.767	980	-13.655	992	-4.783
969	-10.706	981	-12.299	993	-4.457
970	-11.785	982	-11.113	994	-4.158
971	-13.022	983	-10.079	995	-3.887
972	-14.442	984	-9.167	996	-3.641
973	-16.024	985	-8.371	997	-3.417
974	-17.656	986	-7.668	998	-3.210
975	-18.955	987	-7.043	999	-3.023
976	-19.276	988	-6.489	1000	-2.850

## B.2 Radiation pattern data

### B.2.1 Control RMPA azimuthal data

$\Phi$	Amp.	$\Phi$	Amp.	$\Phi$	Amp.	$\Phi$	Amp.
180	-89.4	90	-79.2	0	-65.8	-90	-81.4
175	-89.4	85	-78.0	-5	-65.6	-95	-83.2
170	-89.4	80	-76.8	-10	-66.0	-100	-84.8
165	-89.4	75	-76.8	-15	-66.4	-105	-85.0
160	-89.2	70	-75.6	-20	-67.0	-110	-85.6
155	-88.8	65	-75.8	-25	-67.6	-115	-87.0
150	-89.0	60	-73.0	-30	-68.6	-120	-87.2
145	-88.2	55	-71.8	-35	-69.4	-125	-87.8
140	-88.2	50	-71.0	-40	-70.6	-130	-88.2
135	-87.8	45	-70.2	-45	-71.6	-135	-88.6
130	-87.2	40	-69.4	-50	-72.8	-140	-89.6
125	-86.6	35	-68.4	-55	-73.0	-145	-90.0
120	-86.2	30	-67.8	-60	-74.2	-150	-90.2
115	-85.6	25	-67.2	-65	-74.6	-155	-90.8
110	-84.6	20	-66.8	-70	-75.4	-160	-91.0
105	-83.4	15	-66.4	-75	-76.2	-165	-90.8
100	-82.2	10	-66.0	-80	-77.8	-170	-90.6
95	-80.8	5	-65.8	-85	-79.4	-175	-90.4

### B.2.2 Tuned RMPA azimuth data

$\Phi$	Amp.	$\Phi$	Amp.	$\Phi$	Amp.	$\Phi$	Amp.
180	-90.0	90	-77.0	0	-65.4	-90	-78.2
175	-90.0	85	-76.0	-5	-66.2	-95	-79.4
170	-89.6	80	-74.8	-10	-66.2	-100	-80.6
165	-89.4	75	-74.0	-15	-66.2	-105	-82.4
160	-89.0	70	-73.2	-20	-66.6	-110	-83.6
155	-88.4	65	-72.2	-25	-67.0	-115	-84.4
150	-88.0	60	-71.4	-30	-67.4	-120	-85.4
145	-87.4	55	-70.4	-35	-67.8	-125	-86.2
140	-86.6	50	-69.8	-40	-68.4	-130	-86.6
135	-86.2	45	-69.0	-45	-69.0	-135	-87.2
130	-85.0	40	-68.2	-50	-70.2	-140	-87.6
125	-84.4	35	-67.6	-55	-70.8	-145	-88.4
120	-83.6	30	-67.0	-60	-71.6	-150	-89.2
115	-82.6	25	-66.6	-65	-72.6	-155	-89.6
110	-81.6	20	-66.2	-70	-73.4	-160	-90.2
105	-80.4	15	-65.8	-75	-74.6	-165	-89.6
100	-79.4	10	-65.6	-80	-75.4	-170	-90.0
95	-78.2	5	-65.4	-85	-76.8	-175	-90.0

### B.2.3 Modified RMPA azimuth data

$\Phi$	Amp.	$\Phi$	Amp.	$\Phi$	Amp.	$\Phi$	Amp.
180	-90.8	90	-78.8	0	-69.2	-90	-80.8
175	-90.6	85	-78.0	-5	-69.4	-95	-82.2
170	-90.6	80	-76.8	-10	-69.6	-100	-83.6
165	-90.2	75	-76.0	-15	-69.8	-105	-85.0
160	-89.2	70	-75.0	-20	-70.2	-110	-85.6
155	-88.6	65	-74.4	-25	-70.4	-115	-87.2
150	-88.6	60	-73.8	-30	-70.8	-120	-87.8
145	-88.0	55	-73.2	-35	-71.4	-125	-88.4
140	-87.6	50	-72.6	-40	-72.0	-130	-89.2
135	-87.2	45	-72.0	-45	-72.4	-135	-90.4
130	-86.8	40	-71.6	-50	-73.0	-140	-90.6
125	-85.8	35	-71.0	-55	-73.6	-145	-90.8
120	-85.0	30	-70.6	-60	-74.4	-150	-91.0
115	-84.0	25	-70.2	-65	-75.2	-155	-90.8
110	-83.0	20	-69.8	-70	-76.2	-160	-91.0
105	-82.2	15	-69.6	-75	-77.0	-165	-90.8
100	-80.8	10	-69.4	-80	-78.2	-170	-90.8
95	-79.8	5	-69.2	-85	-79.4	-175	-90.8

### B.2.4 Control RMPA elevation data

$\Phi$	Amp.	$\Phi$	Amp.	$\Phi$	Amp.	$\Phi$	Amp.
180	-77.4	90	-71.8	0	-61.4	-90	-71.6
175	-77.6	85	-70.8	-5	-61.4	-95	-72.4
170	-78.0	80	-69.8	-10	-61.6	-100	-73.4
165	-78.6	75	-68.8	-15	-61.8	-105	-74.6
160	-79.6	70	-67.8	-20	-62.0	-110	-75.6
155	-81.2	65	-67.2	-25	-62.4	-115	-76.8
150	-82.6	60	-66.4	-30	-62.8	-120	-78.2
145	-83.8	55	-65.8	-35	-63.0	-125	-79.2
140	-84.0	50	-65.2	-40	-63.8	-130	-80.4
135	-83.0	45	-64.8	-45	-64.2	-135	-81.4
130	-81.4	40	-64.0	-50	-65.0	-140	-82.0
125	-79.8	35	-63.4	-55	-65.6	-145	-81.6
120	-77.6	30	-63.0	-60	-66.4	-150	-80.6
115	-76.4	25	-62.4	-65	-67.0	-155	-79.8
110	-75.4	20	-62.0	-70	-67.8	-160	-78.8
105	-74.2	15	-61.8	-75	-68.6	-165	-78.2
100	-73.4	10	-61.6	-80	-69.6	-170	-77.6
95	-72.4	5	-61.4	-85	-70.6	-175	-77.4

### B.2.5 Tuned RMPA elevation data

$\Phi$	Amp.	$\Phi$	Amp.	$\Phi$	Amp.	$\Phi$	Amp.
180	-79.2	90	-71.4	0	-61.6	-90	-71.6
175	-79.6	85	-70.8	-5	-61.6	-95	-72.4
170	-80.6	80	-69.6	-10	-61.8	-100	-73.4
165	-82.0	75	-69.2	-15	-62.0	-105	-74.6
160	-83.0	70	-68.6	-20	-62.2	-110	-75.6
155	-83.8	65	-67.6	-25	-62.4	-115	-76.6
150	-83.8	60	-67.0	-30	-62.8	-120	-77.8
145	-83.6	55	-66.2	-35	-63.4	-125	-79.2
140	-82.0	50	-65.6	-40	-64.0	-130	-80.2
135	-80.2	45	-65.0	-45	-64.4	-135	-80.6
130	-78.6	40	-64.6	-50	-65.0	-140	-80.6
125	-77.2	35	-64.0	-55	-65.4	-145	-80.4
120	-76.0	30	-63.6	-60	-66.2	-150	-80.2
115	-75.2	25	-63.0	-65	-67.0	-155	-79.2
110	-74.2	20	-62.6	-70	-67.6	-160	-78.6
105	-73.8	15	-62.0	-75	-68.6	-165	-78.4
100	-72.6	10	-61.8	-80	-69.8	-170	-78.2
95	-72.0	5	-61.8	-85	-70.6	-175	-78.6

### B.2.6 Modified RMPA elevation data

$\Phi$	Amp.	$\Phi$	Amp.	$\Phi$	Amp.	$\Phi$	Amp.
180	-86.0	90	-75.2	0	-66.4	-90	-78.0
175	-86.2	85	-74.8	-5	-68.2	-95	-79.8
170	-87.2	80	-74.0	-10	-68.4	-100	-80.4
165	-87.0	75	-73.6	-15	-68.6	-105	-81.4
160	-86.8	70	-73.0	-20	-68.8	-110	-82.0
155	-86.4	65	-72.0	-25	-69.2	-115	-83.4
150	-86.2	60	-71.4	-30	-69.8	-120	-84.4
145	-86.6	55	-71.0	-35	-70.2	-125	-85.8
140	-84.6	50	-70.2	-40	-70.6	-130	-87.0
135	-83.0	45	-69.8	-45	-71.2	-135	-88.2
130	-81.6	40	-69.2	-50	-72.0	-140	-88.6
125	-80.6	35	-68.4	-55	-72.4	-145	-88.6
120	-79.4	30	-67.8	-60	-73.2	-150	-88.0
115	-78.6	25	-67.6	-65	-73.8	-155	-87.0
110	-77.8	20	-67.2	-70	-74.4	-160	-87.0
105	-77.2	15	-67.0	-75	-75.2	-165	-86.8
100	-76.6	10	-66.8	-80	-76.0	-170	-86.4
95	-75.8	5	-66.6	-85	-76.8	-175	-86.4

# Appendix C

## MATLAB Code

### C.1 RMPA dimensions

```
%%%%%%%%%%%%%%%%%%%%%%%%%%%%%%%%%%%%%%%%%%%%%%%%%%%%%%%%%%%%%%%%%%%%%%%%  
  
% garg.m  
  
%  
  
% script prompts user to enter design specifications  
  
% for a rectangular microstrip patch antenna using  
  
% design procedures from Antenna Theory (Balanis)  
  
% Microstrip Antenna Design Handbook (Garg, et. al.)  
  
%  
  
% by Ron Lewis (10/11/06)  
  
%%%%%%%%%%%%%%%%%%%%%%%%%%%%%%%%%%%%%%%%%%%%%%%%%%%%%%%%%%%%%%%%%%%%%%%%
```

```

% user defined specs

%

fr=input('desired resonant frequency (MHz) >');

e_r=input('substrate dielectric constant >');

h=input('substrate height (mm) >');

%

% constants: permittivity of free space

% permeability of free space

% wavelength in freespace

% frequency in Hz

%

epsilon0=8.854*10^(-12);

mu0=4*pi*10^(-7);

lambda=1/(epsilon0*mu0*fr);

f=fr*10^6;

%

% calculate width of patch element

%

W=1/(2*f*sqrt(mu0*epsilon0))*sqrt(2/(e_r+1));

%

% calculate effective dielectric constant for antenna

```

```

%
e_re=(e_r+1)/2 + (e_r-1)/2*(1+12*h/W)^(-.5);
%
% calculate xi parameters
%
x1=0.434907* ( (e_re^0.81+0.26) / (e_re^0.81-0.189) ) *
( ( (W/h)^0.8544+0.236) / ( (W/h)^0.8544+0.87) )
x2=1+ ( ((W/h)^0.371) / (2.358*e_r+1) )
x3=1+( (0.5274*(atan(0.084*(W/h)^(1.9413/x2) ))) / (e_re^0.9236) )
x4=1+0.0377*atan(0.067*( (W/h)^1.456))*(6-5*exp(0.036*(1-e_r)) )
x5=1-0.218*exp(-7.5*(W/h))
%
% calculate additional length due to fringing
%
DeltaL=h*((x1*x3*x5)/x4)
L= 1/(2*f*sqrt(e_re)*sqrt(mu0*epsilon0))-2*DeltaL
%
%end
%%%%%%%%%%

```

## C.2 Feed line dimensions

```
%%%%%%%%%%%%%%%%%%%%%%%%%%%%%%%%%%%%%%%%%
% feed.m
%
% script prompts user to enter design specifications
% for a microstrip feed for a RMPA using procedures
% from Microwave Engineering (Pozar)
%
% by Ron Lewis (10/12/06)
%%%%%%%%%%%%%%%%%%%%%%%%%%%%%%%%%%%%%%%%%
% user defined specs
%
fr=input('desired resonant frequency (MHz) >');
er=input('substrate dielectric constant >');
h=input('substrate height (mm) >');
Z0=input('impedance > ');
%
% constants: freespace speed of light
% frequency in Hz%
% wave number
%
```

```

c=2.998*10^8;

f=fr*10^6;

k0=2*pi*f/c;

%

% calculates microstrip feed line length and width

% prompt user to estimate ratio W/h

if input('\nIs the ratio W/h greater than two?(y,n)\n?','s')== 'y'

B=377*pi/(2*Z0*sqrt(er));

w=h*(2/pi)*(B-1-log(2*B-1)+((er-1)/(2*er))*(log(B-1)+.39-.61/er));

width=w

else

A=Z0/60*sqrt((er+1)/2)+ (er-1)/(er+1)*(.23+.11/er);

w=h*(8*exp(A))/(exp(2*A)-2);

width=w

end

%

% effective dielectric constant

%

ere=(er+1)/2 + (er-1)/2*(1+12*h/w)^(-.5);

%

% determine length in millimeters

```

```
%  
  
length=pi/2*1/(sqrt(ere)*k0)*1000  
  
%  
  
% end  
  
%%%%%%%%%
```

# C.3 Impedance matching network

## C.3.1 M-script

```

%%%%%%%%%%
% match.m
%
% Impedance Matching Network Developer for single feed MPA
%
% script prompts user to enter MPA parameters and
% returns impedances for a n-resonator Chebychev network
% based on "An Impedance-Matching Technique for Increasing
% the Bandwidth of Microstrip Antennas (Pues and Van de Capelle)
%
% by Ron Lewis (10/01/06)
%%%%%%%%%%
% user given antenna model parameters
%
fr=input('Enter the resonant frequency > ');
R0=input('Enter the resonant antenna resistance > ');
Q=input('Enter the quality factor > ');
Z0=50;

```

```

%
%Designer choices
%
n=input('Enter the order of the matching network >');
B=input('Enter a bandwidth improvement factor as a percentage >');
%
% Network parameter calculation
%
Alpha=tan(pi/2*B);
delta=pi/(2*Alpha*Q);
%
% gi parameters from definition and lookup table
%
g0=1;
g1=1/(delta);
%
n
delta
%
g2=input('Enter g2 based on n and delta >');
g3=input('Enter g3 based on n and delta >');

```

```

g4=input('Enter g4 based on n and delta >');

%%%%%%%%%%

% calculation of J "admittance inverters, Y characteristic admittance, and

% Z characteristic impedance based on a series resonant model or a parallel

% resonant model

%%%%%%%%%%

%

Gamma=tan(pi/4*B);

%

a2=1;

%

a3=1;

%

if input('\nIs the matching network based

on a series resonant model?(y,n)\n?', 's')== 'y'

Zc1=(pi)/2*(R0/Q);

Yc2=g2/(Alpha*R0);

Yc3=Yc2;

J23=(Alpha)*sqrt((Yc2*Yc3)/(g2*g3));

J34=sqrt((Alpha*Yc3)/(g3*g4*Z0));

Y23c=J23*cos(pi/4*B);

```

```

Y34c=J34*cos(pi/4*B);
Yyc2=(Yc2*Alpha-(Y23c)*Gamma)*((a2-Gamma^2)/((1+a2)*Gamma));
Yyc3=(Yc3*Alpha-(Y23c+Y34c)*Gamma)*((a3-Gamma^2)/((1+a3)*Gamma));
end
if input('\nIs the matching network based on a parallel model?(y,n)\n?','s')== 'y'
trace=input('Select an impedance for the centre interconnecting feed segment >');
dummy=sqrt(g2*g3)*(1/trace)/(Alpha*cos((pi/4)*B));
Yc2=dummy;
Yc3=Yc2;
Zc1=Q*(2/(pi))*R0;
J12=sqrt((Alpha*Yc2)/(R0*g2));
b=1;
J23=(Alpha)*sqrt((Yc2*Yc3)/(g2*g3));
J34=sqrt((Alpha*Yc3)/(g3*g4*Z0));
Y12c=J12*cos(pi/4*B);
Y23c=J23*cos(pi/4*B);
Y34c=J34*cos(pi/4*B);
Yyc2=(Yc2*Alpha-(Y12c+Y23c)*Gamma)*((a2-Gamma^2)/((1+a2)*Gamma));
Yyc3=(Yc3*Alpha-(Y23c+Y34c)*Gamma)*((a3-Gamma^2)/((1+a3)*Gamma));
end
%
```

```

% calculate impedances from admittances

%

Yyyc2=a2*Yyc2;

Yyyc3=a3*Yyc3;

Z12c=1/Y12c

Z23c=1/Y23c

Z34c=1/Y34c

Zzc2=1/Yyc2

Zzzc2=1/Yyyc2

Zzc3=1/Yyc3

Zzzc3=1/Yyyc3

%

% end

%%%%%%%%%%

```

### C.3.2 Running M-script

Using Toolbox Path Cache. Type "help toolbox\_path\_cache" for more info.

To get started, select "MATLAB Help" from the Help menu.

>> sample

Enter the resonant frequency > 900

Enter the resonant antenna resistance > 47.59

Enter the quality factor  $> 36.4344$

Enter the order of the matching network  $> 3$

Enter a bandwidth improvement factor as a percentage  $> .1$

$n = 3$

$\delta = 0.2722$

Enter  $g_2$  based on  $n$  and  $\delta > .484$

Enter  $g_3$  based on  $n$  and  $\delta > 2.31$

Enter  $g_4$  based on  $n$  and  $\delta > .365$

Is the matching network based on a series resonant model?(y,n)

?n

Is the matching network based on a parallel model?(y,n)

?y

Select an impedance for the centre interconnecting feed segment  $> 130$

$Z_{12c} = 53.2977$

$Z_{23c} = 130$

$Z_{34c} = 72.1050$

$Z_{zc2} = 26.0640$

$Z_{zzc2} = 26.0640$

$Z_{zc3} = 24.5105$

$Z_{zzc3} = 24.5105$







